

Ethylene polymerization with zirconocene catalyst  
on zeolite A support derived from fly ash



A Thesis Submitted in Partial Fulfillment of the Requirements  
for the Degree of Master of Engineering in Chemical Engineering

Department of Chemical Engineering

FACULTY OF ENGINEERING

Chulalongkorn University

Academic Year 2022

Copyright of Chulalongkorn University

เอทิลีนพอลิเมอร์ไรเซชันด้วยตัวเร่งปฏิกิริยาเซอร์โคโนซีน  
บนตัวรองรับซีโอไลท์เอทีได้จากถ้ำลอย



วิทยานิพนธ์นี้เป็นส่วนหนึ่งของการศึกษาตามหลักสูตรปริญญาวิศวกรรมศาสตรมหาบัณฑิต  
สาขาวิชาวิศวกรรมเคมี ภาควิชาวิศวกรรมเคมี  
คณะวิศวกรรมศาสตร์ จุฬาลงกรณ์มหาวิทยาลัย  
ปีการศึกษา 2565  
ลิขสิทธิ์ของจุฬาลงกรณ์มหาวิทยาลัย

Thesis Title                      Ethylene polymerization with zirconocene catalyston  
zeolite A support derived from fly ash  
By                                      Miss Natthapat Warintha  
Field of Study                      Chemical Engineering  
Thesis Advisor                      Professor BUNJERD JONGSOMJIT, Ph.D.

---

Accepted by the FACULTY OF ENGINEERING, Chulalongkorn University in  
Partial Fulfillment of the Requirement for the Master of Engineering

..... Dean of the FACULTY OF  
ENGINEERING  
(Professor SUPOT TEACHAVORASINSKUN, D.Eng.)

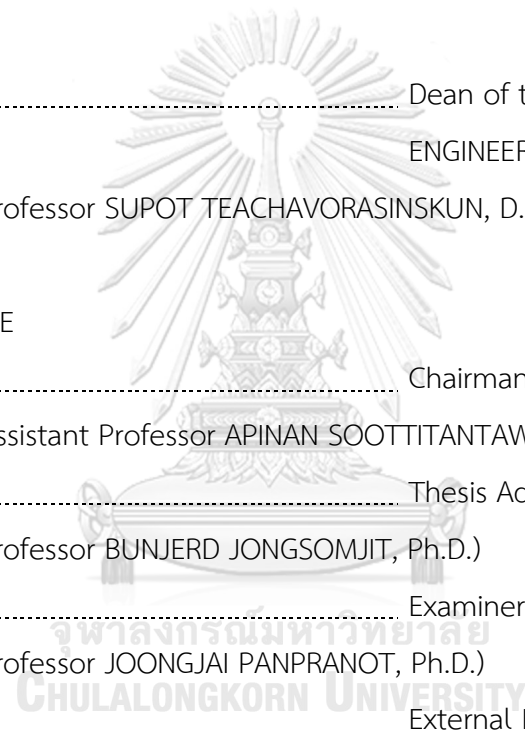
THEESIS COMMITTEE

..... Chairman  
(Assistant Professor APINAN SOOTTITANTAWAT, D.Eng.)

..... Thesis Advisor  
(Professor BUNJERD JONGSOMJIT, Ph.D.)

..... Examiner  
(Professor JOONGJAI PANPRANOT, Ph.D.)

..... External Examiner  
(Associate Professor Ekrachan Chaichana, Ph.D.)



ณัฐภัทร วรินทร์รา : เอทิลีนพอลิเมอร์ไรเซชันด้วยตัวเร่งปฏิกิริยาเซอร์โคโนซีนบนตัวรองรับซีโอไลต์เอที่ได้จากเถ้าลอย. ( Ethylene polymerization with zirconocene catalyston zeolite A support derived from fly ash) อ.ที่ปรึกษาหลัก : ศ. ดร. บรรเจิด จงสมจิตร

การสังเคราะห์ซีโอไลต์เอ (LTA) จากเถ้าลอยถูกนำไปใช้งานมากมาย ซึ่งการนำมาใช้งานเป็นตัวรองรับของตัวเร่งปฏิกิริยาเมทัลโลซีนนั้นพบได้ไม่บ่อยนัก โดยงานวิจัยนี้ประกอบด้วยสามส่วน โดยในส่วนแรกเราได้ศึกษาผลของวิธีการตรึงเมทิลอะลูมิเนียมออกเซน (MAO) และตัวเร่งปฏิกิริยาเซอร์โคโนซีนบนตัวรองรับซิลิกา พบว่า วิธีการตรึงตัวเร่งปฏิกิริยาร่วมก่อนตามด้วยการตรึงตัวเร่งปฏิกิริยาเมทัลโลซีนมีความสามารถในการเร่งปฏิกิริยาที่สูงที่สุด ซึ่งจะถูกนำไปศึกษาในส่วนถัดไป ส่วนที่สองทำการศึกษาอุณหภูมิและอัตราส่วน  $[Al]_{MAO}/[Zr]_{cat}$  ที่เหมาะสมสำหรับกระบวนการสังเคราะห์พอลิเอทิลีนโดยใช้เครื่องปฏิกรณ์แบบกึ่งกะภายใต้การทำงานแบบแอเดียแบติก โดยใช้ตัวเร่งปฏิกิริยาเมทัลโลซีนบนตัวรองรับซีโอไลต์เอ สภาวะที่เหมาะสมที่อุณหภูมิ 80 องศาเซลเซียส และอัตราส่วนระหว่าง  $[Al]_{MAO}/[Zr]_{cat}$  เท่ากับ 2000 ส่วนส่วนสุดท้ายเปรียบเทียบการใช้ตัวรองรับซีโอไลต์ทั้งสามชนิดสำหรับกระบวนการสังเคราะห์พอลิเอทิลีนและเอทิลีน/1-เฮกเซนพอลิเมอร์ไรเซชัน พบว่า LTA-MAO/Zr มีความสามารถในการเร่งปฏิกิริยาที่ดีกว่าตัวรองรับ ZSM5 และ BEA เนื่องจากมีอัตราส่วนระหว่างอะลูมิเนียมต่อเซอร์โคเนียมสูงกว่าและมีความเป็นกรดเลอวิสที่สูง ซึ่งสอดคล้องกับความสามารถในการเร่งปฏิกิริยาของตัวเร่งปฏิกิริยา อย่างไรก็ตาม เราไม่สามารถสรุปได้ว่าตัวรองรับซีโอไลต์ที่มีความเป็นกรดสูงจะทำให้ความสามารถในการเร่งปฏิกิริยาของตัวเร่งปฏิกิริยาสูงขึ้นได้เสมอ เนื่องจากขึ้นอยู่กับปัจจัยหลายประการ ดังนั้นซีโอไลต์เอจึงเป็นตัวรองรับของตัวเร่งปฏิกิริยาเมทัลโลซีนที่เหมาะสมที่สุด

สาขาวิชา วิศวกรรมเคมี

ปีการศึกษา 2565

ลายมือชื่อนิสิต .....

ลายมือชื่อ อ.ที่ปรึกษาหลัก .....

# # 6470378321 : MAJOR CHEMICAL ENGINEERING

KEYWORD: Fly ash, zeolite A, zirconocene, supported metallocene, ethylene polymerization, ethylene/1-hexene copolymerization

Natthapat Warintha : Ethylene polymerization with zirconocene catalyst on zeolite A support derived from fly ash. Advisor: Prof. BUNJERD JONGSOMJIT, Ph.D.

Zeolite A (LTA) synthesis from fly ash has many applications, in which metallocene catalytic support is uncommon. This research study has three parts. Firstly, investigation of the effects of immobilized MAO cocatalyst and zirconocene catalyst techniques on silica support. Immobilized MAO, followed by metallocene catalyst method had the highest catalytic activity, which was used in the next parts. The second part examined the optimal temperature and  $[Al]_{MAO}/[Zr]_{cat}$  ratio with ethylene polymerization in a semi-batch autoclave reactor utilizing LTA-supported metallocene catalysts. The optimal conditions were found at 80°C and  $[Al]_{MAO}/[Zr]_{cat}$  ratios equal to 2000 that were used in the next section. LTA-MAO/Zr showed lower catalytic activity than silica-supported catalysts. This is because acidity disrupted polymer chain formation and reduced crystallinity. Finally, a comparison of three zeolite supports for ethylene and ethylene/1-hexene polymerization was conducted. LTA-MAO/Zr had the best catalytic activities among ZSM5 and BEA support because of a higher Al/Zr ratio and Lewis acidity, which corresponded to the catalyst activity. However, we cannot generalize that high zeolite support acidity leads to high catalyst activity because it depends on multiple factors. Therefore, LTA was an optimally supported metallocene catalyst system.

Field of Study: Chemical Engineering

Student's Signature .....

Academic Year: 2022

Advisor's Signature .....

## ACKNOWLEDGEMENTS

First and foremost, I would like to express my gratitude to my lovely advisor, Professor Dr. Bunjerd Jongsomjit, for accepting me as a member of the Ziegler-Natta and Metallocene group and providing continuous support of my study and related research, as well as useful suggestions and discussion throughout this thesis. His advice helped me throughout the whole process of researching and writing this thesis, and without him, this research thesis wouldn't have been possible. I sincerely appreciate his support.

Following that, I would also be sincere to Asst. Prof. Apinan Soottitantawat as the chairman, Prof. Joongjai Panpranot as the committee and Assoc. Prof. Ekrachan Chaichana as the external examiner for their insightful comments, excellent guidance, continuous support for more understanding in the synthesis of supported catalysts and ethylene polymerization throughout my research.

A special thanks is extended to the Ziegler-Natta and Metallocene group and the students of the Center of Excellence on Catalysis and Catalytic Reaction Engineering. I am immensely grateful for the stimulating discussions, shared spirit, encouragement, and support that we have had over the past two years. The camaraderie and fun we experienced together made this academic journey even more memorable.

Lastly, I would like to convey my deepest appreciation to my beloved family. Their continuous support, inspiration, and encouragement have been the driving force behind my achievements. This thesis and my graduation are dedicated to them.

Natthapat Warintha

## TABLE OF CONTENTS

	Page
.....	iii
ABSTRACT (THAI).....	iii
.....	iv
ABSTRACT (ENGLISH).....	iv
ACKNOWLEDGEMENTS.....	v
TABLE OF CONTENTS.....	vi
LIST OF TABLES.....	xi
LIST OF FIGURES.....	xiii
CHAPTER 1 INTRODUCTION.....	1
1.1 Introduction.....	1
1.2 Research objective.....	3
1.3 Benefits.....	3
1.4 Research scope.....	3
CHAPTER 2 THEORY AND LITERATURE REVIEWS.....	7
2.1 Polyethylene.....	7
2.2 Polyolefin Catalyst.....	10
2.3 Metallocene Catalytic system.....	11
2.3.1 Metallocene catalyst.....	11
2.3.2 Cocatalyst and scavenger.....	14
2.4 Polymerization reaction.....	16
2.5 Supported metallocene catalysts.....	19

2.6. Zeolite .....	22
2.7 Literature reviews.....	32
CHAPTER 3 EXPERIMENTAL.....	36
3.1 Materials and Chemicals.....	36
3.2 Equipment .....	37
3.2.1 Schlenk line.....	37
3.2.2 Schlenk tube.....	38
3.2.3 Vacuum pump.....	39
3.2.4 Glove box .....	39
3.2.5 Slurry phase polymerization.....	39
3.2.6 Magnetic stirrer and heater.....	40
3.3 Preparation of support.....	40
3.3.1 Preparing Zeolite A.....	40
3.3.2 Calcination.....	40
3.3.3 Immobilization.....	40
3.4 Ethylene polymerization.....	42
3.5 Characterization of supports catalysts, catalysts and polymer.....	43
3.5.1 Scanning Electron Microscopy-Energy Dispersive X-Ray (SEM-EDX) .....	43
3.5.2 X-ray Diffractometer (XRD).....	43
3.5.3 Thermogravimetric Analysis and Differential Scanning Calorimetry (TGA-DSC).....	44
3.5.4 Fourier transform Infrared (FT-IR).....	44
3.5.5 N <sub>2</sub> physisorption .....	44
3.5.6 Laser particle size distribution analyzer (PSD) .....	44



3.5.7 Temperature-programmed desorption of ammonia (NH <sub>3</sub> -TPD).....	45
3.6 Research plan .....	46
CHAPTER 4 RESULTS AND DISCUSSION.....	47
4.1 Effect of different immobilization methods of MAO/zirconocene catalysts on silica support.....	47
4.1.1 Characterizations of silica support and MAO/Zirconocene catalyst on silica support .....	48
4.1.1.1 N <sub>2</sub> physisorption (BET) and laser particle size distribution analyzer (PSD).....	48
4.1.1.2 Scanning Electron Microscopy (SEM) and Energy Dispersive X-ray Spectroscopy (EDX).....	49
4.1.1.3 X-ray Diffraction (XRD) .....	51
4.1.1.4 Fourier Transform Infrared Spectroscopy (FTIR).....	51
4.1.2 The catalytic activities of ethylene polymerization .....	52
4.1.3 Characterizations of polyethylene .....	53
4.1.3.1 Scanning Electron Microscopy (SEM) and Energy Dispersive X-ray Spectroscopy (EDX).....	53
4.2 In situ polymerization using zeolite A supported MAO/Zirconocene for ethylene and ethylene/1-hexene polymerization. ....	55
4.2.1 Characteristics of zeolite A (LTA) and LTA-supported catalyst .....	55
4.2.1.1 N <sub>2</sub> physisorption (BET) and Laser particle size distribution analyzer (PSD).....	55
4.2.1.2 Scanning Electron Microscopy (SEM) and Energy Dispersive X-ray Spectroscopy (EDX).....	56
4.2.1.3 X-ray Diffraction (XRD) .....	58
4.2.1.4 Fourier Transform Infrared Spectroscopy (FTIR).....	59

4.2.1.5 Temperature-programmed desorption of ammonia (NH <sub>3</sub> -TPD).....	59
4.2.2 The catalytic activities on polymerization behaviors .....	60
4.2.2.1 Effect of polymerization temperature and cocatalyst (MAO) ratio	60
4.2.2.2 Effect of amount of scavenger (TMA).....	62
4.2.2.3 Ethylene and ethylene/1-hexene polymerization behaviors.....	63
4.2.3 Characterizations of polymer .....	64
4.2.3.1 Scanning Electron Microscopy (SEM) and Energy Dispersive X-ray Spectroscopy (EDX).....	64
4.2.3.2 X-ray Diffraction (XRD) .....	66
4.2.3.3 Thermal gravimetric analysis differential scanning calorimetry (TGA-DSC).....	67
4.2.4 Comparison between silica and zeolite A for supported-metallocene catalyst system. ....	68
4.2.4.1 Characterization of support and immobilized catalyst .....	68
4.2.4.2 Catalyst activity.....	70
4.2.4.3 Characterization of polymer.....	71
4.3 Comparison of different zeolite for supported metallocene catalysts with ethylene polymerization and 1-hexene copolymerization.....	74
4.3.1 Characteristics of different zeolite and zeolite-MAO/metallocene supported catalyst. ....	74
4.3.1.1 N <sub>2</sub> physisorption (BET) and Laser particle size distribution analyzer (PSD).....	74
4.3.1.2 Scanning Electron Microscopy (SEM) and Energy Dispersive X-ray Spectroscopy (EDX).....	75
4.3.1.3 X-ray Diffraction (XRD) .....	77
4.3.1.4 Temperature-programmed desorption of ammonia (NH <sub>3</sub> -TPD).....	79

4.3.1.5 Thermogravimetric Analysis (TGA).....	80
4.3.2 The catalytic activities on Ethylene and ethylene/1-hexene polymerization behaviors .....	81
4.3.3 Characterizations of polymer .....	83
4.3.3.1 Scanning Electron Microscopy (SEM) and Energy Dispersive X-ray Spectroscopy (EDX).....	83
4.3.3.2 X-ray Diffraction (XRD) .....	85
4.3.3.3 Thermal gravimetric analysis differential scanning calorimetry (TGA-DSC).....	86
CHAPTER 5 Conclusion.....	87
5.1 Conclusion .....	87
5.2 Recommendations .....	88
REFERENCES .....	90
APPENDIX A : FOURIER TRANSFORM INFRARED SPECTROSCOPY .....	98
APPENDIX B : THERMAL GRAVIMETRIC ANALYSIS AND DIFFERENTIAL SCANNING CAROLIMETRY .....	104
APPENDIX C : CALCULATION.....	114
APPENDIX D : LIST OF PUBLICATION.....	116
VITA.....	118

## LIST OF TABLES

	Page
Table 1 Classification of polyethylene following various density.....	8
Table 2 Examples of metallocene catalyst.....	12
Table 3 Symmetry of metallocene and polymer tacticity .....	13
Table 4 Example of Si/Al ratio of zeolites .....	25
Table 5 Classification of zeolites by pore size.....	25
Table 6 BET data of commercial zeolite A .....	26
Table 7 General properties of support in this study.....	28
Table 8 The different zeolite synthesis strategies from various raw materials.....	30
Table 9 The chemical used in the reaction by metallocene catalyst system.....	36
Table 10 The surface area, pore size, pore volume and particle size distribution of silica support .....	48
Table 11 Elemental distribution on the catalyst surface (EDX) with different methods. ....	50
Table 12 Catalyst activity with different methods of silica support.....	53
Table 13 The surface area of silica by N <sub>2</sub> physisorption using the Brunauer-Emmett-Teller (BET) method, pore size and pore volume.....	55
Table 14 Elemental distribution on the LTA-supported catalyst surface (EDX).....	57
Table 15 The amount of acid sites of zeolite A .....	60
Table 16 The Catalytic activities of various polymerization temperatures and molar ratios of [Al] <sub>MAO</sub> /[Zr] <sub>cat</sub> via ethylene polymerization.....	61
Table 17 The catalytic activities of various molar ratios of [Al]TMA/[Zr]cat via ethylene polymerization.....	62

Table 18 The activity of MAO/Zirconocene catalyst via ethylene and ethylene/1-hexene polymerization.....	63
Table 19 Melting temperature and crystallization behaviors of polyethylene and copolymers produced from LTA support immobilization. ....	67
Table 20 Comparison of the surface area, pore size, pore volume and particle size distribution between spherical silica and zeolite A .....	68
Table 21 Elemental distribution on the silica and LTA supported catalyst surface. ...	69
Table 22 The activity of the MAO/Zirconocene catalyst via ethylene and ethylene/1-hexene polymerization on silica and LTA support.....	71
Table 23 Melting temperature and crystallization behaviors of polyethylene and copolymer produced from silica and LTA support of immobilization.....	73
Table 24 The surface area of various zeolite supports by N <sub>2</sub> physisorption using the Brunauer-Emmett-Teller (BET) method, pore size and pore volume. ....	74
Table 25 Elemental distribution on the various zeolite-supported catalyst surface...	77
Table 26 The amount of acid sites of various zeolites .....	80
Table 27 The activity of MAO/Zirconocene catalyst via ethylene and ethylene/1-hexene polymerization on various zeolite.....	82
Table 28 Melting temperature and crystallization behaviors of polyethylene and copolymers produced from LTA support immobilization. ....	86

## LIST OF FIGURES

	Page
Figure 1 Polyethylene structure .....	7
Figure 2 The structure of polyethylene.....	9
Figure 3 Generic structure of a metallocene catalyst. ....	11
Figure 4 Examples of metallocene catalysts structure .....	12
Figure 5 Structure of MAO cocatalyst .....	14
Figure 6 MAO cocatalyst activation of zirconocene catalyst .....	15
Figure 7 Catalyst activation with cocatalyst .....	16
Figure 8 Chain initiation.....	17
Figure 9 Monomer propagation.....	17
Figure 10 Chain transfer reaction .....	18
Figure 11 Methods for supporting metallocene .....	21
Figure 12 Some subunits, cages/cavities and chains in several framework types.....	23
Figure 13 Examples of zeolite framework and their micropore systems and dimensions.....	24
Figure 14 LTA framework type.....	26
Figure 15 BEA framework type.....	27
Figure 16 MFI framework type .....	28
Figure 17 Schlenk line. ....	38
Figure 18 Schlenk tube. ....	38
Figure 19 Diagram of Slurry phase polymerization system .....	39
Figure 20 Methods of immobilization for metallocene/MAO catalyst with support ..	41

Figure 21 Immobilization MAO and metallocene on zeolite supports .....	41
Figure 22 Slurry phase polymerization system .....	43
Figure 23 The N <sub>2</sub> adsorption-desorption isotherms and the average particle size distribution of silica support.....	48
Figure 24 Morphology of spherical silica and immobilized catalyst with different methods from the SEM image .....	49
Figure 25 Elemental distribution on spherical silica and immobilized catalysts with different methods from the SEM image .....	50
Figure 26 XRD patterns of silica supports and silica-supported MAO/Zirconocene catalyst with different immobilization methods.....	51
Figure 27 FTIR spectra of silica and silica-supported MAO/Zirconocene catalysts.....	52
Figure 28 Morphology and element distribution of produced polymer via homogeneous system and silica-supported MAO/Zirconocene catalytic system with different immobilization methods .....	54
Figure 29 The N <sub>2</sub> adsorption-desorption isotherms and the average particle size distribution of zeolite A support .....	56
Figure 30 SEM images of zeolite A and immobilized catalyst on zeolite A morphology .....	57
Figure 31 Elemental distribution on zeolite A and immobilized MAO/zirconocene catalyst on zeolite A support.....	58
Figure 32 XRD patterns of LTA and LTA after immobilization .....	58
Figure 33 FTIR spectra of LTA before and after immobilization .....	59
Figure 34 NH <sub>3</sub> -TPD profiles of zeolite A .....	60
Figure 35 Morphology and element distribution of polyethylene and ethylene/1-hexene copolymer produced via homogeneous system and LTA-MAO/Zr catalyst...	65

Figure 36 XRD patterns of polyethylene from homogeneous system and LTA-MAO/Zr catalytic system .....	66
Figure 37 The morphology of silica and zeolite A support and immobilized MAO/zirconocene catalyst.....	69
Figure 38 TGA profiles of silica and LTA-supported metallocene catalysts.....	70
Figure 39 The morphology of polymer from silica and zeolite A support immobilized MAO/zirconocene catalyst.....	71
Figure 40 XRD patterns of polyethylene and ethylene/1-hexene copolymer from SMAO/Zr and LTA-MAO/Zr catalytic system.....	72
Figure 41 The N <sub>2</sub> adsorption-desorption isotherms and the average particle size distribution of various zeolite support.....	75
Figure 42 SEM images of various zeolite and immobilized MAO/zirconocene catalyst on zeolite morphology.....	76
Figure 43 XRD patterns of various zeolites before and after immobilization .....	78
Figure 44 FTIR spectra of various zeolites before and after immobilization.....	79
Figure 45 NH <sub>3</sub> -TPD profiles of various zeolites .....	80
Figure 46 TGA profiles of various zeolite-supported metallocene catalysts .....	81
Figure 47 Morphology and element distribution of polyethylene produced via various zeolite supported catalyst.....	83
Figure 48 Morphology and element distribution of ethylene/1-hexene copolymer produced via various zeolite supported catalyst. ....	84
Figure 49 XRD patterns of polyethylene from various zeolite-supported MAO/zirconocene catalytic system .....	85



# CHAPTER 1

## INTRODUCTION

### 1.1 Introduction

Polyethylene (PE) is a popular and widely used type of plastic in homes and businesses. In 2021, the global polyethylene market by production stood at 108.69 million metric tons and was forecasted to grow to 134.84 million metric tons by 2027 [1]. Also, polyethylene has an important and growing demand from all parts of the world. Due to its many suitable properties, such as low strength and hardness but being very ductile, it has good impact strength, is lightweight, water and chemical resistant, durable, etc., making it suitable for several applications, such as plastic bottles, plastic bags, food packaging, and many other products used in the daily life [2]. Polyethylene is one of the polyolefin families. Types of polyethylene are classified by the degree of crystallinity of the polymer, which depends on its density, the length of its molecular chain, and the amount of branching. Low-density polyethylene (LDPE), high-density polyethylene (HDPE), and linear low-density polyethylene (LLDPE) are the common types of polyethylene, and each type is suitable for different applications [3, 4]. The properties of polyethylene indicate various factors such as the preparation process, catalyst size, morphology, etc.

The common chemical catalysts used to produce polyethylene are Ziegler-Natta and metallocene catalysts. The polymer from the Ziegler-Natta catalytic system has a broad molecular weight distribution (MWD) and broad chemical composition distribution (CCD). Because the Ziegler-Natta catalyst is a multiple-site catalyst, the product has non-uniform properties that are difficult to control. On the other hand, a metallocene catalyst is one catalyst for producing polyethylene. Metallocene is a single-site catalyst. The polymer produced by this catalyst had high activity, a narrow molecular weight distribution (MWD), and a narrow chemical

composition distribution (CCD) [5, 6]. So, a Metallocene catalyst is suitable for ethylene polymerization.

Even so, metallocene catalysts had problems in the homogeneous process, such as being hard to control in terms of shape and foiling in the reactor. So, a supported catalyst for metallocene catalysts can solve these problems [7]. Support for the metallocene catalysts commonly used is provided by inorganic materials such as silica, alumina, titania, zirconia, etc. [7-10].

Nowadays, in Thailand, power plants are located all around the country, such as Mae Moh Power Plant, Bang Pakong Power Plant, Krabi Power Plant, etc. [11]. One of the by-products of this process is fly ash if eliminated non-properly, which affects environmental pollution. Applications of fly ash include materials for construction, agriculture, etc. [12]. Then, Zeolite A is one of those produced wastes from the power generation industry. Produced waste from power generation is fly ash. Mainly containing fly ashes are silica ( $\text{SiO}_2$ ) and alumina ( $\text{Al}_2\text{O}_3$ ), depending on the source of raw materials [13]. At present, Zeolite A is not being used very widely compared to other zeolites. For example, NY-zeolite [14], HY-zeolite [15], ZSM-5 [16], Beta-zeolite [17], etc. However, researchers have focused on zeolite A utilization. Zeolites are crystalline microporous aluminosilicate materials with uniformly sized molecular pores and three-dimensional framework structures [18]. In the past, zeolite A has been used in many applications, such as catalysis [19, 20], absorption for water treatment [21, 22], gas separation [23, 24], and for support catalysts [25, 26], but not as a metallocene catalyst support. So, zeolites A are interested in supporting metallocene catalysts and applying zeolite A to more applications.

In this study, fly ash from the Mae Moh power plant for the synthesis of zeolite A. Zeolite A will study metallocene catalytic. In the preliminary study, the effect of the immobilization method on support was investigated. Due to zeolite A being less synthesized, silica is used as a support that widely used as catalyst support.

This research was divided into two parts. The first part investigates the effect of varying the molar ratios of  $[Al]_{MAO}/[Zr]_{cat}$  and  $[Al]_{TMA}/[Zr]_{cat}$  during the in situ polymerization of ethylene and 1-hexene copolymerization. In the final part, comparisons of the results of different zeolite supports (Beta-zeolite and ZSM-5) on the ethylene polymerization and 1-hexene copolymerization behaviors.

## 1.2 Research objective

- To investigating the use of zeolite A to support a metallocene catalyst in the polymerization of ethylene and the copolymerization of 1-hexene.
- To Compare zeolite A and other zeolites in ethylene polymerization and 1-hexene copolymerization.

## 1.3 Benefits

- Utilizing waste from the electrical industry to decrease environmental pollution caused by waste products.
- In the future, to develop zeolite A as a supported catalyst in the polyethylene or polymer industry.

## 1.4 Research scope

- Bis(cyclopentadienyl)zirconium(IV) dichloride is a commercial metallocene catalyst.
- Zeolite A was synthesized from fly ash from the Mae Moh power plant.
- A commercial spherical silica support was used for the preliminary study.
- ZSM-5 and Beta-Zeolite are commercially supported.

- All support is used as support for MAO and the metallocene catalyst in ethylene polymerization and 1-hexene copolymerization.
- Zeolite-supported MAO and metallocene were prepared by immobilization.
- The performance of the immobilization of cocatalyst/catalyst onto support is determined in the preliminary part using two different methods, including (Method A) immobilized cocatalyst/catalyst/support and (Method B) immobilized cocatalyst/support first, then immobilized catalyst into cocatalyst/support.
- Zeolite supports are characterized by Scanning Electron Microscopy-Energy Dispersive X-Ray (SEM-EDX), X-ray Diffractometer (XRD), N<sub>2</sub> physisorption (BET), Fourier transform Infrared (FT-IR), Laser particle size distribution analyzer (PSD) and Temperature-programmed desorption of ammonia (NH<sub>3</sub>-TPD) methods.
- Zeolite-supported MAO and metallocene catalysts are characterized by Scanning Electron Microscopy-Energy Dispersive X-Ray (SEM-EDX), X-ray Diffractometer (XRD), Thermogravimetric Analysis and Differential Scanning Calorimetry (TGA-DSC) and Fourier transform Infrared (FT-IR) methods.
- Methylaluminoxane (MAO) and trimethylaluminum (TMA) are cocatalysts and scavengers for zirconocene catalysts.
- The temperatures were varied between 50, 60, 70, 80 and 90°C with an  $[Al]_{MAO}/[Zr]_{cat}$  molar ratio of 2000 for ethylene polymerization and 1-hexene copolymerization.
- The molar ratios of  $[Al]_{MAO}/[Zr]_{cat}$  were varied at 1000, 1500, 2000, 2500 and the molar ratios of  $[Al]_{TMA}/[Zr]_{cat}$  were 500, 1000, 150, 2000 and 2500 with an  $[Al]_{MAO}/[Zr]_{cat}$  molar ratio of 1000 for ethylene polymerization and 1-hexene copolymerization.
- The catalyst activities are measured in a 100 mL stainless steel reactor equipped with a magnetic stirrer during ethylene polymerization at design

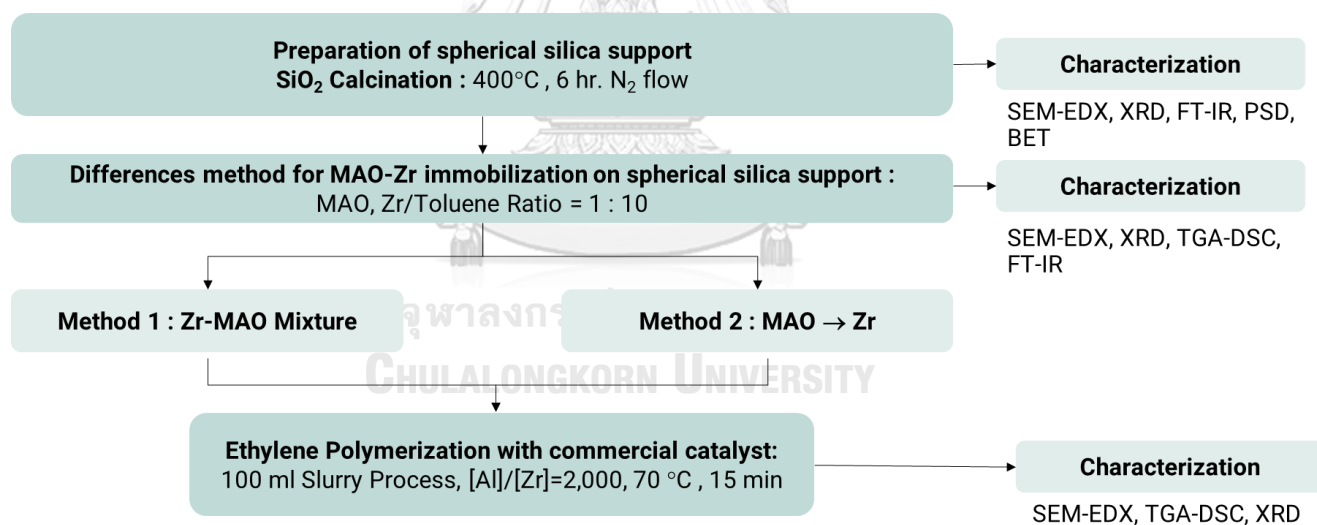
temperature while stirring at 600 rpm under 3.5 bar of ethylene pressure in the slurry process.

- The polyethylene obtained is characterized by Scanning Electron Microscopy-Energy Dispersive X-Ray (SEM-EDX), X-ray Diffractometer (XRD) and Thermogravimetric Analysis and Differential Scanning Calorimetry (TGA-DSC) methods.

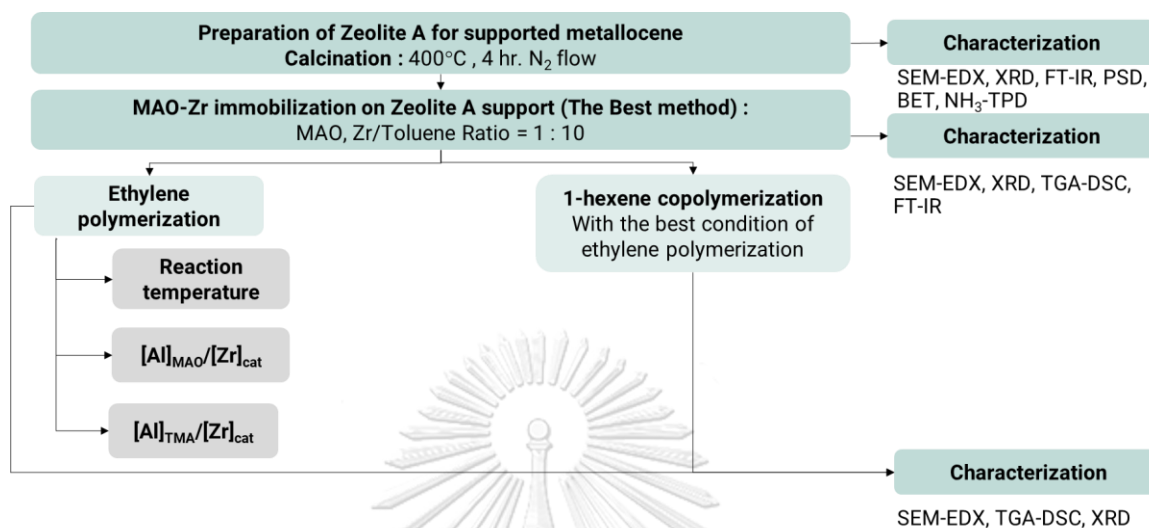
### 1.5 Research methodology

Research methodologies as shown below.

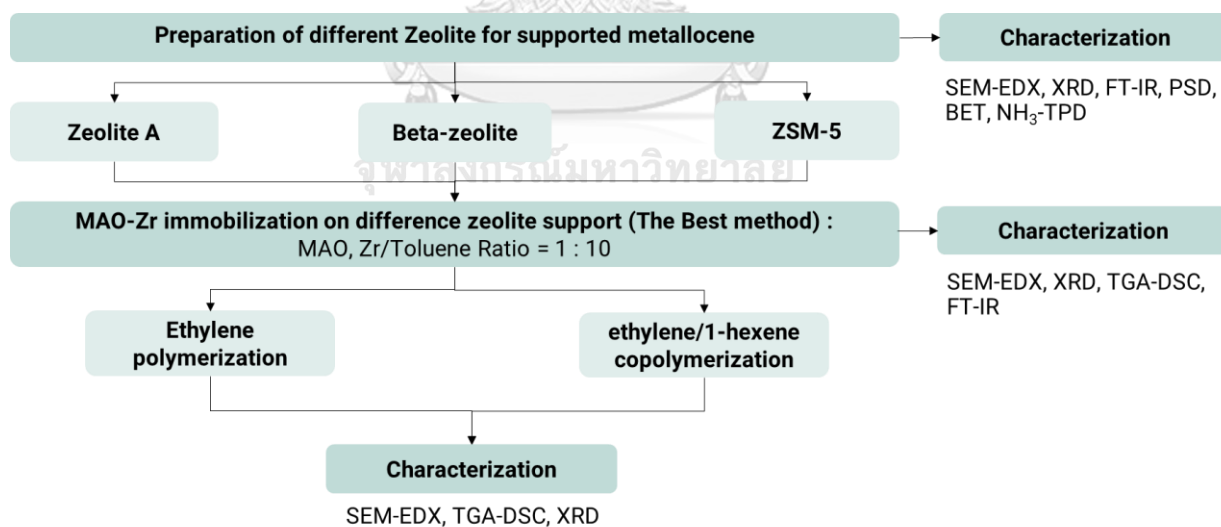
**Preliminary Study :** To determine the effect of different immobilization methods on ethylene polymerization.



**Part I :** To synthesize polyethylene by in situ polymerization using Zeolite A supported MAO-Zr for ethylene polymerization and 1-hexene copolymerization.



**Part II :** To compare Zeolite A, Beta-Zeolite, and ZSM-5 for supported metallocene catalysts with ethylene polymerization and 1-hexene copolymerization.



## CHAPTER 2

### THEORY AND LITERATURE REVIEWS

#### 2.1 Polyethylene

Polyethylene (PE) is one of the polyolefin families. It is the most commonly used plastic in the world. The interesting properties of polyethylene are its light weight, flexibility, ease of processing, durability, resistance to chemicals, and other properties that can be applied to a variety of applications such as bottles for beverages and cosmetics, toys, containers for liquids, chemicals, fuels, household waste, and materials for other applications [27, 28]. Usually, polyethylene consists of alkanes with the formula  $C_{2n}H_{4n+2}$ , where  $n$  is the degree of polymerization. The covalently linked carbon atom with a pair of hydrogen atoms attached to each carbon. The chain ends are terminated by methyl groups [29]. The polyethylene structure in Figure 1.

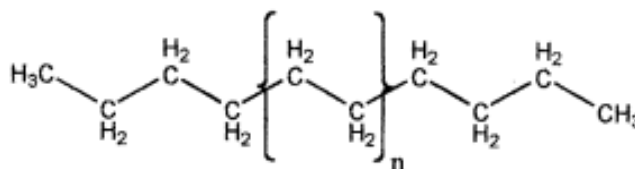


**Figure 1** Polyethylene structure [29]

Therefore, polyethylene was classified mainly based on its molecular weight, density, and branching. The American Society for Testing and Materials (ASTM) has defined types of polyethylene [29, 30] which provides the following classifications based upon density shown in Table 1. For this study, focuses on High-Density Polyethylene (HDPE), Low-Density Polyethylene (LDPE) and Linear low density polyethylene (LLDPE) respectively, that the structures are shown in Figure 2.

**Table 1** Classification of polyethylene following various density.

Types of PE	General named	Density (g/cm <sup>3</sup> )
High density polyethylene	HDPE	> 0.941
Linear medium density polyethylene	LMDPE	0.926-0.940
Medium density polyethylene	MDPE	0.926-0.940
Linear low-density polyethylene	LLDPE	0.919-0.925
Low density polyethylene	LDPE	0.910-0.925

### Low Density Polyethylene (LDPE)

LDPE can only be created through the free radical polymerization of ethylene triggered by organic peroxides or other reagents. Usually, the density ranges from 0.915-0.930 g/cm<sup>3</sup>. LDPE is the most easily processed of the major polyethylene varieties, which are commonly mixed with linear low-density polyethylene (LLDPE) and high-density polyethylene (HDPE). Because of a branch to which other polyethylene chains are linked, LDPE is highly branched and has a comparatively high proportion of amorphous carbon atoms. These branches are quite long and interconnect with other molecules, resulting in great quality in films for food packaging, a significant application.

### High Density Polyethylene (HDPE)

HDPE is made by polymerizing ethylene with Ziegler-Natta or supported chromium ("Phillips") catalysts. Normally, density ranges between 0.94 - 0.97 g/cm<sup>3</sup>. The modulus, yield, crystallinity, and tensile characteristics of HDPE are excellent. HDPE molecules are more linear and generally shorter than LDPE molecules. These side chains are caused by branching and there are extremely few of them. Extruded pipe for potable water/gas and blow-molded packaging for industrial chemicals (HIC) such as bottles, detergents, shampoos, etc. are common applications for HDPE.



## Linear Low-Density Polyethylene (LLDPE)

LLDPE is generated by ethylene copolymerization with Ziegler-Natta, supported chromium, or metallocene catalysts, -olefins, and common comonomers such as 1-butene, 1-hexene, and 1-octene. The normal density ranges from 0.915-0.930 g/cm<sup>3</sup>. LLDPE contains a linear backbone with short, uniform branches, as compared to the longer branches of LDPE. These short branches can move against one another without being entangled like LDPE. LLDPE is highly flexible, high impact strength, good chemical resistance, and excellent stress crack and impact resistance. LLDPE was suitable for various film applications, including general-purpose film, garment packaging, stretch film, agricultural film, etc.

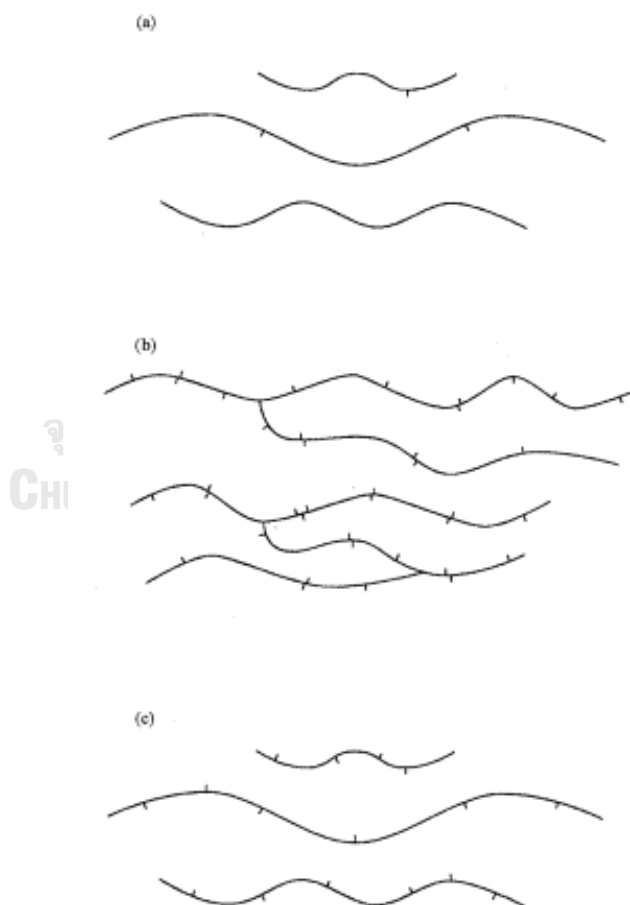


**Figure 2** The structure of polyethylene (a) High Density Polyethylene; (b) Low Density Polyethylene; (c) Linear Low Density Polyethylene [29]

## 2.2 Polyolefin Catalyst

Polyolefins are consistent with polyethylene and polypropylene. Initially, polyolefin was produced by Gibson and Fawcett in the early 1930s and polymerization occurred more than once with free radical initiators under high temperature and high pressure conditions. Early in the 1950s, Phillips Petroleum and Karl Ziegler discovered Phillips and Ziegler catalysts. This catalyst system was composed of a transition metal, typically titanium and a co-catalyst, typically an aluminum alkyl compound. These catalysts provide polymers with nonuniform microstructures, wide molecular weight distributions (MWD) and composition distributions. Metallocene catalysts were discovered in the early 1980s by Walter Kaminsky that metallocene catalysts can control composition distribution, molecular weight distribution (MWD) and stereoregularity. The objective of catalyst development is either to improve polymerization activity or polymer microstructure control. So, the requirement for the good polyolefin's catalyst followed [31-33].

- 1). High stability and productivity
- 2). Good polymer microstructural control
- 3). Production of polymer with good processability
- 4). Production of polymer with controlled particle size distribution, morphology, and high density

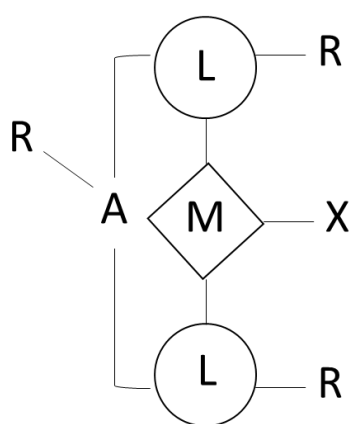
In the present, the development of new catalyst systems has continued, with researchers exploring new organometallic compounds and co-catalysts to improve the control and efficiency of the polymerization process and produce a wide range of materials with specific properties and applications.

## 2.3 Metallocene Catalytic system

Metallocene catalytic systems are a type of homogeneous catalytic system. This catalytic system can be divided into two components. First, metallocene is an organometallic compound. And cocatalyst are an activated component of the metallocene catalytic system. Examples of cocatalysts are aluminoxane, an alkylaluminum, or a combination of aluminoxanes and alkylaluminums. When used alone, these metallocenes have poor activity. Catalytically active species for metallocene/aluminoxane/alkylaluminum complexes, which also produce cationic metallocene catalysts, are well known. [34, 35]

### 2.3.1 Metallocene catalyst

Metallocene catalysts are the organometallic coordination compounds in which one or two  $\pi$ -carbocyclic ligands are called “sandwich compounds”. The two rings may be connected through bridges of different types (Ansa-metallocene). The common transition metals are Zirconocene (Zr), Titanocene (Ti), and Hafnocene (Hf). The general ligands in the metallocene catalyst are Cyclopentadienyl (Cp), Indenyl (Ind) and Fluorenyl (Flu) [36]. The general structure is shown in Figure 3, where metal and cyclic ligand are the main components of the metallocene catalyst and other components are optional.



Where M = Groups 4B, 5B, or 6B transition metal, normally group 4B (Ti, Zr and Hf).

L = Cyclic ligand, normally Cyclopentadienyl (Cp), Indenyl (Ind) and Fluorenyl (Flu)

A = An optional bridging atom usually Si or C atom.

R = A  $\sigma$ -homoleptic hydrocarbyl such as H, alkyl, or other hydrocarbon groups.

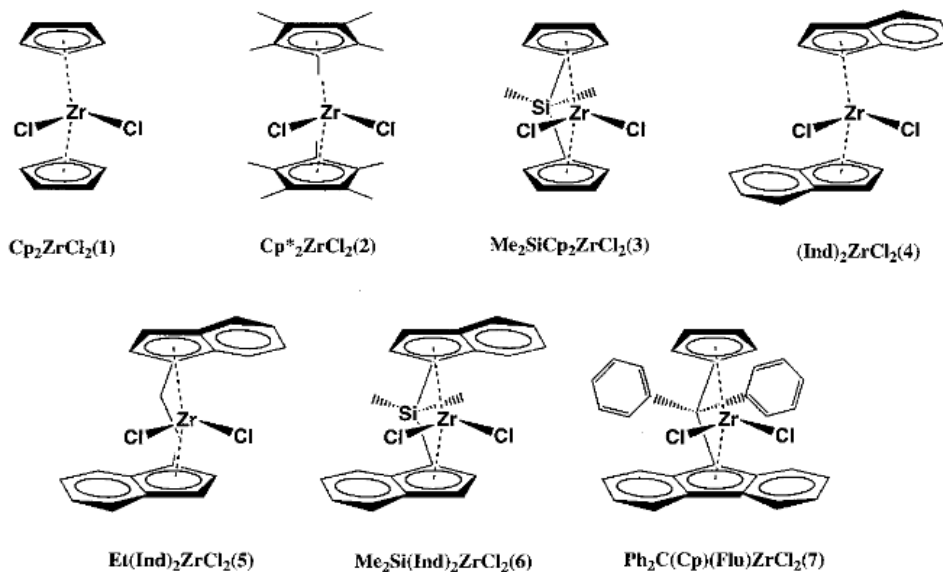
X = chlorine or other halogens from group 7A or an alkyl group.

**Figure 3** Generic structure of a metallocene catalyst.

Table 2 and Figure 4 show examples of each type of metallocene catalyst and some zirconocene catalysts, respectively.

**Table 2** Examples of metallocene catalyst [37]






Category of metallocenes	Metallocene Catalysts
[A] Nonsterrigid metallocenes	1) $Cp_2MCl_2$ (M = Ti, Zr, Hf) 2) $Cp_2ZrR_2$ (M = Me, Ph, $CH_2Ph$ , $CH_2SiMe_3$ ) 3) $(Ind)_2ZrMe_2$
[B] Nonstereorigid ring-substituted metallocenes	1) $(Me_5C_5)_2MCl_2$ (M = Ti, Zr, Hf) 2) $(Me_3SiCp)_2ZrCl_2$
[C] Stereorigid metallocenes	1) $Et(Ind)_2ZrCl_2$ 2) $Et(Ind)_2ZrMe_2$ 3) $Et(IndH_4)_2ZrCl_2$
[D] Cationic metallocenes	1) $Cp_2MR(L)^+ [BPh_4]^-$ (M = Ti, Zr) 2) $[Et(Ind)_2ZrMe]^+ [B(C_6F_5)_4]^-$ 3) $[Cp_2ZrMe]^+ [(C_2B_9H_{11})_2M]^-$ (M = Co)
[E] Supported metallocenes	1) $Al_2O_3-Et(IndH_4)_2ZrCl_2$ 2) $MgCl_2-Cp_2ZrCl_2$ 3) $SiO_2-Et(Ind)_2ZrCl_2$



**Figure 4** Examples of metallocene catalysts structure [38]

However, metallocene composition and type of metal, ligand are varieties. When the two cyclopentadienyl (Cp) rings around the transition metal are unbridged, the metallocene is nonstereorigid and shows  $C_{2v}$  symmetry. Due to an interaction with the other two  $\sigma$ -bonding ligands, the  $Cp_2M$  ( $M = \text{metal}$ ) molecule has a centroid-metal-centroid angle of approximately  $140^\circ$ . When the Cp rings are bridged (two Cp rings arranged in a chiral array and connected with chemical bonds by a bridging group), the stereorigid metallocene, furthermore known as a metallocene, could have either a  $C_1$ ,  $C_2$ , or  $C_s$  symmetry, depending on the substituents on the two Cp rings and the structure of the bridging unit, as depicted in Table 3. [37]

**Table 3** Symmetry of metallocene and polymer tacticity [39]

Symmetry	Metallocene Structure	Sites	Polymer Tacticity	Metallocene Example
$C_{2v}$ achiral		A,A Homotopic	Atactic CE	$Cp_2ZrCl_2$
$C_2$ chiral		E,E Homotopic	Isotactic ES	$rac\text{-}Me_2Si(Ind)_2ZrCl_2$
$C_s$ achiral		A,A Diastereotopic	Atactic CE	Meso- $Me_2Si(Ind)_2ZrCl_2$
$C_s$ prochiral		E,E Enantiotopic	Syndiotactic ES	$Me_2Si(Cp)(9\text{-}Flu)_2ZrCl_2$
$C_1$ chiral		A,A Diastereotopic	Hemiisotactic ES	$Me_2Si(3\text{-}Me\text{-}Cp)(9\text{-}Flu)_2ZrCl_2$

A: aselective, E: enantioselective, CE: Chain-end control, ES: Enantiomorphic site-control

### 2.3.2 Cocatalyst and scavenger

Since the discovery of the metallocene catalyst, there have been many ways to improve the catalytic activity by changing the structure of the catalyst and the polymerization conditions. Cocatalyst is one of the factors that enhances the catalytic activity of ethylene polymerization. Cocatalyst is a compound that is used in combination with a metallocene catalyst in polymerization reactions. Examples of cocatalysts are aluminoxane, an alkylaluminum, or a combination of aluminoxanes and alkylaluminums. The most common types of cocatalysts are alkyl aluminums including methyl aluminoxane (MAO), trimethylaluminum (TMA), triethylaluminum (TEA), triisobutylaluminum (TIBA) and cation forming agents such as  $(C_6H_5)_3C^+(C_6F_5)_4B^-$  and  $B(C_6F_5)_3$  [40, 41] Methyl aluminoxane (MAO) is oligomeric compound (cyclic or linear) chain with  $[-O-Al(Me)-]$  units, as shown in Figure 5.a that a highly effective cocatalyst for metallocene catalyst. MAO are synthesized by controlled hydrolysis of trimethylaluminum (TMA) with water. MAO is formed up of alternate arrangement of aluminum and oxygen atoms, with methyl substituents saturating the free valences. The basic structural unit of MAO is  $[Al_4O_3Me_6]$ . Nevertheless, the aluminum atoms in the unit structure are unsaturated, resulting in agglomerations of molecules that can form cages or clusters of MAO, as shown in Figure 5.b [32, 40, 42]

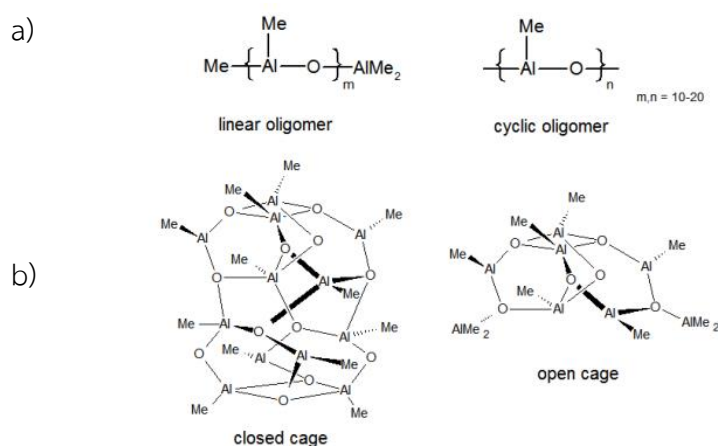
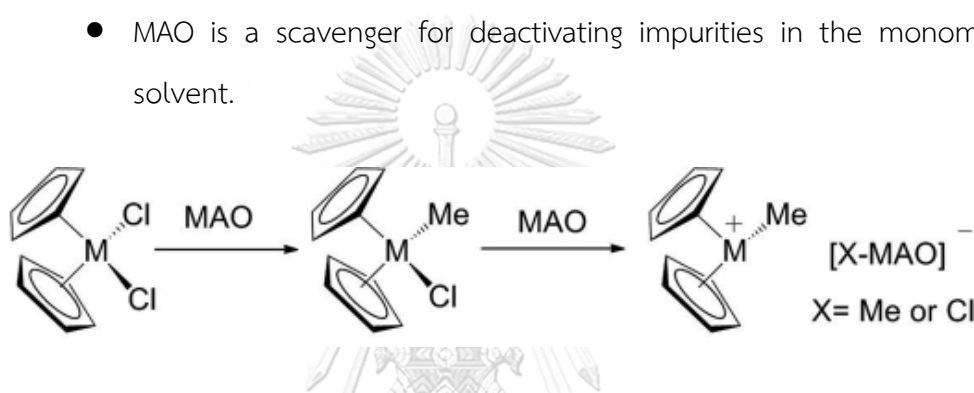


Figure 5 Structure of MAO cocatalyst [37]

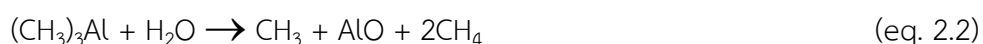
In the case of  $\text{Cp}_2\text{ZrCl}_2$  as precursor, MAO cocatalyst functions can be described as below and show reaction in Figure 6

- MAO methylates the metallocene dihalide ( $\text{Cp}_2\text{ZrCl}_2$ ) to give  $\text{Cp}_2\text{ZrMeCl}$  and  $\text{Cp}_2\text{ZrMe}_2$  species.
- MAO abstracts chloride or methide anion with the formation of a  $[\text{Cp}_2\text{ZrMe}]^+$  cation and a weakly coordinating  $[\text{Cl-MAO}]^-$  or  $[\text{Me-MAO}]^-$  anion.
- MAO is a scavenger for deactivating impurities in the monomer or solvent.



**Figure 6** MAO cocatalyst activation of zirconocene catalyst [43]

In addition, aluminoxane and alkyl aluminum, which are cocatalysts for the metallocene catalytic system, can act as scavengers. Aluminum alkyls scavenge impurities in catalyst poisoning materials (water,  $\text{O}_2$ , etc.) that are often supplied to the reactor during slurry or gas-phase polymerization with MAO/metallocene and traditional Ziegler Natta catalysts. Poisons enter materials as ppm contaminants, such as monomer, comonomer, solvents, and chain transfer agents. In eq. 2.1-2.3 are shown trimethylaluminum (TMA :  $(\text{CH}_3)_3\text{Al}$ ) reacts with impurities. Alkylaluminum derivatives are formed that have no effect on catalytic performance. [44]



## 2.4 Polymerization reaction

Understanding the mechanics and kinetics of the polymerization reaction helps us predict the structure of the resulting polymer. The metallocene-catalyzed polymerization mechanism generally consists of three steps: initiation, propagation, and termination. Important determinants of polymer property formation include kinetics and mechanism. And these parameters also depend on catalyst properties. Mostly, the active center of catalyst is identified to be cationic. Cocatalyst is one of the polymerization factors able to affect simple processes.

The mechanism of ethylene polymerization is shown in Figure 7 - Figure 10. Firstly, the cocatalyst is required to activate the catalyst, but have not provided a mechanism for the reaction. For metallocene catalysts, L indicates a ligand – cyclopentadienyl groups, A is the transition metal active center, and X are halogens. The cocatalyst ( $\text{AlR}_3$ , where R is an alkyl group) extracts two halogen atoms from and transfers one alkyl group to the catalyst. The active site is positively charged, and the cocatalyst product ( $\text{AlR}_2\text{X}_2^-$ ) is a noncoordinating anion needed to stabilize the catalyst. The electron-deficient site is now ready to attract the  $\pi$ -electrons in the olefin double bond. [33, 45, 46]



Figure 7 Catalyst activation with cocatalyst [33]



### Initiation

After the catalyst is activated by reaction with the cocatalyst, the initial mechanism of polymerization begins with the insertion of the first monomer (ethylene) between the transition metal and alkyl group bond. The mechanism showed in bellow.

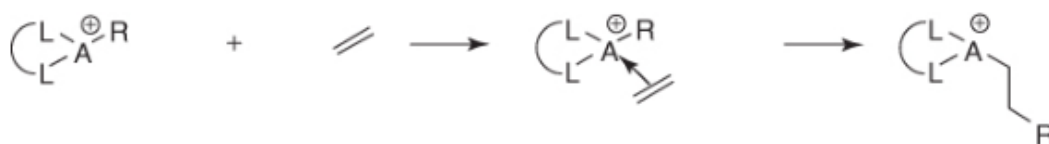


Figure 8 Chain initiation [33]

### Propagation

The insertion of monomers in cationic sites is defined as the propagation step of the polymerization mechanism. The polymer chain is connected by free radicals as shown in Figure 9

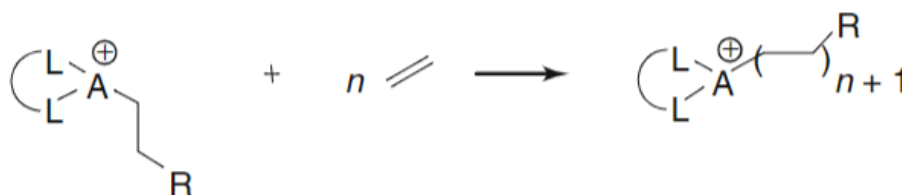


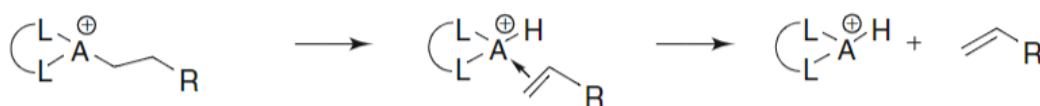
Figure 9 Monomer propagation [33]

### Termination

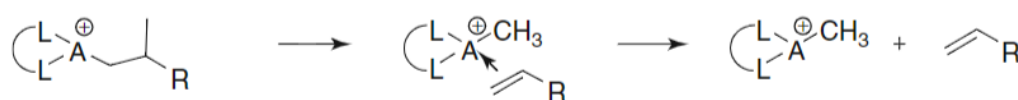
Chain termination reactions on olefin polymerization with metallocene catalyst occur through several reactions such as chain transfer by  $\beta$ -hydride elimination, chain transfer by  $\beta$ -alkyl elimination, chain transfer to monomer, chain transfer to cocatalyst, and chain transfer to hydrogen Figure 10 shows this reaction.

All termination reactions produce a dead chain and a living chain. For ethylene polymerization, a vinyl-terminated chain is formed after  $\beta$ -hydride elimination. However,  $\beta$ -alkyl elimination is possible but far less common than  $\beta$ -hydride elimination. While chain transfer to monomer and cocatalyst are also usually observed during olefin polymerization, And hydrogen is the most often used chain transfer agent. Metallocene and other late transition metal catalysts are very sensitive to hydrogen, but Ziegler-Natta catalysts require a much higher hydrogen concentration to terminate the reaction.

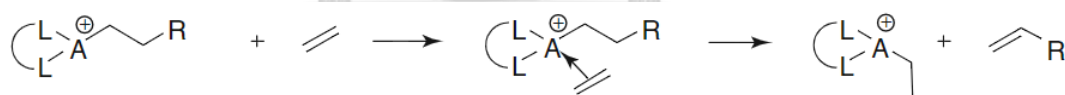
a).  $\beta$ -hydride elimination



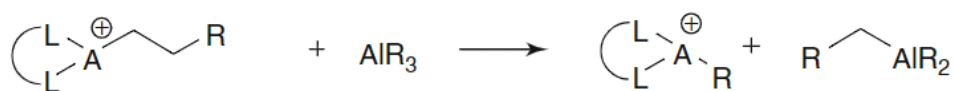
b).  $\beta$ -alkyl elimination



c). Chain transfer to monomer



d). Chain transfer to cocatalyst



e). Chain transfer to hydrogen

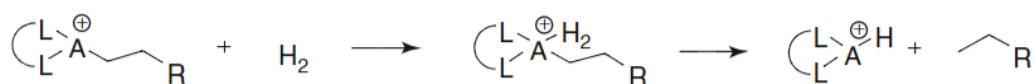


Figure 10 Chain transfer reaction [33]

## 2.5 Supported metallocene catalysts.

Non-supported (homogeneous) metallocene systems can make high-activity olefin polymers with a narrow distribution of molecular weight (MWD) and a narrow distribution of chemical composition (CCD). However, the produced polymer was composed of fine particles (low bulk density) that resulted in the polymer sticking to the walls and equipment of the reactor, commonly referred to as "reactor fouling." So, the metallocene catalyst needs support to help with this problem. Moreover, supported metallocene catalysts have several advantages and disadvantages [5, 6, 47]. Following that is below.

(1) During a polymerization procedure, the activity of some homogeneous metallocene catalysts is significantly reduced. The supported system needs additional stability.

(2) For the high activity, a lot of methylaluminoxane (MAO) is needed as a cocatalyst. For the supported catalysts to be economically viable, this amount must be significantly lowered.

(3) At high polymerization temperatures ( $T_p$ ), most metallocene catalysts in solution generate polyolefins with very low molecular weight (MW) and high  $T_p$ , the supported catalyst should yield greater MW polymers.

(4) Polyolefins produced by homogenous methods have very small particle sizes, a wide size distribution, and a low bulk density. The polymer morphology must be controlled by supporting catalysts.

(5) In solution, metallocene catalysts produce polymers with a narrow MW distribution (MWD) and, as a result, a poor processability-physicmechanical property balance. The supported systems should be able to generate polymers with the broad or bimodal MWD necessary for good rheological and physical properties.

(6) Some supported metallocene catalysts have been found to foul gas-phase reactors. Corrective actions must be taken.

(7) Metallocene catalysts' steric regulation is determined by molecular structure. It would be advantageous if the support could control or even control this.

The most commonly used supports are silica ( $\text{SiO}_2$ ), magnesium chloride ( $\text{MgCl}_2$ ), alumina ( $\text{Al}_2\text{O}_3$ ), magnesium fluoride ( $\text{MgF}_2$ ), calcium fluoride ( $\text{CaF}_2$ ) and zeolite, which have also been used to support metallocene catalysts.

Metallocene catalysts are utilized in homogenous form in only a few polymerization processes. Supported metallocene catalysts are used for the industrial-scale synthesis of polyethylene or isotactic polypropylene. Metallocene must be applied to support existing technical processes (drop-in technology) [34, 42]. Several methods are shown in Figure 11

(A) Immobilized cocatalyst/support: Add MAO cocatalyst on the support first, followed by addition of the metallocene in the polymerization reactor that method is mostly used.

(B) Immobilized cocatalyst/catalyst/support: immobilization of the mixture of metallocene and MAO is adsorbed on the support.

(C) Immobilized catalyst/support: Add the metallocene on the support, followed by addition with MAO in the polymerization reactor.

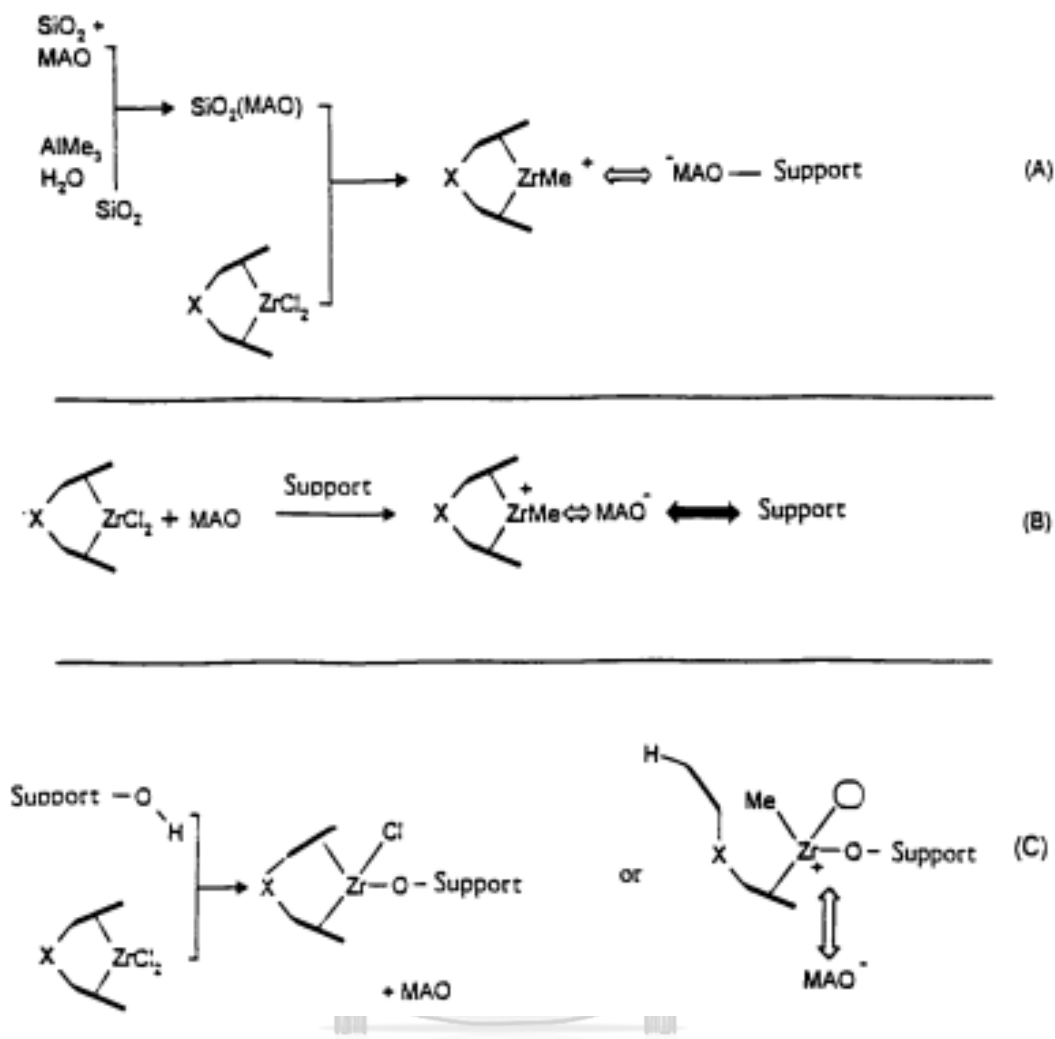


Figure 11 Methods for supporting metallocene [34]

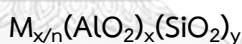
CHULALONGKORN UNIVERSITY

Method C increases the number of active centers in solution by activating the metallocene, shortens the preparation time, and reduces the amount of solvent required for support [48]. But, it is recommended that the catalyst be first added to the support and then zirconocene be introduced into the solution for high catalyst activity [49]. Although Method C is not recommended, it has several advantages. In this research, study sequences of immobilization MAO and metallocene catalysts to develop this method.

## 2.6. Zeolite

Zeolites are microporous crystalline hydrated aluminosilicate minerals with unique structures and properties. Zeolites are widely used in many industrial applications, including catalysis, ion exchange, gas separation, and adsorption. The discovery of zeolites by Cronstedt, a Swedish mineralogist in 1756 was a significant milestone in the history of mineralogy. Since then, many different types of zeolites have been found. Currently, 39 naturally occurring zeolite species have been identified and their structures have been characterized. Nevertheless, more than 100 synthetic species with no known natural analogues have been identified as new zeolites, with the majority still waiting final structural identification [50].

Zeolites contain three-dimensional structures composed of  $TO_4$  tetrahedra ( $SiO_4$  or  $AlO_4$ ) linked by their oxygen atoms to create subunits and, finally, huge lattices composed of duplicate building blocks (unit cells). The structural formula of zeolites (i.e., the chemical composition of the unit cells) is the following:



where  $n$  is the valence of cation  $M$ ,  $x + y$  the total number of tetrahedra per unit cell and  $y/x$  the atomic Si/Al ratio varying from a minimal value of 1 (Lowenstein rule) to infinite [51].

While adsorption and catalytic processes require the diffusion of molecules in zeolite pores that are defined by the size of the ring that forms the pore, denoted as an  $n$ -ring, where  $n$  is the number of T-atoms in the ring. A minimum of 8 tetrahedral (8T) atoms or 8 Membered rings (8MRs) openings are commonly considered to help with this diffusion. Many structural properties (cages, channels, chains, and sheets) are common by a variety of zeolite framework types; therefore, terms such as  $\alpha$ -cavity and  $\beta$ -cage, pentasil unit, crankshaft and double crankshaft chain, and 482

sheet or net have entered general usage [51, 52]. Some of these subunits are shown in Figure 12.

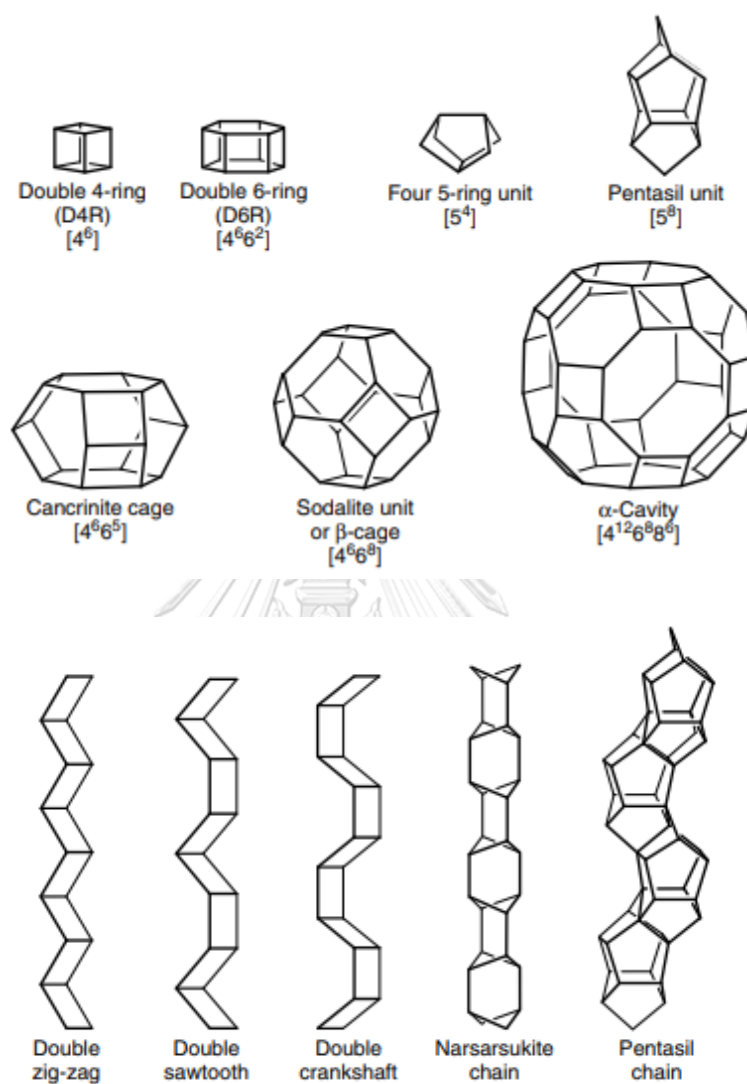


**Figure 12** Some subunits, cages/cavities and chains in several framework types [52]

Zeolite structures are designated by a three-letter code according to rules set by the Commission of the International Zeolite Association (IZA) [53]. The codes are normally derived from the name of the zeolite or “type material,” For instance, **FAU** from the mineral **faujasite** which the well-known X and Y zeolites, **LTA** from **Linde Type A** that is zeolite A, **MFI** from ZSM-5 (**Z**eolite **S**ocony **M**obil - **f**ive) and beta-zeolite (**B**eta polymorph **A** - **BEA**) [51, 52].

Zeolites are classified into different categories such as Crystal structure, Si/Al ratio, and pore size of zeolites. Some common classifications [54, 55]:

**Framework Type:** Zeolites are classified based on their crystal structure, which is determined by the arrangement of their tetrahedral framework. Some examples of zeolite frameworks include the FAU (Faujasite) and MFI (ZSM-5) frameworks shown in Figure 14..

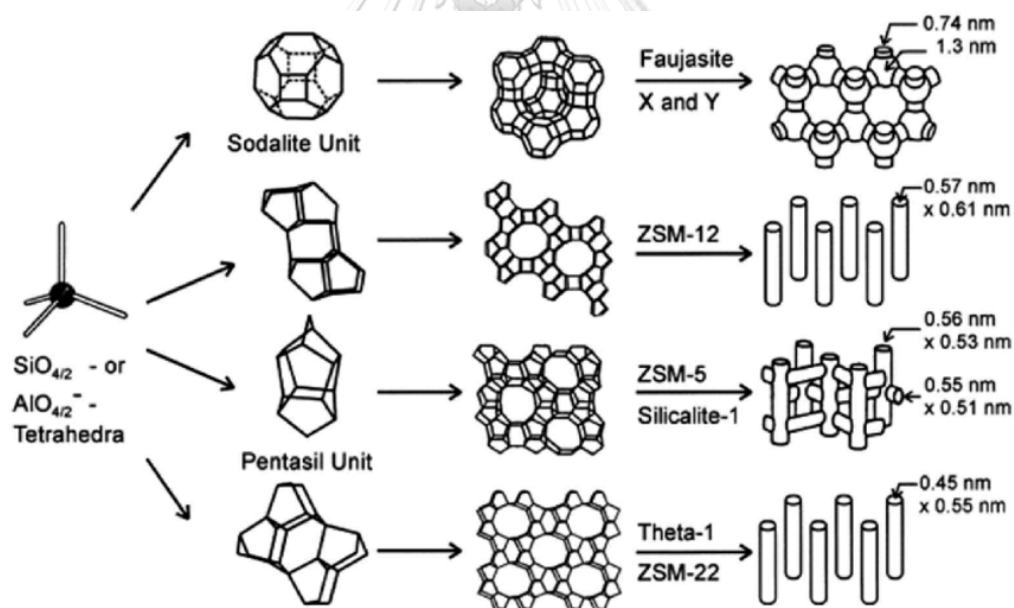


**Figure 13** Examples of zeolite framework and their micropore systems and dimensions [56]



**Si/Al Ratio:** Zeolites can have different ratios of silicon to aluminum (Si/Al) in their framework. This ratio affects the zeolite's acidity, catalytic activity, and selectivity. Zeolites with a low Si/Al ratio are more acidic, while those with a high Si/Al ratio are less acidic. The Si/Al ratio of several zeolites shown in Table 4.

**Table 4** Example of Si/Al ratio of zeolites [54]

	<b>Zeolite</b>	<b>Si/Al mole ratio</b>
<b>Low silica zeolites</b> Si/Al ratio = 1-2	zeolite A	1 – 1.7
	zeolite X	1 -1.5
<b>Medium silica zeolites</b> Si/Al ratio = 3-10	zeolite Y	1 - 5.6
	ZSM-20	3.5 -5
<b>High silica zeolites</b> Si/Al ratio = > 10	ZSM-5	10 - ∞
	Beta-zeolite	12 - ∞

**Pore Size:** Zeolites can also be classified based on the size of their pores. The pore size determines which molecules can be adsorbed or diffused through the zeolite. Some examples of zeolites based on their pore size shown in Table 8.

**Table 5** Classification of zeolites by pore size. [51]

<b>Small pore zeolites</b>	<b>Middle pore zeolites</b>	<b>Large pore zeolites</b>
8 Membered rings (3.0-4.5 Å)	10 Membered rings (4.5-6.0 Å)	12 Membered rings (6.0-8.0 Å)
Zeolite A	Zeolite ZSM-5	Zeolite Beta
Erionite	ZSM-11	Zeolite L
Chabazite	Ferriete	Faujasite (X, Y)
Gismonite	Stibite	Mordenite
Phillipsite	ZSM-23	ZSM-12

However, zeolite-like materials with ultra large pores such as Cloverite (20 T, 0.6 x 1.32 nm), VPI-5 (18 T, 1.27 nm), AIPO4-8 (14 T, 0.79 x 0.87 nm) were recently synthesized.

### Zeolite A (LTA – $[\text{Na}_{12}(\text{H}_2\text{O})_{27}]_8 [\text{Al}_{12}\text{Si}_{12}\text{O}_{48}]_8$ )

The LTA framework type (Figure 14) is a primitive cubic arrangement in which double 4-rings are linked by oxygen bridges as linked to connecting to a single 4-ring. This results in a 3-dimensional, 8-ring channel system and  $\alpha$ -cavity in the center of the unit cell. Zeolite A is used in laundry detergents as an ion exchanger (water softener) and as a desiccant in the laboratory and between the panes of glass in double-glazed windows [52].

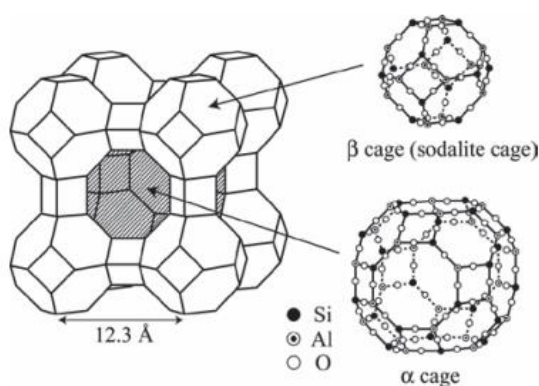


**Figure 14** LTA framework type [54]

Normally, LTA zeolite had various molecular sieves, each with specific properties and applications. Some common types of LTA zeolite molecular sieves include: 3A, 4A or 5A that 4A has a pore size of approximately 4 angstroms ( $\text{\AA}$ ). The commercial zeolites had specific BET data shown in xx. However, depending on the specific manufacturer and grade of LTA zeolite.

**Table 6** BET data of commercial zeolite A [57]

Samples	Specific Surface Area <sup>a</sup> ( $\text{m}^2/\text{g}$ )	Pore volume <sup>b</sup> ( $\text{cm}^3/\text{g}$ )	Pore size <sup>c</sup> (nm)
Commercial zeolite A	559.13	0.2462	58.14

<sup>a</sup>BET method, <sup>b,c</sup>BJH method

### Beta Zeolite (\*BEA – $[\text{Na}_7] [\text{Al}_7\text{Si}_{57}\text{O}_{128}]$ )

Zeolite beta (Figure 15) has well-defined layers that are layered in a more or less random pattern. Layers of saddle-shaped 12-rings are formed by connecting the units with 4-rings. Adjacent layers are connected by a 90-degree rotation. BEA zeolite is a commonly used zeolite due to its high thermal stability, excellent accessibility of acid sites, and high acidity, making it a versatile catalyst and sorbent in various industrial processes. These processes include alkylation and hydroalkylation of aromatics, alkanes alkylation, transalkylation of alkylaromatics, Friedel-Crafts acylation, catalytic cracking, and depollution/decontamination processes such as SCR of NOx and VOC adsorption [52, 58].

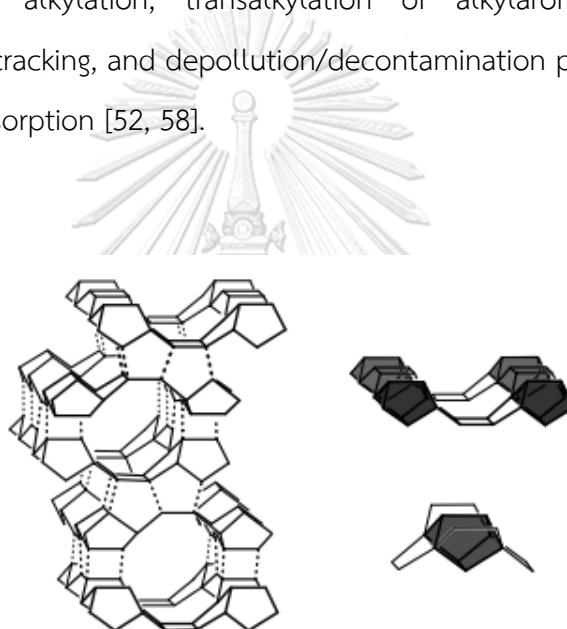


Figure 15 BEA framework type [52]

### ZSM-5 (MFI – $[\text{Na}_x(\text{H}_2\text{O})_{16}] [\text{Al}_x\text{Si}_{96-x}\text{O}_{192}]$ , $x < 27$ )

The high-silica zeolite ZSM-5 framework type (Figure 16) is linked to form pentasil chains, and mirror images of these chains are linked through oxygen bridges to form corrugated sheets with 10-ring holes. The 3-dimensional structure is formed by connecting each sheet with oxygen bridges. An inversion center connects adjacent sheets to one another. Straight 10-ring channels parallel to the corrugations (along y) and sinusoidal 10-ring channels perpendicular to the sheets are produced (along x).

The latter channels connect the straight channels to produce a three-dimensional ten-ring channel structure. Several applications for ZSM-5 have been discovered in refinery and petrochemical operations [52].

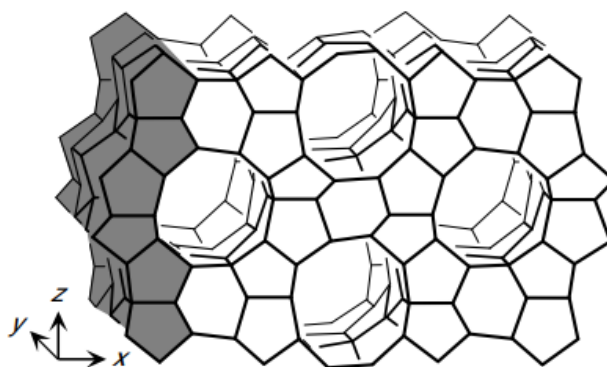


Figure 16 MFI framework type [52]

In this study, we investigate the differences between the four different support materials for a metallocene catalyst. Table 7. showed general properties of each support.

Table 7 General properties of support in this study

Properties	Silica	Zeolite A	ZSM-5	Beta zeolite
	50-150	3.0-4.5	4.5-6.0	6.0-8.0
Pore Size	Mesoporous		Microporous	
Dimensions (Å)	Materials (pore size 2 to 50 nm)		Materials (pore size up to 2 nm)	
Si/Al mole ratio	-	1 – 1.7	10 - ∞	12 - ∞
Acidity	-	High	Medium- Low	Medium- Low

Currently, zeolites can be found occurring naturally or can be created artificially in a laboratory setting. The two main categories of zeolites are natural, including clinoptilolite, mordenite, and garronite, and synthetic, such as zeolite A, P, X, and Y, which are classified based on their silica-alumina ratio. The natural zeolites are more resistant and thermally stable in various environments, with their resistance and stability increasing with a higher silica-alumina ratio and the presence of alkali cations in the zeolite framework. On the other hand, synthetic zeolites are produced with high purity and uniform particle sizes through the synthesis of raw materials like fly ash, rice husk ash, blast furnace slag, municipal solid waste, paper sludge, lithium slag, and kaolin with different synthesis methods [59], as shown in Table 5. Zeolite A can be synthesized from Waste & glass materials, Windshield waste, K-feldspar, Paper sludge, BFS and etc. But, In this research, the zeolite A was used as support for metallocene catalyst by fly ash from the Mae Moh power plant.

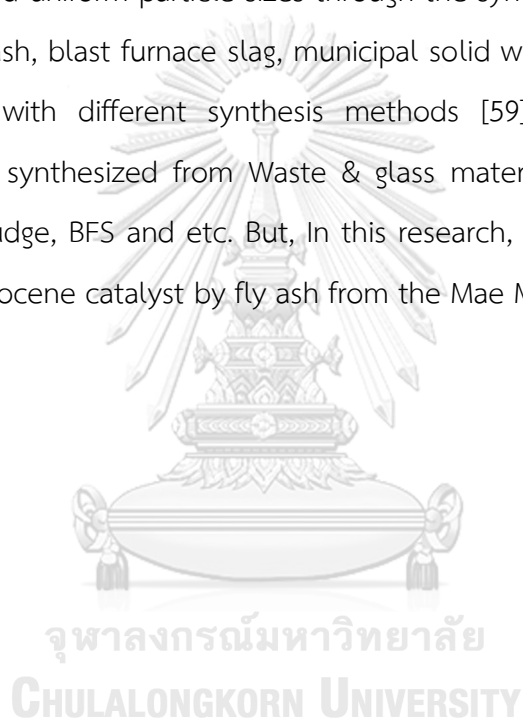


**Table 8** The different zeolite synthesis strategies from various raw materials. [59]

Synthesis method	Raw materials	Type of zeolite	Advantages	Limitations
Hydrothermal method	BFS	Zeolite NaA	High reactivity, minimal energy and pollution use, and superb crystal quality	Corrosive slurries and an expensive autoclave
	Rice husk ash	ZSM-5, Zeolite T		
	Waste & glass materials	Zeolite A		
	Paper sludge	Zeolite NaP		
	Kaolin/metakaolin	Zeolite P, X, ZSM-5		
	Coal fly ash	Zeolite K		
	Lithium slag	Zeolite NaX		
	Windshield waste	Zeolite A		
	Halloysite mineral	Zeolite NaA		
	K-feldspar	Zeolite A		
	Alkali fusion method	BFS		
Waste stone cake		Zeolite X		
Kaolin/ metakaolin		Zeolite Y, Faujasite Zeolite		
Coal fly ash		Zeolite NaX		
Porcelain wastes		Zeolite 13X		
Waste of iron mine tailings		Zeolite A		
SiO <sub>2</sub> sinter and perlite		Zeolite Y, P		
Alkaline hydrothermal method	Paper sludge, BFS	Zeolite A	-	-

Synthesis method	Raw materials	Type of zeolite	Advantages	Limitations
Alkali-leaching method	Rice husk ash	Sodalite Zeolite	Allows impure raw ingredients and produces effective products.	Complicated, pricey, and time-consuming
	Fly ash	A-X zeolite		
Sol-gel method	Rice husk ash	Zeolite NaY	A flexible solution with low energy usage and no requirement for specialized equipment.	Cost of materials, problems in avoiding OH groups and residual porosity, precipitation of a specific oxide during sol-formation
	Alumina disk	ZSM-5		
	Silatrane	MFI zeolite		
	TEOS as precursor	MCM-22		
Microwave synthesis	Coal fly ash	NaP1, Na-A zeolite	Higher temperature, selective heating, and a quicker reaction	Controlling heat forces and water evaporation is challenging.
Iono-thermal synthesis	Metakaolin	NaY zeolite	Large crystal production with accurate crystal composition	Prolonged operation and the manufacturing of hazardous substances.
Solvothermal method	Metakaolin and rice husk ash	Faujasite and P1 zeolite	Easy control over the crystalline product's size, shape distribution, and size	Organic solvent and a costly autoclave are required.
Ultrasound energy method	Sodium aluminosilicate solutions	Zeolite A	Simple, rapid reaction, no complex facilities, high crystal growth rate, homogeneous particle size distribution and morphology, and nucleation control	
	Coal Fly Ash	Zeolite X		
	Metakaolin	LTA, ZSM-5 Zeolite		

## 2.7 Literature reviews

Kaminsky (1994) provided a summary of various metallocene-aluminoxane catalysts used in ethylene polymerization. When the polymerization temperature exceeds 50°C, the zirconium catalyst is more active than the hafnium or titanium systems. Additionally, the titanium complex breaks down at these temperatures. Among the cocatalysts, methylalumoxane (MAO) is significantly more effective than ethylaluminoxane (EAO) or isobutylalumoxane (IBAO) [60]. Therefore, we are interested in utilizing the zirconocene/MAO catalyst system for ethylene polymerization.

Kleinschmidt et al. (1999) investigated the influence of different aluminum alkyls on the polymerization process using stereorigid group 4 ansa-metallocenes as Ziegler-catalysts. triisobutylaluminum (TIBA), triethylaluminum (TMA), triethylaluminum (TEA), tributylaluminum (TBA) are used on scavenger for zirconocene/MAO catalytic for the polymerization process, found that the polymerization activity decreased with increasing size of the substituent (TMA>TEA>TIBA≈TBA) [61].

And Michiels W. and Muñoz-Escalona A. (1995) investigated how combining different cocatalysts, namely  $\text{AlR}_3$  (where R=Me (TMA), Et (TEA), and iBu (TIBA)) and  $\text{B}(\text{C}_6\text{F}_5)_3$  with MAO at varying molar ratios, affected the activities of ethylene polymerization using the  $\text{Cp}_2\text{ZrCl}_2$  catalyst. Results indicated that activities increase at low TMA concentrations with increasing TMA/MAO ratios, peaking at a TMA/MAO ratio of 0.3-0.5, but decrease at higher TMA/MAO ratios. The addition of TEA or TIBA to MAO led to decreased polymerization activities, with the effect being stronger for TEA. The molecular weights of the polyethylene followed the same trend, decreasing with increasing  $\text{AlR}_3$ /MAO ratios [62]. Therefore, we are interested TMA in zirconocene/MAO catalyst system in ethylene polymerization for increase catalyst activity.



Jongsomjit et al. (2006) examined the synthesis of linear low-density polyethylene (LLDPE)/ZrO<sub>2</sub> nanocomposites through in-situ polymerization with a rac-Et(Ind)<sub>2</sub>ZrCl<sub>2</sub>/MAO catalyst. The nano-ZrO<sub>2</sub> filler was evenly distributed and dispersed throughout the polymer matrix. However, the addition of the nano-ZrO<sub>2</sub> filler led to a slight decrease in the melting temperature ( $T_m$ ) and crystallization temperature ( $T_c$ ) due to reduced polymer crystallinity [63].

Additionally, Silveira F. et al. (2010) investigated the effect of different microporous and mesoporous supports on the structure of grafted metallocene species and their performance in ethylene polymerization. All of the supports (MCM-22, ITQ-2, SBA-15, MAO-modified silica, alumina, silica-zirconia and chrysotile). The highest activity in ethylene polymerization was achieved with the supported catalyst using commercial MAO-modified silica.[10].

The study of copolymerization between  $\alpha$ -olefins/ethylene is a fundamental area of research in the field of polymer chemistry. Adding comonomer opens up opportunities for diverse applications of polyethylene. Dong-Ho, Lee, et al. (2000) [64] investigated the copolymerization of ethylene and metallocene using various metallocene catalysts with modified methylaluminoxane cocatalyst. The results showed that the catalyst activity and thermal properties of the polymer depended on both the catalyst structure and the alpha-olefin structure. The addition of 1-hexene as a third monomer exhibited the maximum enhancement in catalyst activity. 1-hexene is suitable for comonomer in zirconocene/MAO catalyst system in ethylene polymerization.

Nowadays, metal-organic frameworks was used for metallocene support. Manianglung C. (2023) used metal-organic frameworks (MOFs) as a support for a metallocene catalyst in ethylene-1-hexene copolymerization, which resulted in

shape-selective polymerization. The resulting polyethylene showed negligible insertion of 1-hexene into the PE chain. The study also found that the loading of the metallocene inside the MOF cages was higher for MOFs with larger window sizes. Additionally, the molecular weight of the resulting polyethylene was greater for MOFs with channel structures compared to those with cage structures. However, the polymerization activity of MOF-supported  $(n\text{-BuCp})_2\text{ZrCl}_2$  was lower than that of the conventional silica-supported one [65]. Therefore, silica is one of inorganic support for metallocene catalyst and provide high catalyst activity. However, other inorganic materials utilized to support metallocene catalysts are zirconia, titania, alumina, and chrysotile. But zeolite was not commonly found to be applied in support metallocene catalysts.

Michelotti M. et al. (2000) investigated the performance of various metallocene complexes of transition metals supported on HY zeolites in the polymerization of ethylene and propylene. The results show that the catalytic activity of the supported catalysts decreased compared to their activity in solution. However, the supported catalysts showed better stability with time and higher molecular weight of the resulting polymers [15].

Moreover, Marques M. d. F. V. and Moreira S. C. (2003) investigated the use of H-ZSM-5 zeolite as a support for impregnating the  $\text{Cp}_2\text{ZrCl}_2$  catalyst in synthesizing polyethylene. The researchers varied the catalyst preparation conditions and analyzed the data using statistical methods to determine the best approach. The results demonstrated that a higher concentration of  $\text{Cp}_2\text{ZrCl}_2$  and pretreatment with MAO were the most effective catalyst preparation conditions. Furthermore, the study discovered that a longer pre-contact time of the supported catalyst with MAO significantly increased the yield of polymerization [16]. Therefore, zeolite was used in metallocene catalysts for a decade because it can improve the stability and molecular weight of polymers. There are many types of zeolites studied, including

those with middle pores (H-ZSM-5) and large pores (HY zeolites). The small pore size of zeolite is not found to be applied in support of metallocene catalysts, which are used in other industries, We are interested in studying the small pores of zeolite for ethylene polymerization that zeolite A is interesting.

Rozhkovskaya A. et al. (2021) succeeded for converting alum sludge into high-quality zeolite LTA using alkali fusion pre-treatment and hydrothermal synthesis. This method improved the quantity and quality of the resulting zeolite LTA, and the preferred synthesis conditions using fusion pre-treatment were identified. The resulting zeolite LTA contained impurities such as iron, calcium, and magnesium, but kinetic studies showed that the exchange of calcium ions with all zeolite samples reached equilibrium within 60 minutes. Equilibrium ion exchange data also revealed that the maximum loading of calcium ions was highest for fusion pre-treated LTA [22].

Al-dahri T. et al. (2022), are interested to learn that Linde-type A zeolite (LTA) can be prepared from coal fly ash (CFA), a byproduct of coal combustion, to produce a valuable material that can address environmental pollution and used as an effective adsorbent for the removal of acidic dyes such as Acid red 66 (AR66) from aqueous solutions. The study's results demonstrate that the synthesized LTA has a high adsorption capacity for AR66 and can effectively remove it from the solution [66]. According to the papers, zeolite A can be synthesized from waste, a by-product in other industries such as water treatment and power plants. Utilization of zeolite A is a sustainable and cost-effective method. Currently, zeolite A is less commonly used to support polyolefin catalysts than other zeolites that are interesting for supporting metallocene catalysts.

## CHAPTER 3

### EXPERIMENTAL

In this research, the research methodology, including all chemicals, the preparation of the catalyst, the experiment of ethylene polymerization and the characterization are explained in this chapter.

#### 3.1 Materials and Chemicals

All chemicals in the supported metallocene catalyst system and the ethylene polymerization process were prepared under an inert atmosphere. Further, oxygen and moisture are controlled by Schlenk lines, including vacuum lines and nitrogen gas with several stopcocks and a glove box, which are specified in detail as follows Table 9:.

**Table 9** The chemical used in the reaction by metallocene catalyst system.

Chemicals	Supplier	Purification
Bis(cyclopentadienyl) zirconium(IV) dichloride ( $Cp_2ZrCl_2$ )	Aldrich Chemical Company, Inc	Used as received
Methylaluminoxane (MAO)		10%wt in toluene
Trimethylaluminum (TMA)		97%
Zeolite A	Department of Chemistry, Faculty of Science, Ubon Ratchathani University, Thailand	Used as received
Beta-Zeolite	Alfa Aesar by Thermo Fisher Scientific	$SiO_2/Al_2O_3$ ratios = 360
Zeolite Socony Mobil-5 (ZSM-5)	Tosoh Asia Pte. Ltd.	$SiO_2/Al_2O_3$ ratios = 40

Chemicals	Supplier	Purification
1-hexene	Aldrich Chemical Company, Inc	97% Soaked in molecular sieve
Ethylene gas	Linde (Thailand) Public Company Limited	99.99%
Hydrochloric acid	Aldrich Chemical Company, Inc	Fuming 37%
Methanol	S.R. Lab	Used as received
Ultra-high purity argon gas	Thai Industrial Gas Co., Ltd.	99.999%

### 3.2 Equipment

The metallocene catalyst system is extremely sensitive to oxygen and moisture. Then, the special equipment will be required to manage the preparation and polymerization processes, which follow as below.

#### 3.2.1 Schlenk line

The Schlenk line consists of a vacuum and nitrogen gas line with several stopcocks. Schlenk lines are used to control and eliminate moisture and oxygen throughout operations to ensure the safe and successful handling of sensitive chemicals. Typically, the gases and solvent vapors generated during evacuation are captured in a liquid nitrogen cold trap to prevent contamination of the vacuum pump. This operation is performed under a vacuum.

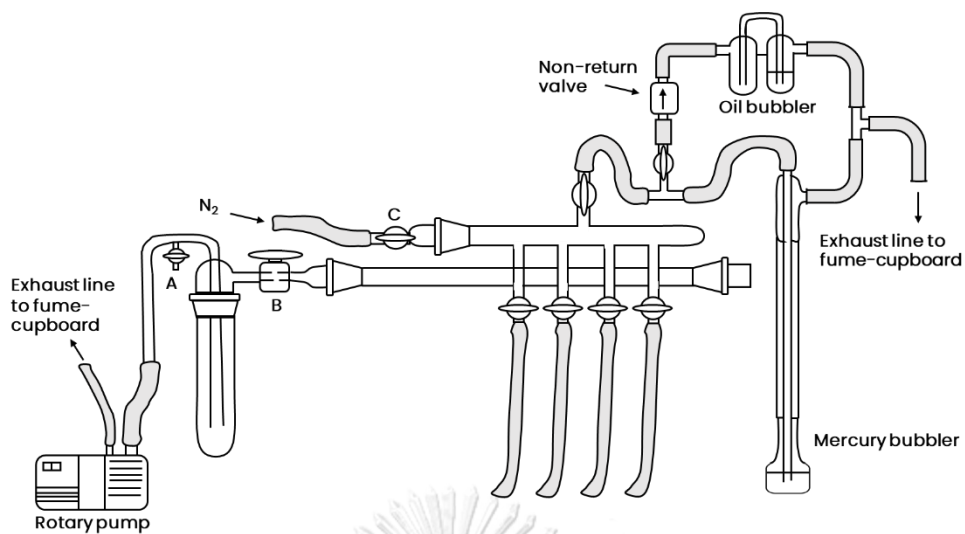


Figure 17 Schlenk line.

### 3.2.2 Schlenk tube

A Schlenk tube is a tube with joints and side arms, with a three-way glass valve. They come in sizes of 50, 100 and 200 ml and are used to store support material and prepare for the immobilization of MAO and metallocene on the support shown in Figure 18.

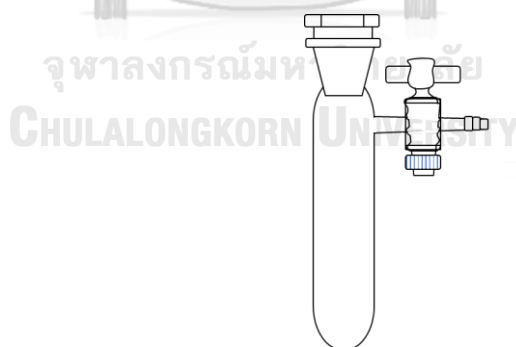


Figure 18 Schlenk tube.

### 3.2.3 Vacuum pump

A model 195 vacuum pump supplied by Labconco Corporation was used to remove oxygen from the system with a pressure of  $10^{-1}$  to  $10^{-3}$  mmHg for the vacuum supply to the vacuum line in the Schlenk line.

### 3.2.4 Glove box

MRBAUN LABstar glove boxes provide an inert environment for handling highly sensitive chemicals to moisture and oxygen. There are two parts to creating an inert atmosphere, a gas cleaning system and a closed gas loop to remove water and oxygen. In addition, moisture and oxygen concentrations in the glove box system were investigated using moisture and oxygen analyzers, including the MB-MO-SE1 and MB-OX-SE1, respectively.

### 3.2.5 Slurry phase polymerization

The reactor is 100 ml stainless steel autoclave with a magnetic stirrer was used in the polymerization process, as shown in Figure 19.

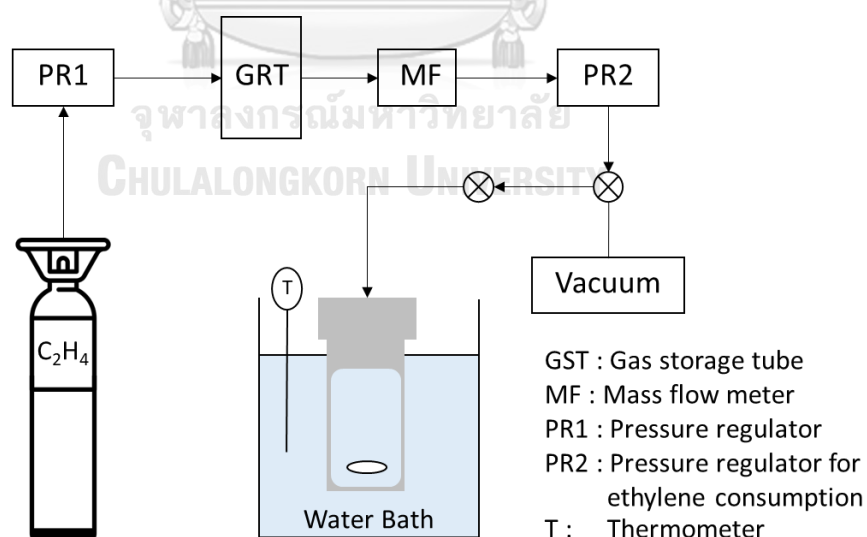


**Figure 19** Diagram of Slurry phase polymerization system

### 3.2.6 Magnetic stirrer and heater

The magnetic stirrer and heater model RTC basis from IKA Labortechnik were used to mix the solution and control the heat of the reaction during ethylene polymerization.

## 3.3 Preparation of support

### 3.3.1 Preparing Zeolite A

Dispersed 5.3 g of silica powder extracted from fly ash in a solution between 10.1 g of NaOH and 71.7 g of water at 100 °C for 45 min. Then, the aluminate solution was prepared by dissolving 5.3 g of sodium aluminate and 0.3 g of NaOH in 76.6 g of distilled water. The aluminate solution was slowly added to the silicate solution while stirring. After that, it was stirred for a further 10 minutes and heated at 90° C in the oven for crystallization. The obtained solid product was filtered and purified to pH 7 with distilled water, then dried at 90 °C overnight.

### 3.3.2 Calcination

All the zeolite support was calcined at 400 °C with a heating rate of 5 °C/min for 4 hours under a nitrogen atmosphere. After that, it was cooled down to room temperature, placed under vacuum for 2 hours, and stored in a bottle under an inert atmosphere.

### 3.3.3 Immobilization

In the research, two methods were used for the preparation of supported metallocene catalyst, as shown in Figure 20 - Figure 21.

**Method A.** Immobilized a mixture of metallocene catalyst and cocatalyst (MAO) with the support. This is designated as “S-Mix”.



**Method B.** Immobilized only cocatalyst (MAO) on the support. After that, a metallocene catalyst was consequently added to the MAO-immobilized support. This is denoted as “SMAO/Zr”.

The support to immobilized materials ratio was fixed at 1:10 with the magnetic stirrer at room temperature. Then, the slurry mixture was stirred for 30 minutes, and the supported catalyst was dried under vacuum until the solid powders of the metallocene-supported catalyst were formed.

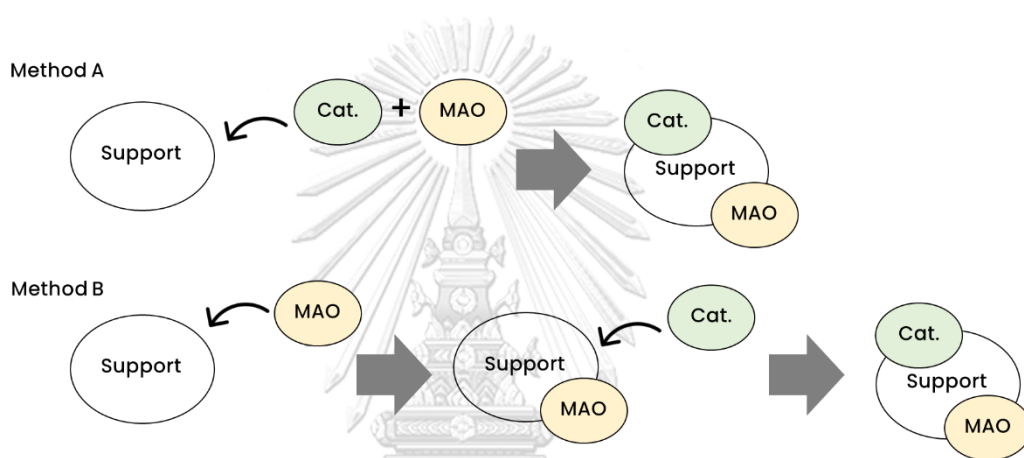


**Figure 20** Methods of immobilization for metallocene/MAO catalyst with support

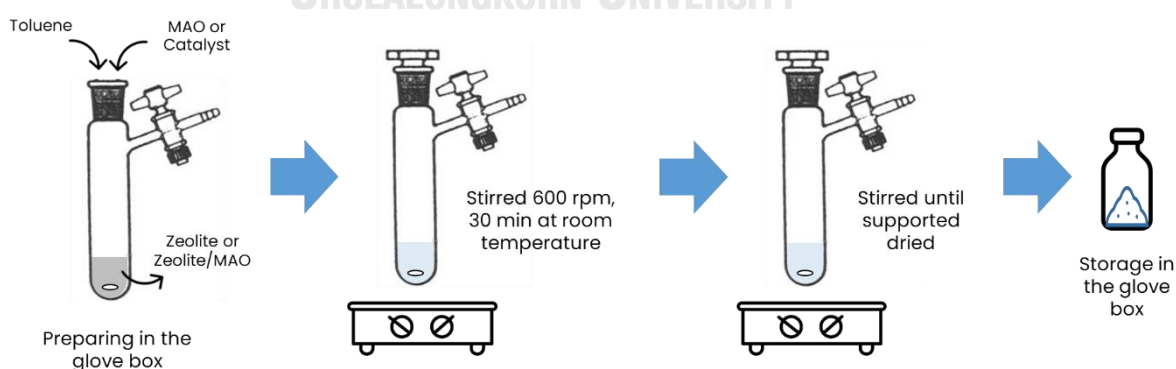


**Figure 21** Immobilization MAO and metallocene on zeolite supports.

### 3.4 Ethylene polymerization

The homopolymerization of ethylene was carried out in a 100 ml semi-batch stainless steel autoclave reactor with a magnetic stirrer (Figure 22). Catalyst, cocatalyst and scavenger were added in the reactor under an inert atmosphere. The system was conducted with fixed molar ratio between metallocene catalyst and MAO at 2,000 ( $[Al]_{MAO}/[Zr]_{Cat}=2,000$ ). First, 1.5 ml of catalyst solution ( $5 \times 10^{-5}$  M of Bis(cyclopentadienyl)zirconium(IV) dichloride) and 2 ml of MAO were added into reactor. Toluene as a solvent was added to make a total volume of 30 ml. The reactor is immersed in liquid nitrogen to stop the reaction to prevent the pre-contact effect in polymerization before being evacuated and purged with nitrogen for 8 min. Finally, The polymerization system heated up to  $70^{\circ}C$ . Ethylene gas was fed into the system under 3.5 bar and operated polymerization time for 15 min. Then, polymerization was terminated by acidic methanol (HCl excess in methanol). The particles of polyethylene were filtered and dried at room temperature.

In added scavenger case, The molar ratio between the metallocene catalyst and scavenger at 1,000 ( $[Al]_{TMA}/[Zr]_{Cat}=1,000$ ). First, added catalyst solution, MAO at the same condition and added TMA. Toluene was added to make a total volume of 30 ml.

For a metallocene-supported catalytic system, catalysts, cocatalysts, and scavengers with various molar ratios of  $[Al]MAO/[Zr]_{cat}$  and  $[Al]TMA/[Zr]_{cat}$  were added in the reactor under an inert atmosphere. In the addition, metallocene-supported catalytic systems instead were added into the reactor, followed by solvent, cocatalyst, and scavenger, which controlled the total molar ratio of  $[Al]MAO/[Zr]_{cat}$  at a determined ratio.

For ethylene/1-hexene copolymerization, after immersing the reactor in liquid nitrogen to stop the reaction, it was evacuated and purged with nitrogen for

8 minutes. Then, 5 ml of 1-hexene was injected into the reactor, followed by the same step.

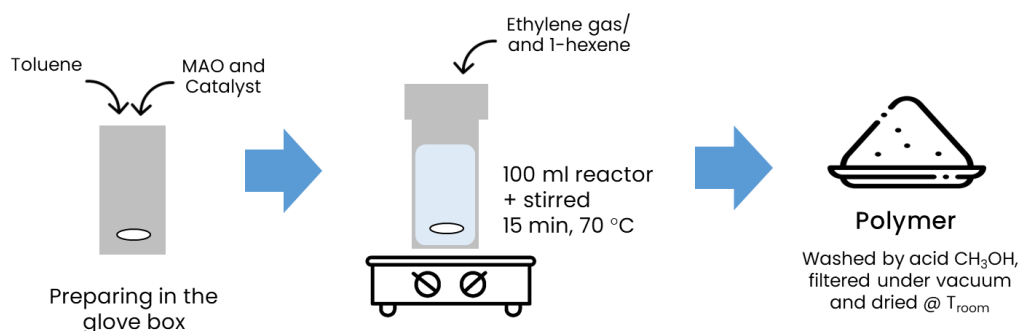


Figure 22 Slurry phase polymerization system

### 3.5 Characterization of supports catalysts, catalysts and polymer.

#### 3.5.1 Scanning Electron Microscopy-Energy Dispersive X-Ray (SEM-EDX)

The investigation of the morphology of support, supports after immobilization and polymer using a JEOL mode JSM-6400 model of SEM. The elemental distributions of Al and Zr were observed by EDX using Link Isis series 300 program to confirm the modification of support after immobilization by MAO and zirconocene catalyst. The samples were coated with gold particles by ion sputtering to provide electrical contact with the specimen.

#### 3.5.2 X-ray Diffractometer (XRD)

X-ray diffraction was used to determine the bulk crystalline phase and crystal structure of the support material, the supports after immobilization and polymer. The diffractometry was performed using a Siemens D-5000 X-ray diffractometer with  $\text{CuK}\alpha$  radiation ( $\lambda = 1.54439 \times 10^{-10}$  m) with Ni filter. The spectrum was scanned in the  $2\theta$  range of 5 to 80 degrees at scan rate of 2.4 degree/min. The sample was put into the center of holder and closed under an argon atmosphere.

### 3.5.3 Thermogravimetric Analysis and Differential Scanning Calorimetry (TGA-DSC)

TGA-DSC was used to analyze the melting temperature ( $T_m$ ) of the support after immobilization and polymers by using the TA Disobedient SDT Q600 analyzer and crystallinity ( $\chi_c$ ) of polymers taking after by DSC 204 F1 phoenix. The investigations were operated at a heating rate of 10 °C/min within the temperature range of room temperature to 600°C.

### 3.5.4 Fourier transform Infrared (FT-IR)

The molecular structure or functional group of support materials and supports after immobilization was determined using FTIR. The samples were cast as a thin layer under inert gas on NaCl plates to provide protection from oxygen and moisture. The Nicolet 6700 FTIR spectrometer was used to examine the tested samples in ATR mode. The FTIR spectra were in the 400–4000  $\text{cm}^{-1}$  scanning range with 100 scans at a 4  $\text{cm}^{-1}$  resolution.

### 3.5.5 $\text{N}_2$ physisorption

Quantachome Autosorb 1 was used to measure the catalyst support. The instrument used a vacuum volumetric method to measure the pore size diameter, the surface area of porous materials, and the pore volume. The method is based on the replacement of porous material by nitrogen gas adsorption (physisorption)/desorption at 77 K (-196.15 °C).

### 3.5.6 Laser particle size distribution analyzer (PSD)

Particle size distribution and particle size of support were measured using the laser diffraction principle by Mastersizer 3000.

### 3.5.7 Temperature-programmed desorption of ammonia (NH<sub>3</sub>-TPD)

The acid properties of the catalysts were measured by using a Micromeritics Chemisorp 2750 Pulse for temperature-programmed desorption of ammonia (NH<sub>3</sub>- TPD). In the experiment, 0.1 g of sample and quartz wool were inserted into a quartz tube and pre-heated at 200°C at a rate of 10°C per minute. After cooling the sample to 40°C, the sample was saturated with 15% NH<sub>3</sub> for 30 minutes and heated up from 40°C to 800°C with heating rate of 10°C/min. The amount of ammonia in effluent was measured as a function of temperature using a TCD signal.





## CHAPTER 4

### RESULTS AND DISCUSSION

This chapter discusses the results and discussion related to this study. The research is divided into three parts; Part 1 is the preliminary study (4.1), which determines the effect of different immobilized MAO cocatalyst and zirconocene catalyst methods on silica support. In Part 2 (4.2), it is described how to synthesize polyethylene by in situ polymerization using Zeolite A supported MAO/Zr by varying temperature,  $[Al]_{MAO}/[Zr]_{cat}$  molar ratios and  $[Al]_{TMA}/[Zr]_{cat}$  ratios as fixed temperature, and  $[Al]_{MAO}/[Zr]_{cat}$  constants for ethylene polymerization and 1-hexene copolymerization. In the last part (4.3), it was brought the most suitable temperature and  $[Al]_{MAO}/[Zr]_{cat}$  ratios for examining the effect of zeolite types by comparing Zeolite A, Beta-Zeolite, and ZSM-5 for supported metallocene catalysts with ethylene polymerization and 1-hexene copolymerization.

#### 4.1 Effect of different immobilization methods of MAO/zirconocene catalysts on silica support

This topic investigated the effect of different immobilization methods using the silica-supported MAO/Zirconocene catalyst. Silica support and MAO/Zirconocene catalyst were characterized by various characterization techniques, including  $N_2$  physisorption (BET), SEM-EDX, XRD and FT-IR. Detailed explanations are provided in the section as follows.

#### 4.1.1 Characterizations of silica support and MAO/Zirconocene catalyst on silica support

##### 4.1.1.1 N<sub>2</sub> physisorption (BET) and laser particle size distribution analyzer (PSD)

The silica support was analyzed by N<sub>2</sub> -physisorption to determine the surface area, pore volume, and pore size. And then, analyzed by laser particle size distribution analyzer to determine particle size distribution.

**Table 10** The surface area, pore size, pore volume and particle size distribution of silica support

Samples	BET Surface	Pore volume <sup>b</sup>	Pore size <sup>c</sup>	Particle size <sup>d</sup>
	Area <sup>a</sup> (m <sup>2</sup> /g)	(cm <sup>3</sup> /g)	(nm)	(μm)
Silica	298.1	1.249	14.5	36.9

<sup>a</sup>BET method, <sup>b</sup>BJH method, <sup>d</sup>PSD analysis

The results of BET surface area and pore characteristics of silica support are summarized in Table 10 and N<sub>2</sub> adsorption-desorption isotherms are shown in Figure 23. It was found that silica has BET surface area of only 298.1 m<sup>2</sup>/g, the pore volume of 1.249 cm<sup>3</sup>/g, and the average pore size of 14.5 nm.

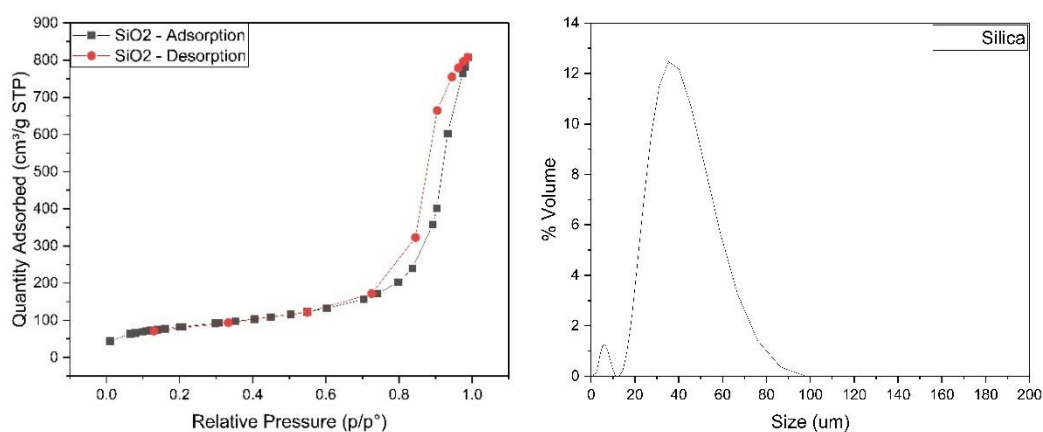


**Figure 23** The N<sub>2</sub> adsorption-desorption isotherms and the average particle size distribution of silica support



According to IUPAC classification, the isotherm of silica represents type IV, with a hysteresis of type H1 [67]. This form of isotherm is common in mesoporous materials and has a uniform size and shape. The PSD curve indicates that the average size of silica particles is approximately  $36.9 \mu\text{m}$ .

#### 4.1.1.2 Scanning Electron Microscopy (SEM) and Energy Dispersive X-ray Spectroscopy (EDX)

The morphology of silica particles and MAO/Zirconocene catalysts with the different immobilized method was analyzed by SEM image as shown in Figure 24. The silica support had spherical shapes and the shape of the support would affect the morphology of the immobilized MAO/Zr catalyst on different methods that have spherical shapes.

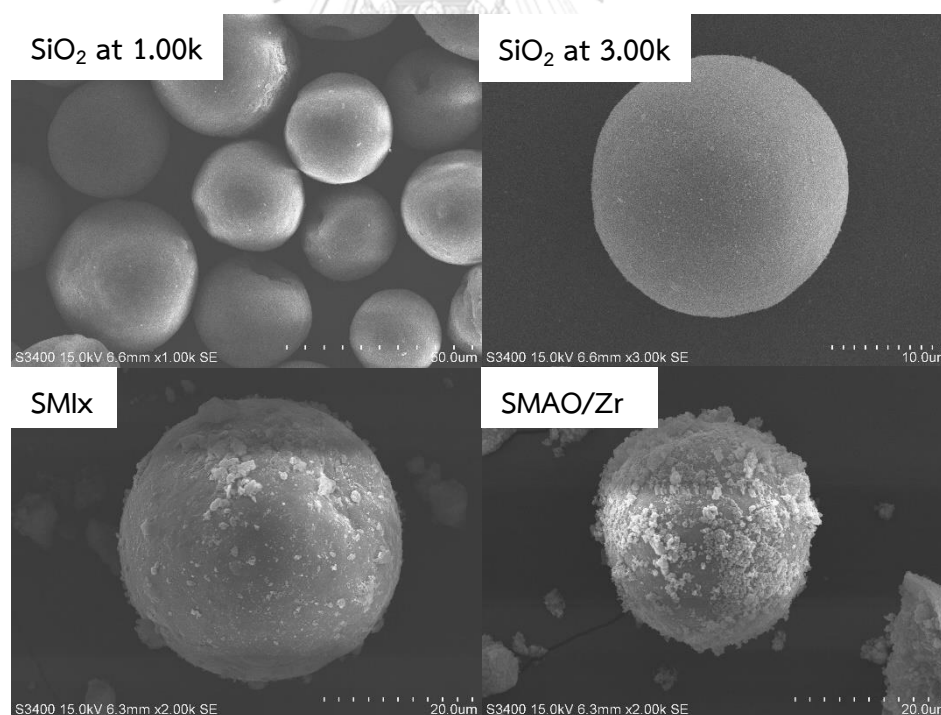


**Figure 24** Morphology of spherical silica and immobilized catalyst with different methods from the SEM image

The SMix refers to the immobilization of the metallocene catalyst and MAO together, while SMAO/Zr refers to the immobilization of the MAO first, followed by the catalyst. It was found that SMAO/Zr had a higher amount of components on the surface of the silica support than SMix as seen by EDX analysis in Table 11 and Figure 25, it revealed that SMAO/Zr had a higher amount of Al and Zr deposition on the silica support than that using SMix. So, the Al and Zr content in both methods were significantly different.

**Table 11** Elemental distribution on the catalyst surface (EDX) with different methods.

Samples	Element content (wt%)				[Al]/[Zr] molar
	O	Al	Si	Zr	ratios
Silica support	47.03	52.97	-	-	-
SMix	44.89	6.93	33.16	15.02	1.56
SMAO/Zr	41.82	11.92	27.65	18.61	2.17

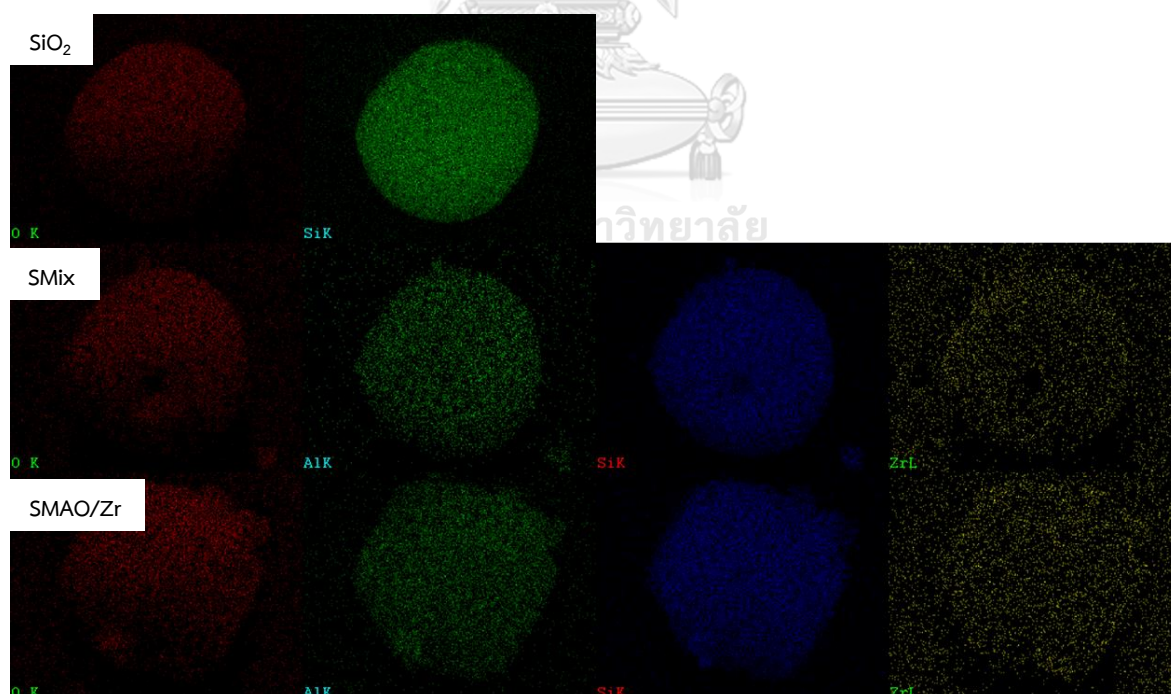


**Figure 25** Elemental distribution on spherical silica and immobilized catalysts with different methods from the SEM image

#### 4.1.1.3 X-ray Diffraction (XRD)

Figure 26 shows the X-ray diffraction (XRD) patterns of silica support and silica-supported MAO/Zirconocene catalysts. The results present similar XRD patterns comprised of a broad peak between approximately  $20^\circ$  and  $30^\circ$ , which corresponds to amorphous silica. The XRD patterns of MAO/Zirconocene catalyst on silica support were nearly identical to those of silica before impregnation. This indicated that the immobilized MAO and metallocene catalyst were well dispersed on silica or had a crystallite size less than 2 nm which XRD could not detect (no sharp peaks were observed).

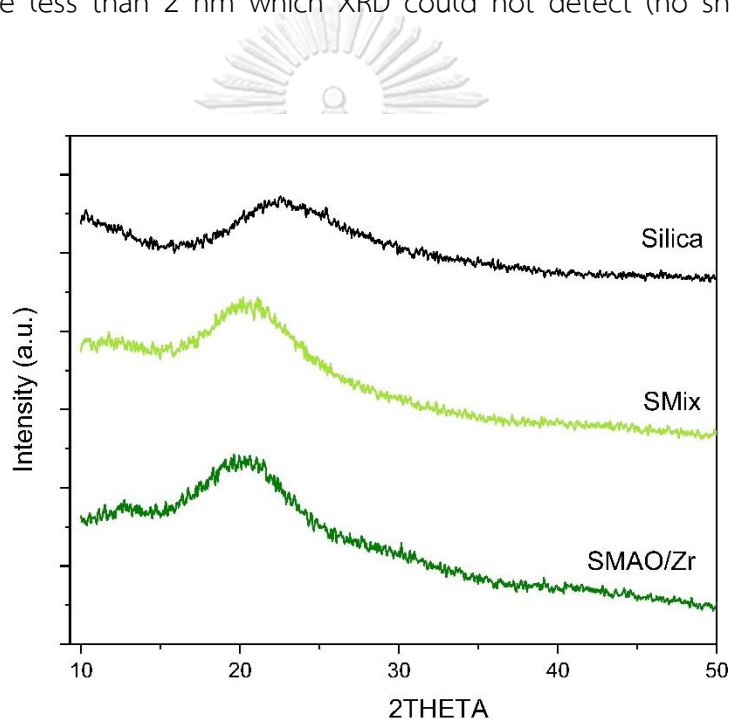


**Figure 26** XRD patterns of silica supports and silica-supported MAO/Zirconocene catalyst with different immobilization methods.

#### 4.1.1.4 Fourier Transform Infrared Spectroscopy (FTIR)

The FTIR analysis is shown in Figure 27. The functional group on silica support exhibited a broad band in the range between  $3000$  to  $3600\text{ cm}^{-1}$ , which was an indication of the stretching vibration of the bond for the hydroxyl group (-OH group).

The broad absorption peak at  $2912\text{ cm}^{-1}$  was assigned to the C–H stretching vibrations of the methyl groups in the methylaluminoxane [68]. The strong band at  $1090\text{ cm}^{-1}$ , was attributed to the Si–O–Si stretching, which was present in silica [69]. Also, the Zr–O (at about  $1108\text{ cm}^{-1}$ ) and C–H (at about  $2981\text{ cm}^{-1}$ ) are found in the spectra assigned to the metallocene catalysts [70].

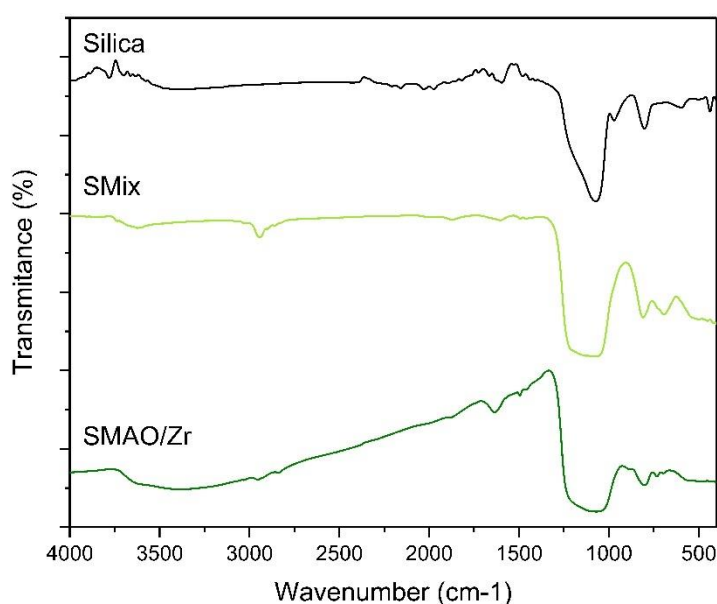


Figure 27 FTIR spectra of silica and silica-supported MAO/Zirconocene catalysts

#### 4.1.2 The catalytic activities of ethylene polymerization

Table 12, presents the MAO/Zirconocene catalytic systems (runs 2-3) in which the silica has lower catalytic activities than the homogeneous system (run 1). This is because negative effects such as monomers cannot react with active sites due to the lower amount of active sites resulting from interactions with the support surface. Besides, MAO or catalyst is bulkier in the supported system. In addition, different immobilized methods (runs 2-3) showed that SMAO/Zr (run 3) had more catalyst activity than SMix (run 2). From the EDX result, the SMAO/Zr show a good distribution of Al and/or Zr covered on the external support surface after immobilization of MAO.

Moreover, it can be observed that SMAO/Zr had a higher amount of Al and Zr than SMix. Furthermore, immobilize MAO first method, MAO is involved in the formation of cationic active sites for metallocene catalyst and also formation of a "crown-alumoxane complex" by immobilization with MAO to stabilize the anion, which can prevent anion that attacks the metallocene cation nucleophilically, that terminate process in cationic ethylene polymerization [71] And immobilization mixing of MAO and metallocene catalyst method probably less produced crown structure and can be expected that Zr<sup>+</sup> cations are more difficult to generate and stabilize in the case of supports with weak Lewis acid character. As a result, SMAO/Zr demonstrated higher activity and polymer yield than other immobilization methods. Different immobilization methods had a significant amount of active site from the catalyst to interact with the surface of the silica support and affect catalyst activity.

**Table 12** Catalyst activity with different methods of silica support

Run	Catalysts	Yield (g.)	Catalyst Activity <sup>a</sup> (g.PE/g.cat*h)
1	PE-Homo	4.85	43,795.9
2	PE-SMix	0.09	368.8
3	PE-SMAO/Zr	0.16	632.0

<sup>a</sup> The measurement at polymerization condition of  $[Zr]_{cat} = 5 \times 10^{-5}$  M,  $[Al]_{MAO} / [Zr]_{cat} = 2,000$  70 °C, 15 min, Total pressure = 3.5 bar in toluene with total volume = 30 ml.

### 4.1.3 Characterizations of polyethylene

#### 4.1.3.1 Scanning Electron Microscopy (SEM) and Energy Dispersive X-ray Spectroscopy (EDX)

From Figure 28, the morphology of the polymer investigated by SEM image showed that the homogeneous system had a fine particle of polymer with an irregular shape that was different from the polymer in the heterogeneous system,

which had an agglomeration of polymer making a larger polymer. Considering the polymer produced from the SMix catalyst, polymers were produced around the surface of the silica support and did not occur on the surface of the support. Probably, it occurred on the leached active site on support. Produced polyethylene from SMAO/Zr catalyst was formed and coated around on silica support, indicating the catalyst in the polymer texture. Polymerization can occur with active sites on silica support.

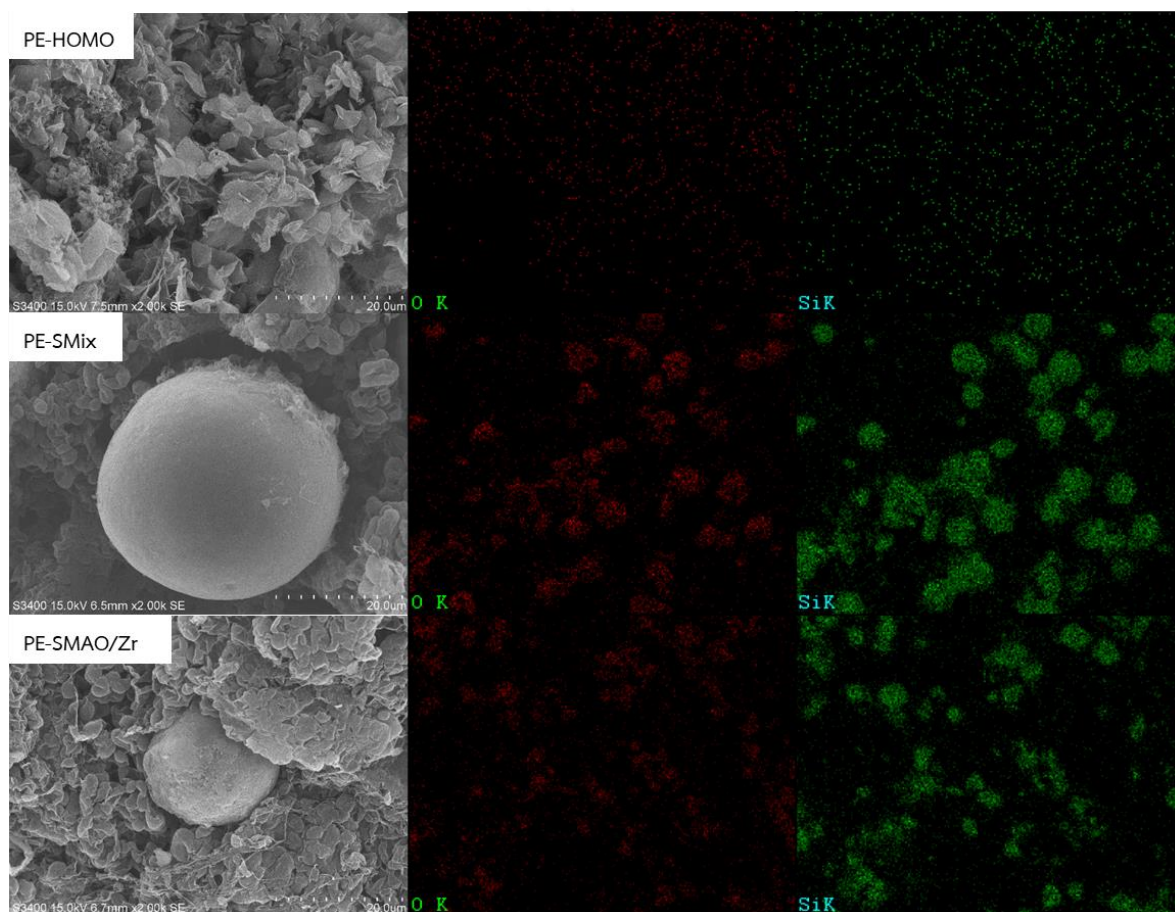


**Figure 28** Morphology and element distribution of produced polymer via homogeneous system and silica-supported MAO/Zirconocene catalytic system with different immobilization methods



## 4.2 In situ polymerization using zeolite A supported MAO/Zirconocene for ethylene and ethylene/1-hexene polymerization.

In this part, we studied the zeolite A-supported MAO/zirconocene catalyst effect of various temperatures and  $[Al]_{MAO}/[Zr]_{cat}$  ratios for suitable conditions for ethylene and ethylene/1-hexene polymerization and compared it with silica-supported system. In addition, we investigated the effect of the amount of scavenger MAO/zirconocene catalyst on ethylene polymerization.  $N_2$  physisorption (BET), SEM-EDX, XRD, FT-IR,  $NH_3$ -TPD, TGA and DTA were applied for characterization. Detailed explanations are provided in the section that follows.

### 4.2.1 Characteristics of zeolite A (LTA) and LTA-supported catalyst

#### 4.2.1.1 $N_2$ physisorption (BET) and Laser particle size distribution analyzer (PSD)

The zeolite A supports were analyzed by  $N_2$ -physisorption to determine the surface area, pore volume, and pore size and analyzed by laser particle size distribution analyzer to determine particle size distribution. In Table 13 and Figure 29, the results of BET surface area and pore characteristics of zeolite A supports are summarized along with the  $N_2$  adsorption-desorption isotherms.

**Table 13** The surface area of silica by  $N_2$  physisorption using the Brunauer-Emmett-Teller (BET) method, pore size and pore volume.

Samples	BET Specific Surface Area <sup>a</sup> (m <sup>2</sup> /g)	V <sub>meso</sub> <sup>b</sup> (cm <sup>3</sup> /g)	V <sub>micro</sub> <sup>b</sup> (cm <sup>3</sup> /g)	Pore size <sup>c</sup> (nm)	Particle size <sup>d</sup> (μm)
LTA	17.0	0.016	0.303	10.1	13.3

<sup>a</sup>BET method (Mesopore and Micropore), <sup>b,c</sup>BJH method, <sup>d</sup>PSD analysis

The specific surface area of LTA was 17.0 m<sup>2</sup>/g that significant difference from commercial LTA (559.1 m<sup>2</sup>/g) [57] and The mesopore and micropore volume were 0.016 and 0.303 cm<sup>3</sup>/g, respectively. The average adsorption pore diameter was 10.1

nm. The  $N_2$  adsorption-desorption Isotherms of zeolite A that according to IUPAC classification are isotherm types I and IV. It found microporous and mesoporous materials [72] and the average particle size of zeolite A was  $13.3 \mu\text{m}$ .

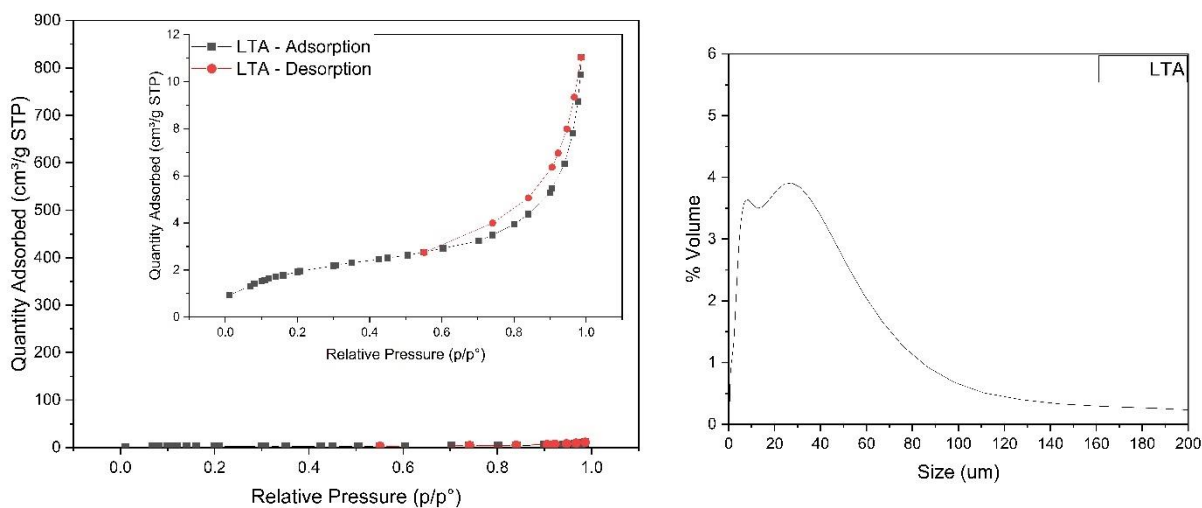


**Figure 29** The  $N_2$  adsorption-desorption isotherms and the average particle size distribution of zeolite A support

#### 4.2.1.2 Scanning Electron Microscopy (SEM) and Energy Dispersive X-ray Spectroscopy (EDX)

The morphology of the zeolite A support and immobilized catalyst was determined by the SEM image. The shape of zeolite A is shown in Figure 30. The structure consisted of cubic crystals with rough and smooth sides. This describes the zeolite A (LTA framework topology) characteristics [73]. The morphology of the LTA immobilization with MAO and zirconocene catalyst (LTA-MAO/Zr) was spheroidal with rough surfaces. It was observed that LTA-MAO/Zr had larger particles than LTA support and lots of adhesion of small particles on the support surface, indicating the presence of MAO and zirconocene catalysts onto the support surface, which correlated with the EDX results from Table 14. The Al and Zr content had increased from the initial zeolite A support.



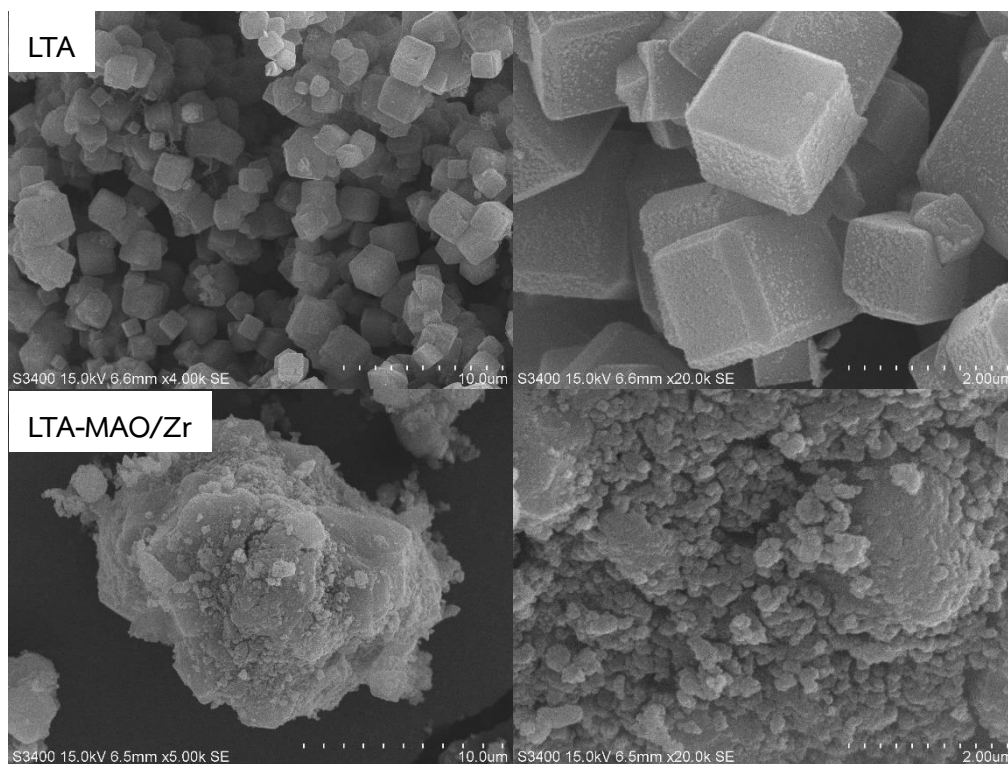


**Figure 30** SEM images of zeolite A and immobilized catalyst on zeolite A morphology

From Table 14, the amounts of components on the surface of the LTA support were seen by EDX analysis. LTA had a Si/Al molar ratio equal to 1.12 and LTA after immobilization (LTA-MAO/Zr) had a Si/Al ratio less than LTA which indicates increased dispersion on the surface of the amount of Al from MAO. In addition, the increased Zr content shows that the zirconocene catalyst is immobilized on the LTA surface.

**Table 14** Elemental distribution on the LTA-supported catalyst surface (EDX)

Samples	Element content (wt%)				[Si]/[Al]	[Al]/[Zr]
	O	Al	Si	Zr	molar ratios	molar ratios
LTA	44.57	25.57	29.86	-	1.12	-
LTA-MAO/Zr	41.34	21.61	9.41	27.64	0.42	2.64

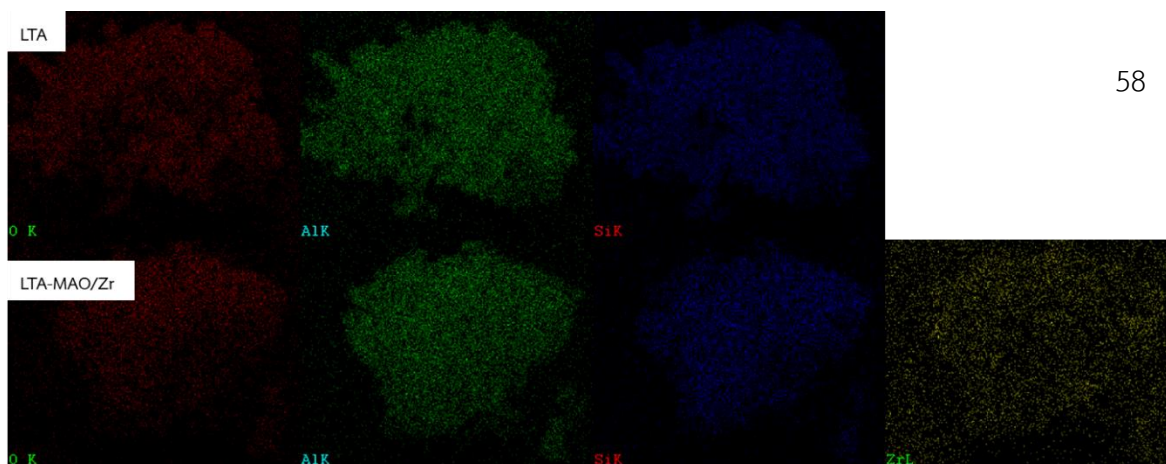


**Figure 31** Elemental distribution on zeolite A and immobilized MAO/zirconocene catalyst on zeolite A support

#### 4.2.1.3 X-ray Diffraction (XRD)

In Figure 32 for XRD analysis, the characteristic peaks of LTA support are located at 7.2, 10.1, 12.4, 16.1, 21.7, 24.1, 26.1, 27.2, 30.0, 30.9, 32.6, and 34.2 [74]. The XRD peak of LTA-MAO/Zr had the LTA support peak pattern, but was less sharp than LTA support, which indicated MAO/zirconocene catalyst immobilization and not modified LTA structure. The immobilized MAO and metallocene catalyst were dispersed on LTA to make a decreased crystallite and an increased amorphous structure that according to the EDX having an increase in Al and Zr content.

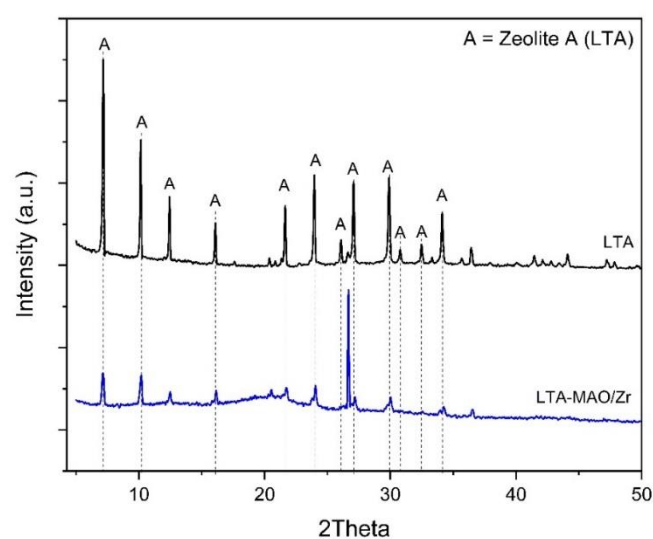


**Figure 32** XRD patterns of LTA and LTA after immobilization

#### 4.2.1.4 Fourier Transform Infrared Spectroscopy (FTIR)

The FTIR analysis was used to determine the bonding form and functional group of LTA supports and LTA supports after immobilization with MAO and zirconocene catalyst, which are shown in Figure 33. The broad band in the range between 3000 to 3600  $\text{cm}^{-1}$  was an indication of the stretching vibration of the bond for the hydroxyl group (-OH group) and the band at 1630  $\text{cm}^{-1}$  was due to the vibration of the Si-O bond. The generated vibrations by Al-O bonds are shown at 1033  $\text{cm}^{-1}$ , which was present in zeolite [75],[76]. Finally, it is observed that a broad band around 800  $\text{cm}^{-1}$  showing the presence of MAO, can be assigned to the Al-O bond [77].

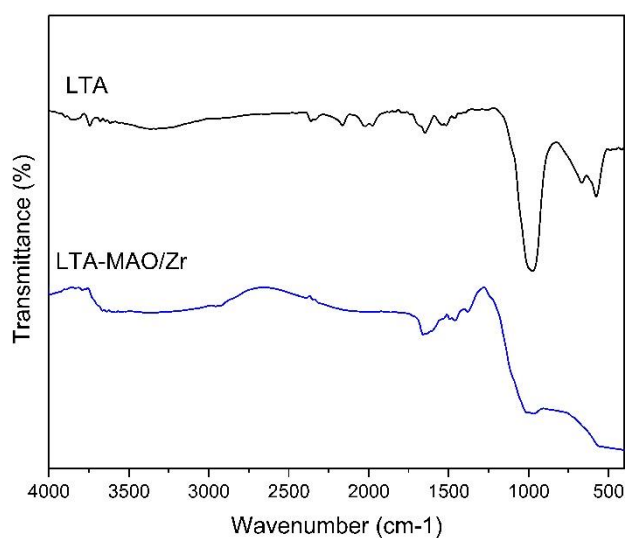


**Figure 33** FTIR spectra of LTA before and after immobilization

#### 4.2.1.5 Temperature-programmed desorption of ammonia ( $\text{NH}_3$ -TPD)

The  $\text{NH}_3$ -TPD profiles of zeolite A, shown in Figure 34, consisted mainly of two desorption peaks of weak acid sites (50 -350°C) and medium acid sites (350-450°C). The peaks of LTA presented a slight shift to the higher temperature, and the

corresponding amount of acid was calculated by curve deconvolution as shown in Table 15. The total amount of acid in LTA is 274.31  $\mu\text{mol/g}$

**Table 15** The amount of acid sites of zeolite A

Samples	Si/Al molar ratio	Acid capacity ( $\mu\text{mol/g}$ )			
		Total	Weak	medium	Strong
LTA	1.12	274.31	179.80	94.51	-

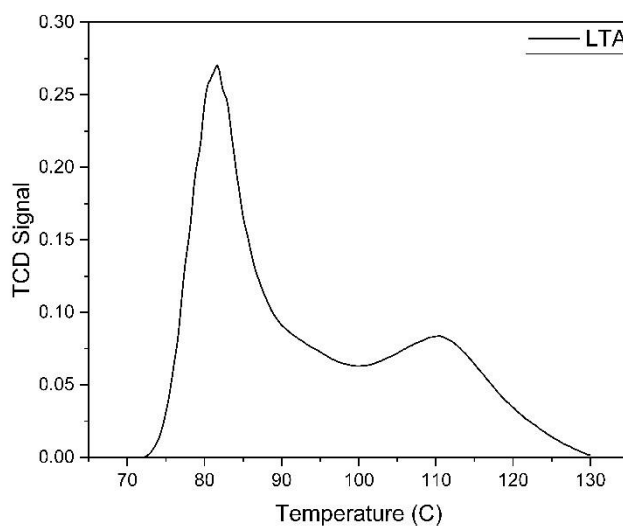


**Figure 34**  $\text{NH}_3$ -TPD profiles of zeolite A

## 4.2.2 The catalytic activities on polymerization behaviors

### 4.2.2.1 Effect of polymerization temperature and cocatalyst (MAO) ratio

The MAO/zirconocene catalyst on zeolite A support was used at various polymerization temperatures including 50, 60, 70, 80, and 90°C for ethylene polymerization. From Table 16, it shows that at 80°C, polyethylene yields were up to 0.13 g and had the highest activity of 210.6 g<sub>PE</sub>/g<sub>cat</sub>.hr. The yield of polyethylene rose to 80°C, which rendered the highest yield and activity of polyethylene. After

that, the polyethylene yield decreased at 90°C. This is likely due to catalyst deactivation as temperatures increase or an increased chain transfer reaction. In this work, the optimal temperature for ethylene polymerization was 80°C.

**Table 16** The Catalytic activities of various polymerization temperatures and molar ratios of  $[Al]_{MAO}/[Zr]_{cat}$  via ethylene polymerization

Run	Temperature (°C)	$[Al]_{MAO}/[Zr]_{cat}$ Ratio	Yield (g.)	Catalyst activity <sup>a</sup> (g.PE/g.cat*h)
1	50	2,000	0.02	96.0
2	60	2,000	0.04	159.2
3	70	2,000	0.04	154.6
<b>4</b>	<b>80</b>	<b>2,000</b>	<b>0.05</b>	<b>210.6</b>
5	90	2,000	0.03	131.6
6	80	1,000	0.04	153.0
7	80	1,500	0.04	160.2
<b>8</b>	<b>80</b>	<b>2,000</b>	<b>0.05</b>	<b>210.6</b>
9	80	2,500	0.04	174.6

<sup>a</sup> The measurement at polymerization condition of  $[Zr]_{cat} = 5 \times 10^{-5}$  M, for 15 min, Total pressure = 3.5 bar in toluene with total volume = 30 ml.

In addition, The MAO/zirconocene catalyst on zeolite A support was used at various molar ratios of  $[Al]_{MAO}/[Zr]_{cat}$  for ethylene polymerization. At  $[Al]_{MAO}/[Zr]_{cat}$  equal to 2000, there was the highest polyethylene yield up to 0.13 g and the highest activity of 210.6 g.PE/g.cat.hr. was observed, which was a suitable molar ratio for an LTA-supported catalyst for ethylene polymerization. Normally, the catalytic activity of a catalyst tends to increase as the  $[Al]_{MAO}/[Zr]_{cat}$  molar ratios increase. However, the catalyst activity decreased when the Al/Zr ratio was 2500. The excess aluminum probably produced inactive species or blocked the catalyst active sites resulting in a decrease in its activity. According to the research of I. N. Meshkova et al. [78], the Al/Zr ratio was changed from 4620 to 140 in the case of the system with  $Cp_2ZrCl_2$

synthesized on zeolite support. It was observed that increasing the Al/Zr ratio resulted in decreased catalyst activity .

#### 4.2.2.2 Effect of amount of scavenger (TMA)

The effect of various molar ratios of scavenger ( $[Al]_{TMA}/[Zr]_{cat}$ ) with zirconocene catalyst for ethylene polymerization is shown in Table 17. The increased TMA concentration affects increased catalyst activity. In addition, MAO/zirconocene catalysts with the addition of trimethylaluminum (TMA) as a scavenger had higher catalytic activity than MAO/zirconocene catalysts without the addition of TMA due to alkylaluminum also scavenged catalyst poisons that can reduce the amount of impurities in the system, which destroy the active site of catalyst in polymerization processes, leading to an increase in activity.

**Table 17** The catalytic activities of various molar ratios of  $[Al]TMA/[Zr]cat$  via ethylene polymerization.

Run	$[Al]_{MAO}/[Zr]_{cat}$ Ratio	$[Al]_{TMA}/[Zr]_{cat}$ Ratio	Yield (g.)	Catalyst activity <sup>a</sup> (g.PE/g.cat*h)
1	1,000	-	0.04	153.0
2	1,000	500	0.04	144.6
3	1,000	1,000	0.04	162.2
4	1,000	1,500	0.04	170.9
5	1,000	2,000	0.05	193.2
6	1,000	2,500	0.07	267.8

<sup>a</sup> The measurement at polymerization condition of  $[Zr]_{cat} = 5 \times 10^{-5}$  M, 80 °C, 15 min, Total pressure = 3.5 bar in toluene with total volume = 30 ml.

#### 4.2.2.3 Ethylene and ethylene/1-hexene polymerization behaviors

Table 8 presents the ethylene and ethylene/1-hexene polymerization with an LTA immobilized MAO/metallocene catalyst. A comparison of ethylene and ethylene/1-hexene polymerization systems (runs 1, 3) showed that copolymerization had higher catalyst activity than homopolymerization because adding the comonomer to the system increases reactants. The enhancement of activity catalysts by 1-hexene is known as the "comonomer effect" [79].

In addition, ethylene and ethylene/1-hexene polymerization with LTA immobilized MAO/metallocene catalysts (runs 2, 4) showed that the catalyst activity of copolymerization (run 4) was higher than ethylene polymerization. The difference in catalyst activity between the two systems was slight and not significant. However, ethylene/1-hexene copolymerization produced few copolymers (low catalyst activity that could not bring the copolymer to characterization). The conditions of ethylene/1-hexene copolymerization with LTA-MAO/Zr catalyst activity may be unsuitable. Furthermore, High temperatures can deactivate catalysts that affect catalyst activity.

**Table 18** The activity of MAO/Zirconocene catalyst via ethylene and ethylene/1-hexene polymerization.

Systems	Run	Polymers	Yield (g.)	Catalyst Activity <sup>a</sup> (g.PE/g.cat*h)
Ethylene polymerization	1	PE-Homo	4.85	43,795.9
	2	PE-LTA-MAO/Zr	0.05	210.6
Ethylene/1-hexene copolymerization	3	CoPE-Homo	6.75	60,918.1
	4	CoPE-LTA-MAO/Zr	0.06	223.8

<sup>a</sup> The measurement at polymerization condition of  $[Zr]_{cat} = 5 \times 10^{-5}$  M,  $[Al]_{MAO} / [Zr]_{cat} = 2,000$ , 80 °C, 15 min, Total pressure = 3.5 bar in toluene with total volume = 30 ml.

For ethylene polymerization and ethylene/1-hexene copolymerization (runs 1–2 and run 3-4), the supported catalytic system (run 2) has significantly lower catalytic activities than the homogeneous system (run 1) because of the negative effects such as monomer cannot react with active sites due to the lower amount of active sites resulting from interactions with the support surface. Besides, MAO or catalyst is bulkier in the supported system.

### 4.2.3 Characterizations of polymer

#### 4.2.3.1 Scanning Electron Microscopy (SEM) and Energy Dispersive X-ray Spectroscopy (EDX)

The morphology of the polyethylene and ethylene/1-hexene copolymers shown in Figure 35, was observed by scanning electron microscopy. The polyethylene produced by the LTA-MAO/Zr catalyst was investigated by SEM images showing that the particles of the produced polymer were agglomerated like cornflowers and had larger particles than polymers from homogeneous systems.

For the copolymerization system, the morphology of the ethylene/1-hexene copolymer was gel-like or semisolid-like. However, the morphology of the ethylene/1-hexene copolymer formed by the LTA-MAO/Zr catalyst is quite similar to that of the catalyst precursor. Around the catalyst precursor, the molecule of ethylene/1-hexene copolymer formed into a particle and expanded continuously.



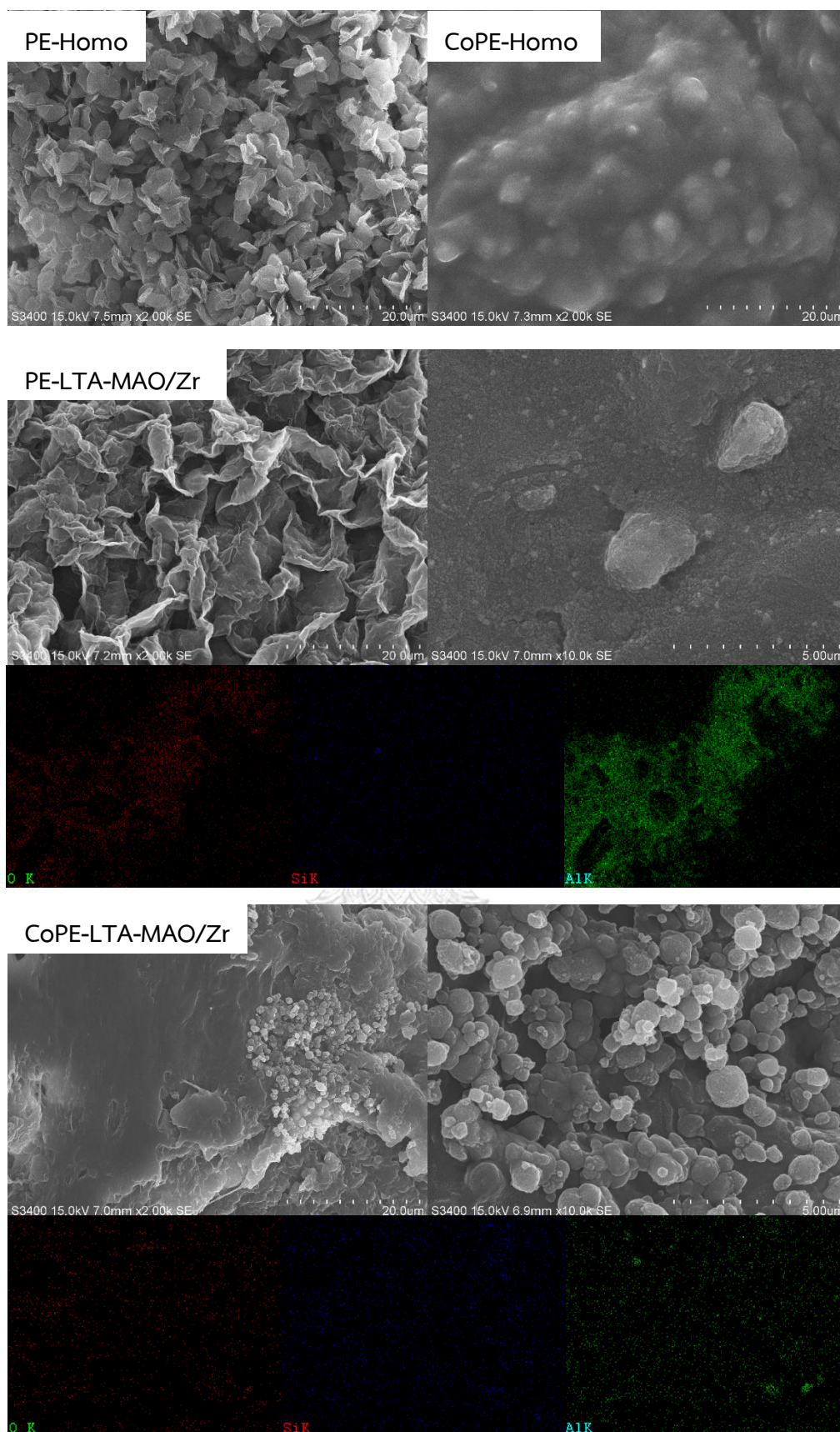


**Figure 35** Morphology and element distribution of polyethylene and ethylene/1-hexene copolymer produced via homogeneous system and LTA-MAO/Zr catalyst.

#### 4.2.3.2 X-ray Diffraction (XRD)

The XRD technique was used to characterize the crystalline structures of all the obtained polymers, as shown in Figure 36. The XRD patterns of polyethylene produced by homogeneous systems and the LTA-MAO/Zr catalyst confirmed that the zeolite A (LTA) was used as a support for the immobilization of MAO/zirconocene as a catalyst for ethylene polymerization. The XRD patterns of obtained polyethylene were similar, demonstrating two peaks of  $21.3^\circ$  and  $23.7^\circ$ , which conform to the orthorhombic crystalline structure of polyethylene [80]. For copolymerization, the XRD pattern is less shaped because 1-hexene insertion affects the decreased crystalline structure of polyethylene.

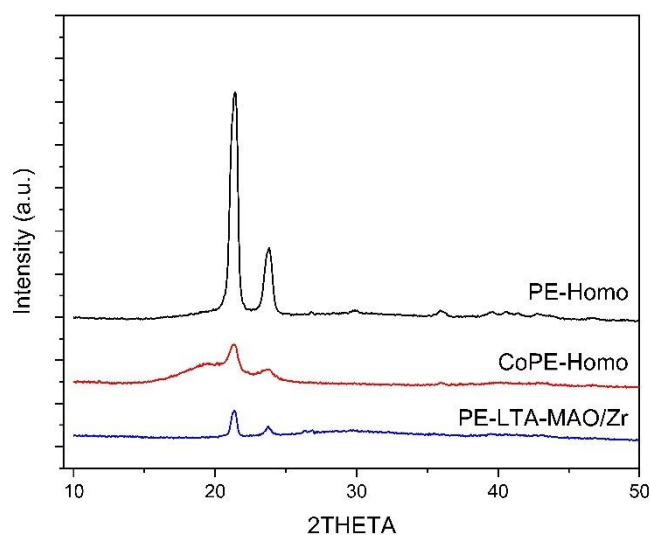


**Figure 36** XRD patterns of polyethylene from homogeneous system and LTA-MAO/Zr catalytic system

Noted : CoPE-LTA-MAO/Zr not determined.

#### 4.2.3.3 Thermal gravimetric analysis differential scanning calorimetry (TGA-DSC)

To investigate the melting temperature ( $T_m$ ) and crystallinity ( $\chi_c$ ) of the obtained polyethylene from LTA immobilized Mao/zirconocene catalyst, the TGA-DSC technique was used for this purpose. As shown in Table 19, the melting temperature of polyethylene was 129.30°C which is more than the melting temperature of the ethylene/1-hexene copolymer of 114.72°C. The melting temperature of polymer from LTA-MAO/Zr catalyst was higher than polymer from homogeneous catalyst, so adding support for metallocene catalyst was able to increase thermal stability.

Furthermore, LTA was used to determine the ethylene/1-hexene copolymer. 1-hexene addition is able to decrease the crystallinity of polymers, and the insertion of 1-hexene leads to a decrease in crystallinity. As a result, polymers with a lower melting point and density, and increased flexibility and processibility were obtained [81].

**Table 19** Melting temperature and crystallization behaviors of polyethylene and copolymers produced from LTA support immobilization.

Run	Polymers	Melting temperature <sup>a</sup> (°C)	$\Delta H_{\text{exp}}$ <sup>b</sup> (J/g)	Crystallinity <sup>a</sup> (% $\chi_c$ )
1	PE-Homo	129.30	186.70	65.28
2	PE-LTA-MAO/Zr	133.14	130.00	45.45
3	CoPE-Homo	114.72	6.60	2.31
4	CoPE-LTA-MAO/Zr	n.d.	n.d.	n.d.

<sup>a</sup> Melting temperature ( $T_m$ ) measured by DSC measurement.

<sup>b</sup> Heat of fusion ( $\Delta H_{\text{exp}}$ ) measured by DSC measurement.

<sup>c</sup> Crystallinity ( $\chi_c$ ) was calculated from the equation; %crystallinity= $(\Delta H_{\text{sample}}/\Delta H_{100\% \text{ crystallinity}}) \times 100$ , the  $\Delta H_{100\% \text{ crystallinity}}$  of polyethylene is 286 J/g.

n.d. = not determined

#### 4.2.4 Comparison between silica and zeolite A for supported-metallocene catalyst system.

##### 4.2.4.1 Characterization of support and immobilized catalyst

The results revealed that silica Table 20 had a pore volume (1.249 cm<sup>3</sup>/g) greater than LTA (0.016 cm<sup>3</sup>/g.). The average pore size diameter of silica was larger than LTA , a slight difference. In addition, the surface areas and particle sizes of spherical silica and LTA were significantly different. The surface area and particle size of silica appeared to be larger when compared to zeolite A support. The physical properties are very important for catalyst and product properties.

**Table 20** Comparison of the surface area, pore size, pore volume and particle size distribution between spherical silica and zeolite A

Samples	Specific Surface Area <sup>a</sup> (m <sup>2</sup> /g)	V <sub>meso</sub> <sup>b</sup> (cm <sup>3</sup> /g)	V <sub>micro</sub> <sup>b</sup> (cm <sup>3</sup> /g)	Pore size <sup>c</sup> (nm)	Particle size <sup>d</sup> (μm)
Silica	298.1	1.249	-	14.5	36.9
LTA	17.0	0.016	0.303	10.1	13.3

<sup>a</sup>BET method (Mesopore and Micropore), <sup>b,c</sup>BJH method, <sup>d</sup>PSD analysis

The morphology of silica support and LTA support was determined using scanning electron microscopy (SEM) as shown in Figure 37. It was found that the silica had a spherical shape. Zeolite A presents a cubic shape and a rough surface area. So, the shape and surface of the silica and LTA were different. However, both support immobilized MAO/zirconocene catalysts were found and the elemental distribution was also performed using EDX mapping on the external surface as seen in Table 21. The LTA-MAO/Zr had a higher Al and Zr content ratio on the surface than the SMAO/Zr, but only a slight difference.

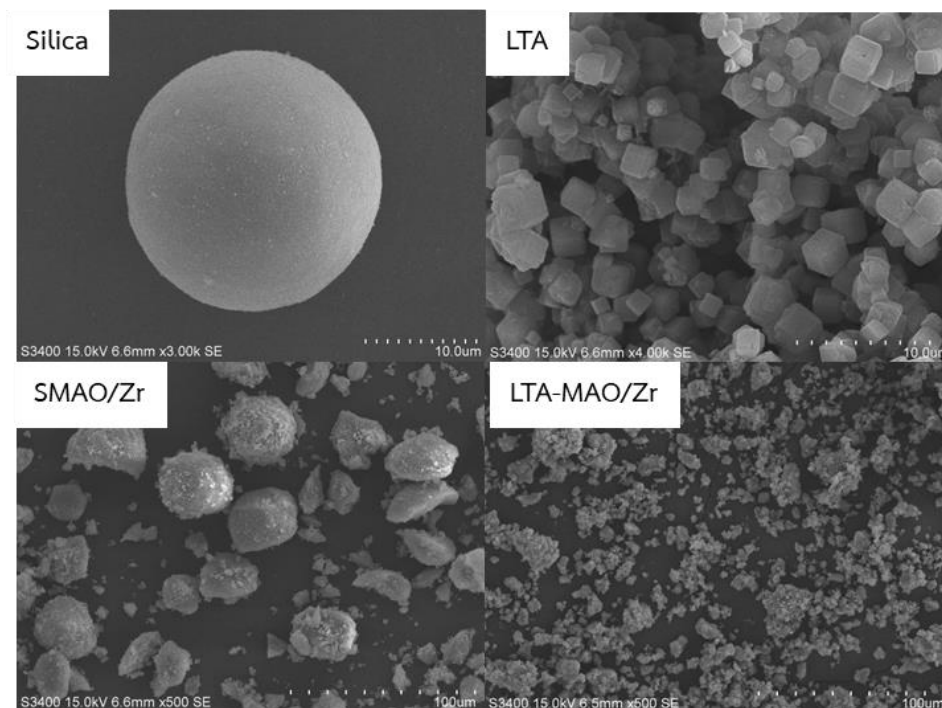


**Figure 37** The morphology of silica and zeolite A support and immobilized MAO/zirconocene catalyst

**Table 21** Elemental distribution on the silica and LTA supported catalyst surface.

Samples	Element content (wt%)				[Al]/[Zr] molar ratios
	O	Al	Si	Zr	
SMAO/Zr	41.82	11.92	27.65	18.61	2.17
LTA-MAO/Zr	41.34	21.61	9.41	27.64	2.64

TGA was used to investigate the thermal stability of different supported catalysts with % weight loss. As shown in Figure 38, it was found that compared to this curve, the weight loss of both supported catalysts decreased significantly and had a similar trend. It was observed that SMAO/Zr has the least %weight loss at 11% and LTA-MAO/Zr has %weight loss at 18%. The first period of temperature before 105°C displayed decomposition moisture. After that, the modified supported catalyst decreased continuously as follows: volatile matter, and ash. And after 600°C, the

residues are fixed carbon. The supported metallocene catalyst has strong thermal stability, and both supported catalysts had a slight %weight loss difference.

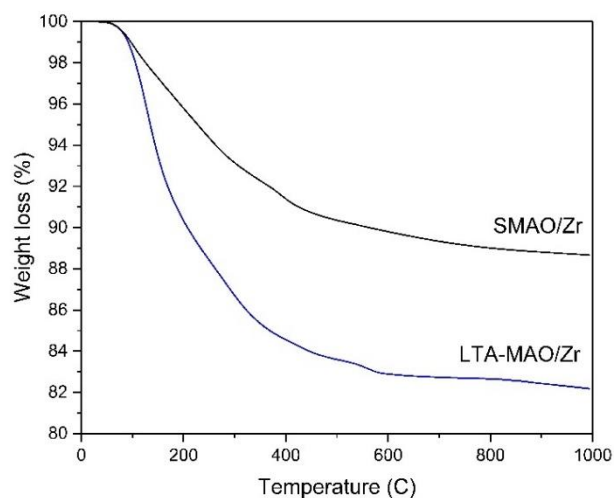


**Figure 38** TGA profiles of silica and LTA-supported metallocene catalysts

#### 4.2.4.2 Catalyst activity

The MAO/zirconocene catalyst on silica support and zeolite A via ethylene and ethylene/1-hexene polymerization is shown in Table 22. The yield of polyethylene and catalyst activity of SMAO/Zr were higher than those of LTA-MAO/Zr. The LTA-supported catalyst activity is less than silica, about 0.26 and 0.57 times in ethylene polymerization and ethylene/1-hexene copolymerization, respectively. Silica-supported catalysts had a surface area greater than LTA, and the particle size of silica was suitable for supported metallocene catalysts, as seen in Table 20. The LTA had an acidity that probably affected catalyst activity. In addition, ethylene/1-hexene polymerization with silica-supported MAO/metallocene catalyst activity is more active than ethylene polymerization. Normally, copolymerization systems have a higher yield and catalyst activity than homogeneous systems [81], indicating that the conditions of ethylene/1-hexene copolymerization with a supported catalyst may be unsuitable.

**Table 22** The activity of the MAO/Zirconocene catalyst via ethylene and ethylene/1-hexene polymerization on silica and LTA support.

Systems	Run	Catalysts	Yield (g.)	Catalyst Activity <sup>a</sup> (g.PE/g.cat*h)	Catalyst activity ratio
Ethylene polymerization	1	PE-SMAO/Zr	0.21	820.8	1
	2	PE-LTA-MAO/Zr	0.05	210.6	0.26
Ethylene/1-hexene copolymerization	3	CoPE-SMAO/Zr	0.10	394.4	1
	4	CoPE-LTA-MAO/Zr	0.06	223.8	0.57

<sup>a</sup> The measurement at polymerization condition of  $[Zr]_{cat} = 5 \times 10^{-5}$  M,  $[Al]_{MAO} / [Zr]_{cat} = 2,000$  80 °C, 15 min, Total pressure = 3.5 bar in toluene with total volume = 30 ml.

#### 4.2.4.3 Characterization of polymer

The morphology of the obtained polyethylene from homogeneous and heterogeneous systems as measured by SEM/EDX is shown in Figure 39. It was found that silica-supported can produce polyethylene coated around a surface, which is similar to silica having a spherical shape. The agglomerated polymer was produced from an LTA-supported catalyst that had small particles of LTA.

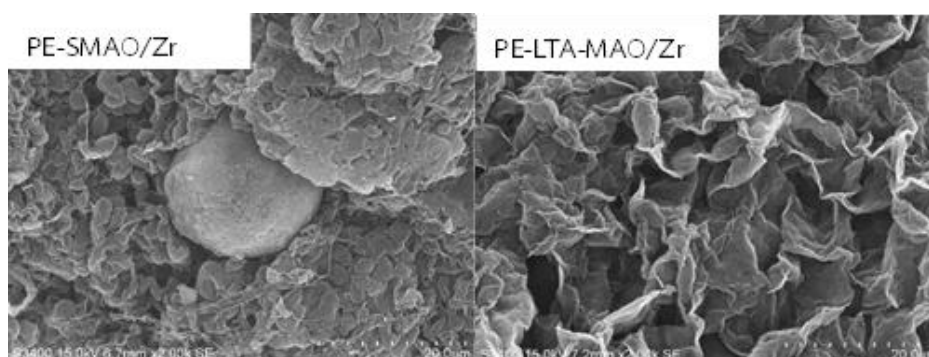


**Figure 39** The morphology of polymer from silica and zeolite A support immobilized MAO/zirconocene catalyst



The XRD technique, obtained polymers from different support as shown in Figure 40. The XRD patterns of polyethylene between SMAO/Zr and the LTA-MAO/Zr catalyst were similar, demonstrating two peaks of  $21.3^\circ$  and  $23.7^\circ$ , which conform to the orthorhombic crystalline structure of polyethylene [80]. And for copolymer from SMAO/Zr, the XRD pattern is similar to copolymer from homogeneous system that decreased crystalline structure when adding comonomer.

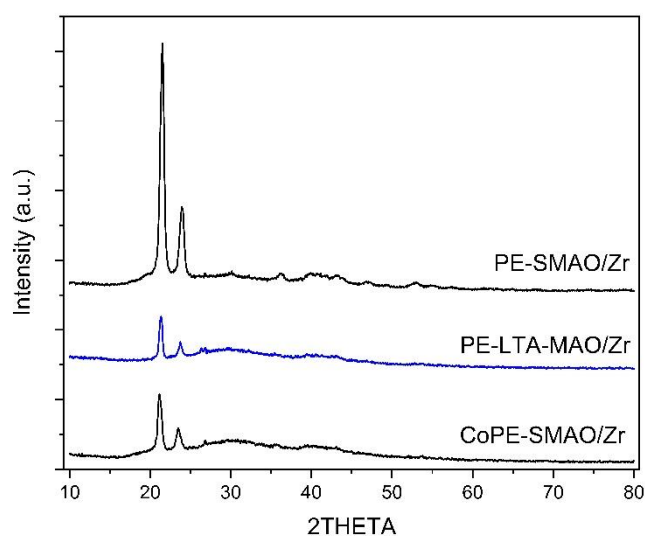


**Figure 40** XRD patterns of polyethylene and ethylene/1-hexene copolymer from SMAO/Zr and LTA-MAO/Zr catalytic system

Noted : CoPE-LTA-MAO/Zr not determined.

The TGA-DSC technique was used for this purpose as shown in Table 23, the melting temperatures of polyethylene between SMAO/Zr and LTA-MAO/Ze catalysts were slightly different. However, the crystallinity of the polymer from silica support was higher than that from LTA support related to the XRD patterns that showed the strong peak of the crystalline structure of polyethylene. This was probably due to LTA support had small particles ( $13.3 \mu\text{m}$ ) that low catalyst activity with reduced the crystallization of polyethylene [82] or the acidity of LTA support can lead to the



formation of branched or crosslinked structures, which can disrupt the formation of polymer chains and reduce crystallinity

**Table 23** Melting temperature and crystallization behaviors of polyethylene and copolymer produced from silica and LTA support of immobilization.

Run	Polymers	Melting temperature <sup>a</sup> (°C)	$\Delta H_{\text{exp}}$ <sup>b</sup> (J/g)	Crystallinity <sup>a</sup> (% $\chi_c$ )
1	PE-SMAO/Zr	138.16	222.00	77.62
2	PE-LTA-MAO/Zr	133.14	130.00	45.45
3	CoPE-SMAO/Zr	110.86	91.82	32.10
4	CoPE-LTA-MAO/Zr	n.d.	n.d.	n.d.

<sup>a</sup> Melting temperature ( $T_m$ ) measured by DSC measurement.

<sup>b</sup> Heat of fusion ( $\Delta H_{\text{exp}}$ ) measured by DSC measurement.

<sup>c</sup> Crystallinity ( $X_c$ ) was calculated from the equation; %crystallinity= $(\Delta H_{\text{sample}}/\Delta H_{100\% \text{ crystallinity}}) \times 100$ , the  $\Delta H_{100\% \text{ crystallinity}}$  of polyethylene is 286 J/g.

n.d. = not determined

### 4.3 Comparison of different zeolite for supported metallocene catalysts with ethylene polymerization and 1-hexene copolymerization.

In the last part, the characteristics and activity of catalysts using various zeolite supports, including zeolite A, ZSM5 and beta zeolite (BEA) were investigated. The various zeolites are analyzed using various techniques such as N<sub>2</sub> physisorption (BET), SEM-EDX, XRD, FT-IR, NH<sub>3</sub>-TPD, and TGA-DSC. Next, the different zeolite-supported catalysts were used under the conditions from Part 2 with the temperature of 80°C and a molar ratio of Al and Zr was 2000 for ethylene and ethylene/1-hexene copolymerization. Finally, the obtained polyethylene was characterized in terms of morphology, crystallinity, and thermal properties.

#### 4.3.1 Characteristics of different zeolite and zeolite-MAO/metallocene supported catalyst.

##### 4.3.1.1 N<sub>2</sub> physisorption (BET) and Laser particle size distribution analyzer (PSD)

In Table 24 and Figure 41, the results of BET surface area and pore characteristics of various zeolite supports are summarized with the N<sub>2</sub> adsorption-desorption isotherms.

**Table 24** The surface area of various zeolite supports by N<sub>2</sub> physisorption using the Brunauer-Emmett-Teller (BET) method, pore size and pore volume.

Samples	BET Specific Surface Area <sup>a</sup> (m <sup>2</sup> /g)	V <sub>meso</sub> <sup>b</sup> (cm <sup>3</sup> /g)	V <sub>micro</sub> <sup>b</sup> (cm <sup>3</sup> /g)	Pore size <sup>c</sup> (nm)	Particle size <sup>d</sup> (μm)
LTA	17.0	0.016	0.303	10.1	13.3
ZSM5	648.2	0.030	0.174	2.6	88.1
BEA	996.4	0.113	0.325	4.2	1.8

<sup>a</sup>BET method (Mesopore and Micropore), <sup>b,c</sup>BJH method, <sup>d</sup>PSD analysis

Comparing their N<sub>2</sub> adsorption-desorption isotherms between LTA, ZSM5, and BEA, it revealed differences in their porosity and surface area characteristics. The three zeolites exhibit a combination of micropores and mesopores. The BEA exhibited the highest BET surface area, followed by the ZSM-5 and LTA as 996.4, 648.2 and 17.0 m<sup>2</sup>/g, respectively. In addition, it was found that the particle sizes of the various zeolite samples presented were in the range of 10-250 μm. The particle size of LTA appeared to be larger and had a broader particle size distribution when compared to other zeolite types. The results of the particle size effect in ethylene and ethylene/1-hexene polymerization will be examined further.

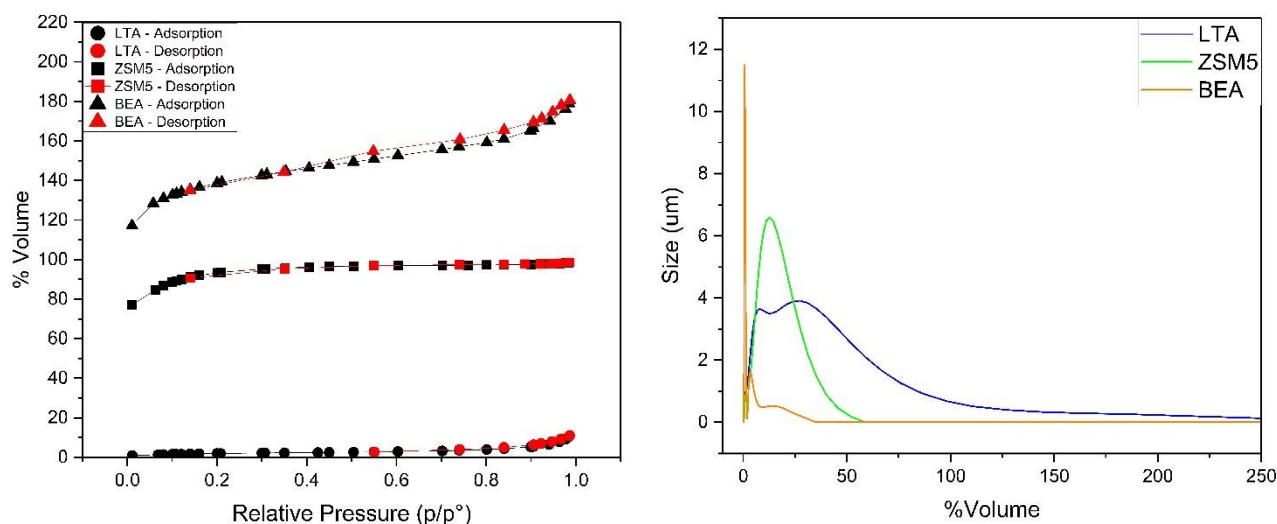


**Figure 41** The N<sub>2</sub> adsorption-desorption isotherms and the average particle size distribution of various zeolite support

#### 4.3.1.2 Scanning Electron Microscopy (SEM) and Energy Dispersive X-ray Spectroscopy (EDX)

The morphology of various zeolite supports was characterized using scanning electron microscopy (SEM) as shown in Figure 42. The shape of zeolite A consisted of cubic crystals with rough and smooth sides. ZSM5 consists of cubic-like crystallites. The BEA morphology had a spheroidal shape. The various zeolite particles after

immobilization had a spheroidal shape and a larger particle size than initially. However, the particle size of BEA and BEA-supported MAO/zirconocene catalysts showed that they were smaller when compared to other zeolites.

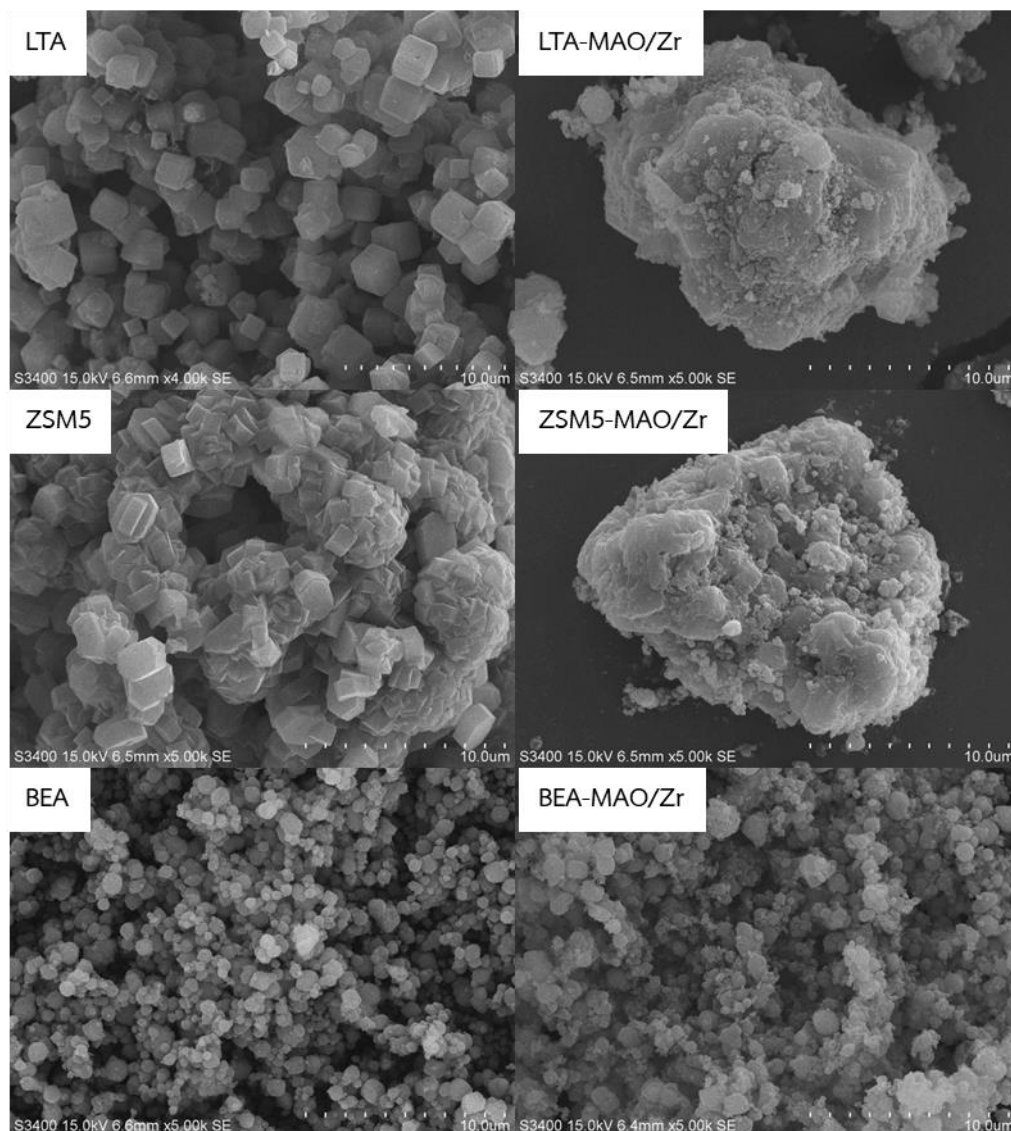


**Figure 42** SEM images of various zeolite and immobilized MAO/zirconocene catalyst on zeolite morphology

From Table 25, the amount of components on the surface of the zeolite support and zeolite after immobilization was measured by EDX analysis. The Si/Al ratio of various zeolites between before and after immobilization showed that the

Si/Al ratio after immobilization had increased when compared to before, which indicated that Al from MAO was depressed on zeolite. In addition, the increased Zr content showed that the zirconocene catalyst was immobilized on the zeolite surface. The different Si/Al ratio affected the structural morphology and led to a different surface area. Moreover, the Si/Al ratio of each zeolite is related to BET surface area and pore volume [83]. The LTA had a lower Si/Al ratio, BET surface areas, and pore volume than other zeolites.

**Table 25** Elemental distribution on the various zeolite-supported catalyst surface

Samples	Element content (wt%)				[Si]/[Al]	[Al]/[Zr]
	O	Al	Si	Zr	molar ratios	molar ratios
LTA	44.57	25.57	29.86	-	1.12	-
ZSM5	44.04	3.11	52.84	-	16.31	-
BEA	53.98	0.54	45.48	-	80.49	-
LTA-MAO/Zr	41.34	21.61	9.41	27.64	0.42	2.64
ZSM5-MAO/Zr	38.21	14.68	18.64	28.47	1.22	1.74
BEA-MAO/Zr	39.71	10.06	21.00	29.23	2.00	1.16

#### 4.3.1.3 X-ray Diffraction (XRD)

In this task, we will compare the XRD patterns of three zeolite types, including LTA, ZSM5, and BEA before and after immobilization with MAO/zirconocene catalyst, as seen in Figure 43 . The three zeolite types are zeolite frameworks with a well-ordered crystal structure. The three zeolites are zeolite frameworks with a well-ordered crystal structure. The XRD peaks of LTA are observed at 7.2, 10.1, 12.4, 16.1, 21.7, 24.1, 26.1, 27.2, 30.0, 30.9, 32.6, and 34.2 [74] which confirms the presence of the LTA framework. The main XRD pattern of ZSM5 shows 8.0, 8.9, 9.1, 13.1, 13.9, 14.8, 15.5, 15.9, 20.3, 20.8, 23.1, 23.7, 23.9 and 24.4 [74]. These peaks indicate the presence of the ZSM5 framework in the sample. The XRD pattern of BEA typically

observed at 7.9, 13.6, 14.7, 21.8, 22.8, 27.3, and 30.9 [74], confirmed the presence of the BEA zeolite.

In addition, the XRD patterns of LTA, ZSM5, and BEA after immobilization with MAO/zirconocene catalyst were decreased when compared to zeolite support because of the decreased crystallites and increased the amorphous structure of the support, which indicated MAO/zirconocene catalyst immobilization can disperse on zeolite support. The EDX result showed an increase in Al and Zr content on various zeolite samples.

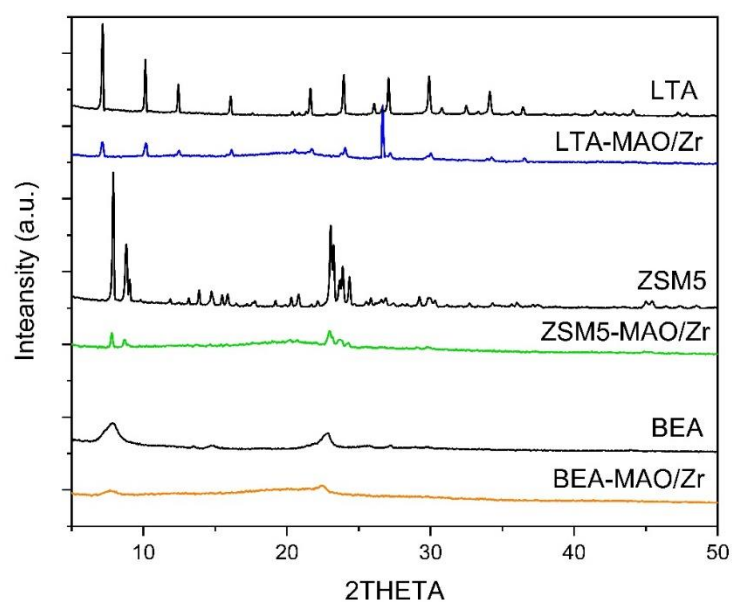


**Figure 43** XRD patterns of various zeolites before and after immobilization

#### 4.3.1.4 Fourier Transform Infrared Spectroscopy (FTIR)

From Figure 44, IR analysis of all supports and supports after immobilization with MAO and zirconocene catalyst. In the FTIR spectrum of all zeolite supports, characteristic absorption bands are present around 1500–400  $\text{cm}^{-1}$  indicating structural zeolite frameworks that consist of the vibration of the Si-O bond and Al-O bond [84]. And zeolite-supported catalysts showed IR spectra with a broad band

around  $800\text{ cm}^{-1}$ , presence of MAO, which can be assigned to the Al-O bond [77]. The broad band in the range between  $3000$  and  $3600\text{ cm}^{-1}$  was an indication of the stretching vibration of the bond for the hydroxyl group (-OH group) that BEA-MAO/Zr had observable, indicating -OH group on the zeolite structure that affects the active site and catalyst activity.

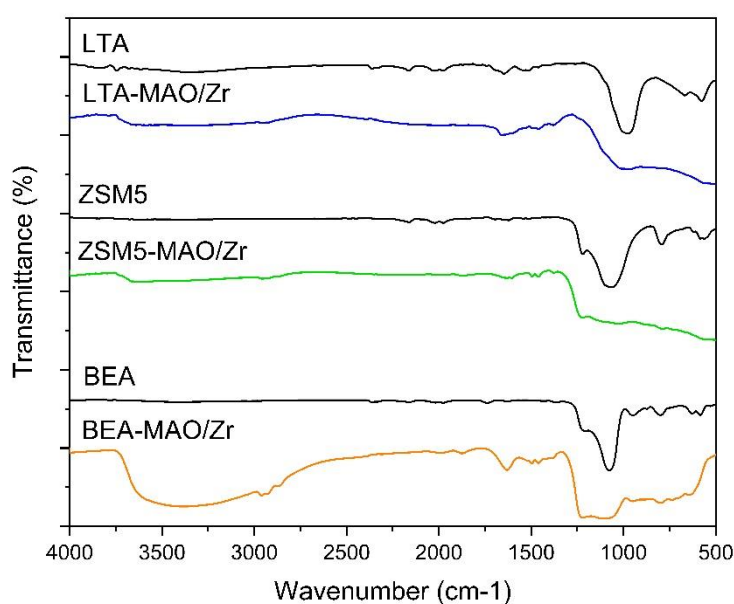


**Figure 44** FTIR spectra of various zeolites before and after immobilization

#### 4.3.1.4 Temperature-programmed desorption of ammonia ( $\text{NH}_3$ -TPD)

The  $\text{NH}_3$ -TPD profiles of various zeolites, shown in Figure 45, consisted mainly of three desorption peaks: weak acid sites ( $50$ - $300^\circ\text{C}$ ), medium sites ( $300$ - $450^\circ\text{C}$ ) and strong acid sites ( $450$ - $600^\circ\text{C}$ ). At the lower temperature, it was known to associate with the Lewis acid sites, while the higher temperature is ascribed to the Bronsted acid sites [85]. All zeolites had mostly weak and medium acid sites. LTA had weak and medium acid referred to the highest Lewis acid among other zeolite supports. The corresponding amount of acid was calculated by curve deconvolution, as shown in Table 26. The LTA had the highest total acid capacity of  $274.31\ \mu\text{mol/g}$  followed

by ZSM-5 and BEA, respectively. This suggested that the Si/Al ratio affected the acid strength of zeolites, and it was likely that increasing the aluminium content led to a stronger acid strength [83].

**Table 26** The amount of acid sites of various zeolites

Samples	Si/Al molar ratio	Acid capacity ( $\mu\text{mol/g}$ )			
		Total	Weak	Medium	Strong
LTA	1.12	274.31	179.80	94.51	-
ZSM5	16.31	182.60	120.71	40.21	21.68
BEA	80.49	167.73	87.80	60.99	18.94

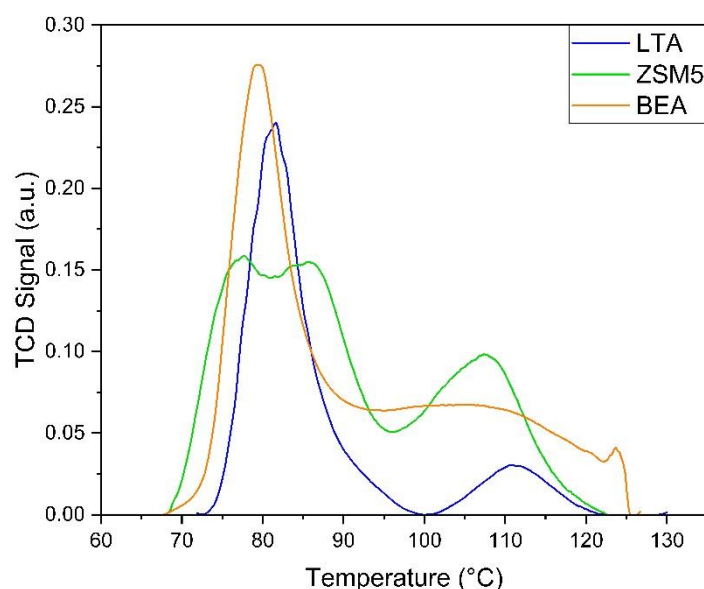


**Figure 45**  $\text{NH}_3$ -TPD profiles of various zeolites

#### 4.3.1.5 Thermogravimetric Analysis (TGA)

The TGA results presented in Figure 16 demonstrate the thermal stability of different supported catalysts by measuring their weight loss. It was found that compared to this curve, the weight loss of various zeolite supported catalysts decreased significantly and had a similar trend. The ZSM5-MAO/Zr has the least



%weight loss at 15% followed LTA-MAO/Zr of 18% and BEA-MAO/Zr of 19%, respectively. The initial temperature range, which was lower than 105 degrees Celsius, exhibited the decomposition moisture. After that, the volatile matter and ash released by the modified supported catalyst began to slowly decrease. And after 600°C, the remains are fixed carbon. The supported metallocene catalyst exhibits good thermal stability, as well as there was slightly different in the amount of weight loss between the three zeolites supported catalysts.

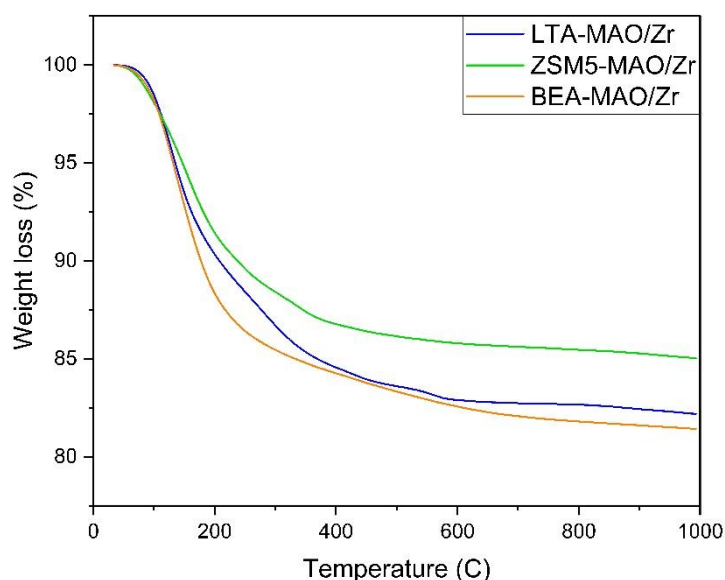


Figure 46 TGA profiles of various zeolite-supported metallocene catalysts

#### 4.3.2 The catalytic activities on Ethylene and ethylene/1-hexene polymerization behaviors

Table 27 shows the polymerization of ethylene and ethylene/1-hexene using a variety of zeolites that have been immobilized with MAO/metallocene catalysts. With the ethylene/1-hexene copolymerization system, the various zeolite support catalysts exhibited greater activity than with the ethylene polymerization system. The difference in catalyst activity between the two systems was negligible and insignificant. In addition, The LTA supported catalytic system has higher catalytic

activities than ZSM5 and BEA support, respectively for ethylene and ethylene/1-hexene polymerization. Although BEA had the largest surface area that was a good support for catalyst, but BEA-MAO/Zr had a lot of OH groups in its structure as seen in the FTIR results. The OH group can participate in side-reactions during the polymerization process. For example, it can act as a chain transfer agent, leading to the termination of the polymer chain, which leads to lower catalyst activity when compared to other zeolite supports. In contrast, LTA-MAO/Zr had the highest yield and catalyst activity because of the higher Al/Zr ratio on the LTA support than other zeolite supports, and the LTA had the highest acidity of Lewis acid, which directly correlated with the activity of the catalysts [85].

However, the catalyst activity depended on many factors, for example, surface area of the support, amount of catalyst and cocatalyst, temperature, acidity, etc., that cannot be directly compared between the three zeolites because of differences in textural properties. In this study, LTA support was an optimally supported metallocene catalyst system that probably had suitable textural properties and acidity.

**Table 27** The activity of MAO/Zirconocene catalyst via ethylene and ethylene/1-hexene polymerization on various zeolite

Systems	Run	Polymers	Yield (g.)	Catalyst Activity <sup>a</sup> (g.PE/g.cat*h)
Ethylene polymerization	1	PE-LTA-MAO/Zr	0.05	210.6
	2	PE-ZSM5-MAO/Zr	0.04	163.2
	3	PE-BEA-MAO/Zr	0.03	137.8
Ethylene/1-hexene copolymerization	4	CoPE-LTA-MAO/Zr	0.06	223.8
	5	CoPE-ZSM5-MAO/Zr	0.03	169.4
	6	CoPE-BEA-MAO/Zr	0.03	152.4

<sup>a</sup> The measurement at polymerization condition of  $[Zr]_{cat} = 5 \times 10^{-5}$  M,  $[Al]_{MAO} / [Zr]_{cat} = 2,000$ , 80 °C, 15 min, Total pressure = 3.5 bar in toluene with total volume = 30 ml.

### 4.3.3 Characterizations of polymer

#### 4.3.3.1 Scanning Electron Microscopy (SEM) and Energy Dispersive X-ray Spectroscopy (EDX)

The morphologies of the polyethylene and ethylene/1-hexene copolymers shown in Figure 47 and Figure 48, were observed by scanning electron microscopy.

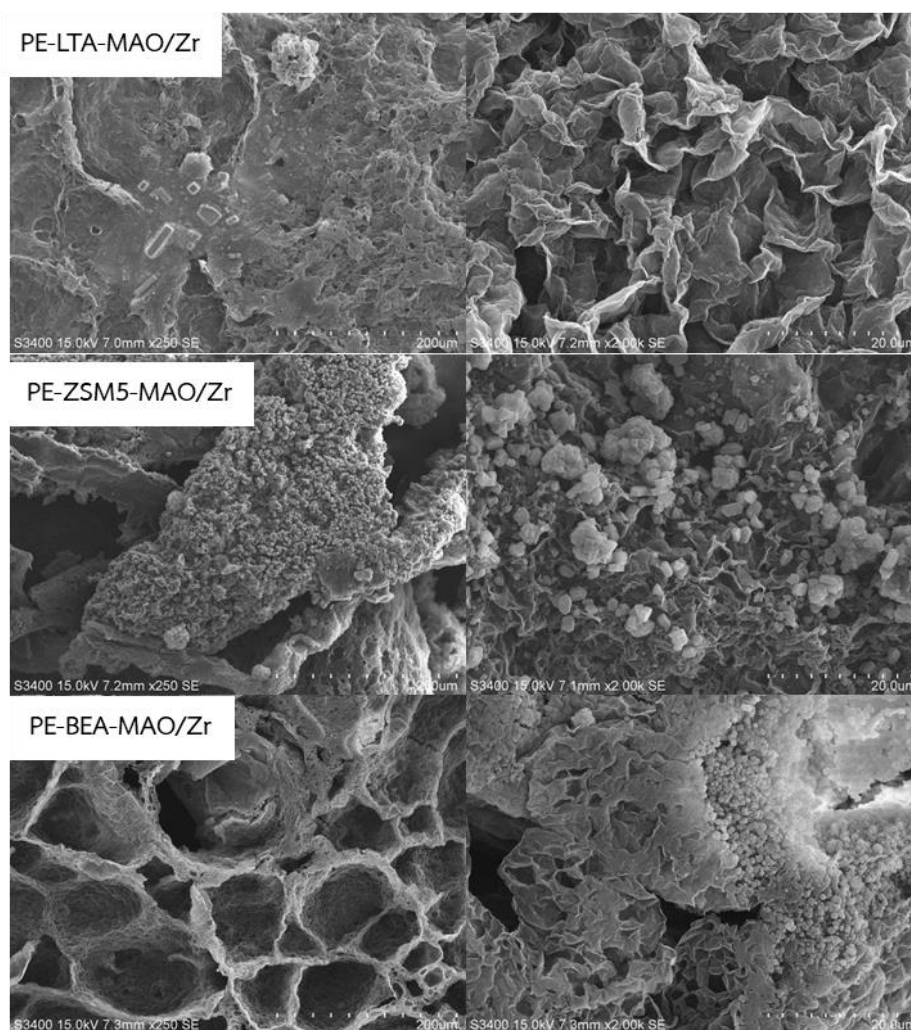


**Figure 47** Morphology and element distribution of polyethylene produced via various zeolite supported catalyst.

The polyethylene produced by the zeolite after immobilization with catalyst was investigated by SEM images showing that the particles of the produced polymer

were agglomerated like cornflowers and had large spheroidal lumps. The particles of polyethylene in LTA-MAO/Zr had the largest size, followed by polyethylene in ZSM5-MAO/Zr and BEA-MAO/Zr, respectively. In addition, with the low yield of polyethylene in ZSM 5-MAO/Zr and BEA-MAO/Zr. it can be seen hollow polyethylene, which occurs when the few polyethylene chains cannot agglomerate into solid polymers.

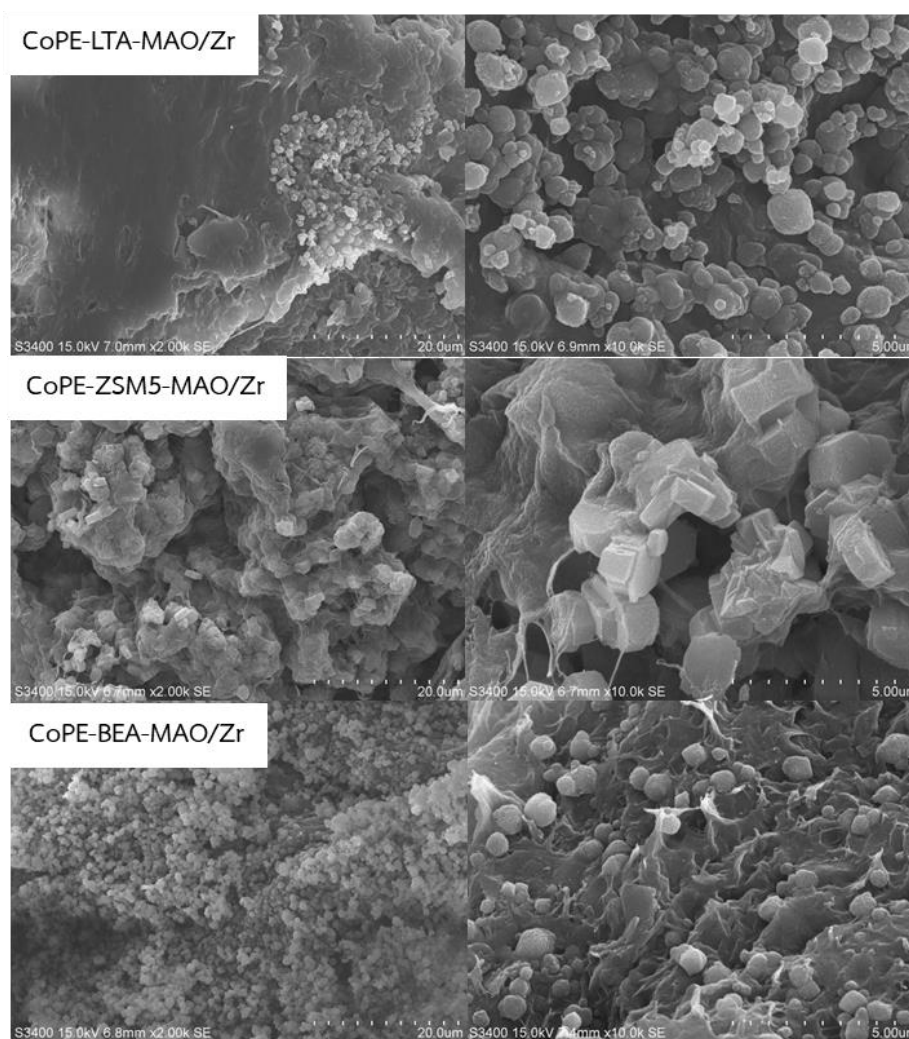


**Figure 48** Morphology and element distribution of ethylene/1-hexene copolymer produced via various zeolite supported catalyst.

For the copolymerization system, the morphology of the ethylene/1-hexene copolymer was produced by various zeolite supported catalysts that had large

lumps. The texture of the copolymer was semisolid-like copolymer from a homogeneous system coated support. However, the morphology of the ethylene/1-hexene copolymer formed by the three zeolite-supported catalyst is quite similar to that of the catalyst precursor.

#### 4.3.3.2 X-ray Diffraction (XRD)

The XRD technique was used to characterize the crystalline structures of all the obtained polymers, as shown in Figure 49. The XRD patterns of obtained polyethylene were similar, demonstrating two peaks of  $21.3^\circ$  and  $23.7^\circ$ , which conform to the orthorhombic crystalline structure of polyethylene [80]. Polyethylene from LTA-MAO/Zr had more crystallinity when compared to polyethylene from other zeolite supported catalysts. The XRD patterns of polyethylene produced by various zeolite supported catalysts confirmed that the zeolite was used as a support for the immobilization of MAO/zirconocene as a catalyst for ethylene polymerization.

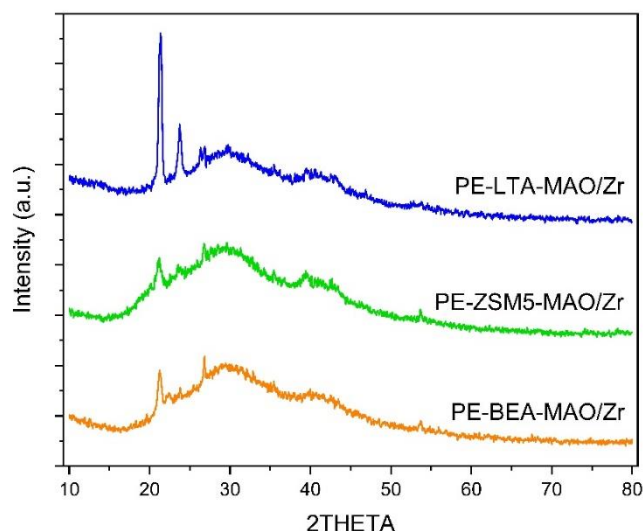


**Figure 49** XRD patterns of polyethylene from various zeolite-supported MAO/zirconocene catalytic system

Noted : Copolymer is not determined.

#### 4.3.3.3 Thermal gravimetric analysis differential scanning calorimetry (TGA-DSC)

The obtained polyethylene from zeolite immobilized MAO/zirconocene catalysts were determined the melting temperature ( $T_m$ ) and crystallinity ( $\chi_c$ ) by TGA-DSC technique that was used for this purpose, as shown in Table 28. The melting point of polyethylene is somewhere in the range of 130 to 133 °C. In comparison to PE-ZSM5/Zr and PE-BEA-MAO/Zr, the melting temperature of PE-LTA-MAO/Zr was the greatest. As a result, no significant difference in melting temperature was observed for all polymers. On the other hand, it was found that the crystallinity values of these polyethylene depending on the type of zeolite supported catalysts. PE-ZSM5-MAO/Zr exhibited the highest crystallinity, followed by PE-LTA-MAO/Zr and PE-BEA-MAO/Zr, respectively. It suggested that the various catalysts supported by zeolite influenced the polymer crystallization.

**Table 28** Melting temperature and crystallization behaviors of polyethylene and copolymers produced from LTA support immobilization.

Run	Polymers	Melting temperature <sup>a</sup> (°C)	$\Delta H_{exp}$ <sup>b</sup> (J/g)	Crystallinity <sup>a</sup> (% $\chi_c$ )
1	PE-LTA-MAO/Zr	133.14	130.00	45.45
2	PE-ZSM5-MAO/Zr	132.26	164.70	57.59
3	PE-BEA-MAO/Zr	130.47	125.55	43.90
4	CoPE-LTA-MAO/Zr	n.d.	n.d.	n.d.
5	CoPE-ZSM5-MAO/Zr	n.d.	n.d.	n.d.
6	CoPE-BEA-MAO/Zr	n.d.	n.d.	n.d.

<sup>a</sup> Melting temperature ( $T_m$ ) measured by DSC measurement.

<sup>b</sup> Heat of fusion ( $\Delta H_{exp}$ ) measured by DSC measurement.

<sup>c</sup> Crystallinity ( $\chi_c$ ) was calculated from the equation; %crystallinity= $(\Delta H_{sample}/\Delta H_{100\% \text{ crystallinity}}) \times 100$ , the  $\Delta H_{100\% \text{ crystallinity}}$  of polyethylene is 286 J/g.

n.d. = not determined

## CHAPTER 5

### Conclusion

#### 5.1 Conclusion

Part 1 is the preliminary study (4.1), which determines the effect of different immobilized MAO cocatalyst and zirconocene catalyst methods on silica support. It was found that immobilization MAO first, followed by the metallocene catalyst method, increased Al/Zr content on silica support and catalyst activity. SMAO/Zr can produce a "crown-alumoxane complex" to stabilize the anion, preventing the process from terminating more than other methods. Produced polymer having a greater morphology when compared to a homogeneous system. The polymer had agglomerates, and the shape of the polymer was quite spherical.

In Part 2 (4.2), zeolite A supported MAO/Zr by varying temperature,  $[Al]_{MAO}/[Zr]_{cat}$  molar ratios and  $[Al]_{TMA}/[Zr]_{cat}$  ratios at fixed temperature, and  $[Al]MAO/[Zr]_{cat}$  constants for ethylene polymerization were determined. The activity of LTA-MAO/Zr catalysts increased with increasing  $[Al]MAO/[Zr]_{cat}$  molar ratios and temperature, but when they reached the optimum point, catalyst activity decreased. The suitable conditions for polyethylene polymerization are 80°C and  $[Al]MAO/[Zr]_{cat}$  molar ratios equal to 2000. Therefore, the addition of TMA to LTA-MAO/Zr catalysts slightly increased catalytic activity. This is because added TMA can reduce the amount of impurities, leading to an increase in activity. In addition, comparison of ethylene and ethylene/1-hexene polymerization with LTA-MAO/Zr showed that the catalyst activity of copolymerization was higher than ethylene polymerization because of the commoner effect. However, the catalyst activity of the two systems was slightly different, indicating copolymerization conditions were not optimal. Although, LTA-MAO/Zr had lower catalyst activity than silica supported catalysts, the acidity of LTA support can disrupt the formation of polymer chains and reduce crystallinity. LTA support is produced from fly ash that can be used to

support metallocene. It can produce polyethylene and ethylene/1-hexene copolymerization. The obtained polymer had morphology and thermal properties quite similar to those of polymers from silica supported catalysts that are benchmarked in the present.

In the last part (4.3), immobilization of MAO and zirconocene onto three zeolite supports for ethylene polymerization and ethylene/1-hexene copolymerization at 80°C and  $[Al]_{MAO}/[Zr]_{cat} = 2000$ . It was found that LTA-MAO/Zr has higher catalytic activities than ZSM5 and BEA support, respectively because of the higher Al/Zr ratio on the LTA support than other zeolite supports, and the LTA had the highest acidity of Lewis acid, which directly correlated with the activity of the catalysts. However, we cannot conclude that high acidity from zeolite support leads to high catalyst activity in which it depends on many factors that are superimposed on each other. In this study, LTA support was an optimally supported metallocene catalyst system that probably had suitable textural properties and acidity.

## 5.2 Recommendations

- To determine various temperature on ethylene/1-hexene copolymerization with LTA-supported metallocene catalyst.
- To determine various acidity of LTA support, for example added some acid before immobilizing with cocatalyst/catalyst on support.
- To determine additive of pretreatment LTA before using supported metallocene catalyst for higher catalyst activity such as adding Spacer groups for better dispend of active site.
- To determine various reaction time on ethylene/1-hexene copolymerization with LTA-supported metallocene catalyst.





จุฬาลงกรณ์มหาวิทยาลัย  
**CHULALONGKORN UNIVERSITY**

## REFERENCES

1. Global Polyethylene Market: Analysis By Demand, By Production, By Product Density, By Application, By Region Size & Forecast with Impact Analysis of COVID-19 and Forecast up to 2027. Research and markets; 2022.
2. McCartney I. 2019. Available from: <https://kempner.co.uk/2019/05/08/the-advantages-and-disadvantages-of-polyethylene-blog/>.
3. Patel R, Jain P, Story B, Chum S. Polyethylene: An Account of Scientific Discovery and Industrial Innovations. 10002008. p. 71-102.
4. Ronca S. Chapter 10 - Polyethylene. In: Gilbert M, editor. Brydson's Plastics Materials (Eighth Edition): Butterworth-Heinemann; 2017. p. 247-78.
5. Jongsomjit B. Development of linear low-density polyethylene synthesis using supported metallocene catalysts. 2009.
6. Chadwick JC, Garoff T, Severn JR. Traditional Heterogeneous Catalysts. Tailor-Made Polymers 2008. p. 43-78.
7. Ciardelli F, Altomare A, Michelotti M. From homogeneous to supported metallocene catalysts. Catalysis Today. 1998;41(1):149-57.
8. Covarrubias C, Quijada R. High catalytic activity of SBA-15-supported metallocene toward ethylene polymerization: The effect of the ordered porous structure of the support. Catalysis Communications. 2009;10(6):995-1001.
9. Abdul Kaleel SH, Kottukkal Bahuleyan B, De SK, Jabarulla Khan M, Sougrat R, Al-Harhi MA. Effect of Mn doped-titania on the activity of metallocene catalyst by in situ ethylene polymerization. Journal of Industrial and Engineering Chemistry. 2012;18(5):1836-40.
10. Silveira F, Alves MdCM, Stedile FC, Pergher SB, dos Santos JHZ. Microporous and mesoporous supports and their effect on the performance of supported metallocene catalysts. Journal of Molecular Catalysis A: Chemical. 2010;315(2):213-20.
11. Thailand EGAo. Power Plants & Dams 2022 [Available from: <https://www.egat.co.th/home/en/powerplants-and-dams/>].
12. Ferreira C, Ribeiro A, Ottosen L. Possible applications for municipal solid waste

fly ash. *Journal of Hazardous Materials*. 2003;96(2):201-16.

13. Iqbal RM, Alyatikah E, Toepak EP, Rasidah R, Tambunan LR, Siswo S, et al. Chemical characteristic of fly ash from 3 Kalimantan's power plants as potential source for synthesis of aluminosilicate-based material. *AIP Conference Proceedings*. 2021;2349(1):020011.

14. Zhu M, An X, Gui T, Wu T, Li Y, Chen X. Effects of ion-exchange on the pervaporation performance and microstructure of NaY zeolite membrane. *Chinese Journal of Chemical Engineering*. 2023.

15. Michelotti M, Arribas G, Bronco S, Altomare A. Effect of the zeolite HY-support on the monoalkene polymerization by group IV metallocenes. *Journal of Molecular Catalysis A: Chemical*. 2000;152(1):167-77.

16. Marques MdFV, Moreira SC. ZSM-5 acid zeolite supported metallocene catalysts for ethylene polymerization. *Journal of Molecular Catalysis A: Chemical*. 2003;192(1):93-101.

17. Yu F, Zhang C, Geng R, Zhou H, Dong Q, Liu S, et al. Hydrocracking of naphthalene over Beta zeolite coupled with NiMo/ $\gamma$ -Al<sub>2</sub>O<sub>3</sub>: Investigation of metal and acid balance based on the composition of industrial hydrocracking catalyst. *Fuel*. 2023;344:128049.

18. Indira V, Abhitha K. A review on recent developments in Zeolite A synthesis for improved carbon dioxide capture: Implications for the water-energy nexus. *Energy Nexus*. 2022;7:100095.

19. Zahmakiran M. Preparation and characterization of LTA-type zeolite framework dispersed ruthenium nanoparticles and their catalytic application in the hydrolytic dehydrogenation of ammonia-borane for efficient hydrogen generation. *Materials Science and Engineering: B*. 2012;177(8):606-13.

20. Đặng T-H, Chen B-H, Lee D-J. Optimization of biodiesel production from transesterification of triolein using zeolite LTA catalysts synthesized from kaolin clay. *Journal of the Taiwan Institute of Chemical Engineers*. 2017;79:14-22.

21. Cheong Y-W, Wong K-L, Ooi BS, Ling TC, Khoerunnisa F, Ng E-P. Effects of Synthesis Parameters on Crystallization Behavior of K-MER Zeolite and Its Morphological

Properties on Catalytic Cyanoethylation Reaction. Crystals [Internet]. 2020; 10(2).

22. Rozhkovskaya A, Rajapakse J, Millar GJ. Synthesis of high-quality zeolite LTA from alum sludge generated in drinking water treatment plants. Journal of Environmental Chemical Engineering. 2021;9(2):104751.

23. Zhou X, Miao G, Xu G, Luo J, Yang C, Xiao J. Mixed (Ag<sup>+</sup>, Ca<sup>2+</sup>)-LTA zeolite with suitable pore feature for effective separation of C<sub>3</sub>H<sub>6</sub>/C<sub>3</sub>H<sub>8</sub>. Chemical Engineering Journal. 2022;450:137913.

24. Huang A, Wang N, Caro J. Synthesis of multi-layer zeolite LTA membranes with enhanced gas separation performance by using 3-aminopropyltriethoxysilane as interlayer. Microporous and Mesoporous Materials. 2012;164:294-301.

25. Sun T, Wei J, Zhou C, Wang Y, Shu Z, Zhou J, et al. Facile preparation and enhanced photocatalytic hydrogen evolution of cation-exchanged zeolite LTA supported TiO<sub>2</sub> photocatalysts. International Journal of Hydrogen Energy. 2023.

26. Qian K, Li L, Chen P, Xiu Y, E Y, Gies H. Copper-nickel doped LTA zeolite as a high- efficiency methanol oxidation reaction catalyst in alkaline solution. International Journal of Hydrogen Energy. 2021;46(46):23898-905.

27. Britannica E. Polyethylene | Properties, Structures, Uses, & Facts 2022 [Available from: <https://www.britannica.com/science/polyethylene>].

28. Portal PGP. Properties and uses of polyethylene in industry and in households - PCC Group Product Portal 2022 [Available from: <https://www.products.pcc.eu/en/blog/properties-and-uses-of-polyethylene-in-industry-and-in-households/>].

29. Peacock A. Handbook of Polyethylene Structures: Properties, and Applications. Boca Raton: 2000.

30. Introduction to Polymers of Ethylene. Introduction to Industrial Polyethylene 2010. p. 1-22.

31. Jeremic D. Polyethylene. Ullmann's Encyclopedia of Industrial Chemistry. p. 1-42.

32. Kashiwa N, Imuta J-i. Recent progress on olefin polymerization catalysts. Catalysis Surveys from Asia. 1997;1(1):125-42.

33. Introduction to Polyolefins. Polyolefin Reaction Engineering 2012. p. 1-13.

34. Kaminsky W. Metallocene catalysts for olefin polymerization. In: Hattori H, Otsuka K, editors. *Studies in Surface Science and Catalysis*. 121: Elsevier; 1999. p. 3-12.
35. Kaminsky W. Highly active metallocene catalysts for olefin polymerization. *Journal of the Chemical Society, Dalton Transactions*. 1998(9):1413-8.
36. *Polymerization Catalysis and Mechanism. Polyolefin Reaction Engineering* 2012. p. 53-86.
37. Gupta VK, Satish S, Bhardwaj IS. Metallocene Complexes of Group 4 Elements in the Polymerization of Monoolefins. *Journal of Macromolecular Science, Part C*. 1994;34(3):439-514.
38. Naga N, Imanishi Y. Copolymerization of Ethylene and Cyclopentene with Zirconocene Catalysts: Effect of Ligand Structure of Zirconocenes. *Macromolecular Chemistry and Physics*. 2002;203(1):159-65.
39. Miri M, Pritchard B, Cheng H. A versatile approach for modeling and simulating the tacticity of polymers. *Journal of molecular modeling*. 2010;17:1767-80.
40. Chien JCW, Wang B-P. Metallocene–methylaluminoxane catalysts for olefin polymerization. I. Trimethylaluminum as coactivator. *Journal of Polymer Science Part A: Polymer Chemistry*. 1988;26(11):3089-102.
41. Yang X, Stern CL, Marks TJ. Cation-like homogeneous olefin polymerization catalysts based upon zirconocene alkyls and tris(pentafluorophenyl)borane. *Journal of the American Chemical Society*. 1991;113(9):3623-5.
42. Pauer W, Dube B, Hungenberg KDDCD, Lei EJCKL, Li B-G, McKenna TFL, et al. *Polymer Reaction Engineering of Dispersed Systems: Volume I. Polymer Reaction Engineering of Dispersed Systems*. 2018.
43. Zijlstra HS, Harder S. Methylalumoxane – History, Production, Properties, and Applications. *European Journal of Inorganic Chemistry*. 2015;2015(1):19-43.
44. Nguyen HMT, Tang H-Y, Huang W-F, Lin MC. Mechanisms for reactions of trimethylaluminum with molecular oxygen and water. *Computational and Theoretical Chemistry*. 2014;1035:39-43.
45. Ortega DE, Matute RA, Toro-Labbé A. Exploring the Nature of the Energy Barriers on the Mechanism of the Zirconocene-Catalyzed Ethylene Polymerization: A Quantitative Study from Reaction Force Analysis. *The Journal of Physical Chemistry C*.

2020;124(15):8198-209.

46. Resconi LM, Camurati I, Sudmeijer O. Chain transfer reactions in propylene polymerization with zirconocene catalysts. *Topics in Catalysis*. 1999;7:145-63.
47. Chien JCW. Supported metallocene polymerization catalysis. *Topics in Catalysis*. 1999;7(1):23-36.
48. Hlatky GG. Heterogeneous Single-Site Catalysts for Olefin Polymerization. *Chemical Reviews*. 2000;100(4):1347-76.
49. Tumawong P, Chaichana E, Jongsomjit B. Effect of Immobilization Methods on the Production of Polyethylene-cellulose Biocomposites via Ethylene Polymerization with Metallocene/MAO Catalyst. *Bulletin of Chemical Reaction Engineering & Catalysis*. 2020;15:752-64.
50. Maesen T. Chapter 1 - The Zeolite Scene – An Overview. In: Čejka J, van Bekkum H, Corma A, Schüth F, editors. *Studies in Surface Science and Catalysis*. 168: Elsevier; 2007. p. 1-12.
51. Guisnet M, Gilson J-P. Zeolites for Cleaner Technologies 2005.
52. McCusker LB, Baerlocher C. Chapter 2 - Zeolite Structures. In: Čejka J, van Bekkum H, Corma A, Schüth F, editors. *Studies in Surface Science and Catalysis*. 168: Elsevier; 2007. p. 13-37.
53. Database of Zeolite Structures: Database of Zeolite Structures; [Available from: <http://www.iza-structure.org/databases/>].
54. Garcia Mendoza JG. Synthesis and applications of low silica zeolites from bolivian clay and diatomaceous earth: Luleå University of Technology; 2017.
55. Sadeghbeigi R. Chapter 4 - FCC Catalysts. In: Sadeghbeigi R, editor. *Fluid Catalytic Cracking Handbook (Third Edition)*. Oxford: Butterworth-Heinemann; 2012. p. 87-115.
56. Mohd Nazir LS, Yeong YF, Chew TL. Methods and synthesis parameters affecting the formation of FAU type zeolite membrane and its separation performance: a review. *Journal of Asian Ceramic Societies*. 2020;8:1-19.
57. Sowunmi A, Folayan CO, Anafi F, Ajayi O, Omisanya NO, Obada D, et al. Dataset on the comparison of synthesized and commercial zeolites for potential solar adsorption refrigerating system. *Data in Brief*. 2018;20.

58. Bok TO, Andriako EP, Knyazeva EE, Ivanova II. Engineering of zeolite BEA crystal size and morphology via seed-directed steam assisted conversion. *RSC Advances*. 2020;10(63):38505-14.
59. Khaleque A, Alam MM, Hoque M, Mondal S, Haider JB, Xu B, et al. Zeolite synthesis from low-cost materials and environmental applications: A review. *Environmental Advances*. 2020;2:100019.
60. Kaminsky W. Zirconocene catalysts for olefin polymerization. *Catalysis Today*. 1994;20(2):257-71.
61. Kleinschmidt R, van der Leek Y, Reffke M, Fink G. Kinetics and mechanistic insight into propylene polymerization with different metallocenes and various aluminium alkyls as cocatalysts. *Journal of Molecular Catalysis A: Chemical*. 1999;148(1):29-41.
62. Michiels W, Muñoz-Escalona A. Mixed cocatalyst systems in metallocene ethylene polymerization. *Macromolecular Symposia*. 1995;97(1):171-83.
63. Jongsomjit B, Panpranot J, Okada M, Shiono T, Praserttham P. Characteristics of LLDPE/ZrO<sub>2</sub> Nanocomposite Synthesized by In-situ Polymerization using a Zirconocene/MAO Catalyst. *Iranian Polymer Journal*. 2006;15:433-9.
64. Lee DH, Jung HK, Kim WS, Min KE, Park LS, Seo KH, et al. Copolymerization of ethylene and cycloolefin with metallocene catalysts : I. Effect of catalyst. 2000;24.
65. Manianglung C, Lee JS, Ko YS. Olefin polymerization behavior of metallocene immobilized inside pore of metal-organic frameworks. *Catalysis Today*. 2023;411-412:113893.
66. Al-dahri T, AbdulRazak AA, Rohani S. Preparation and characterization of Linde-type A zeolite (LTA) from coal fly ash by microwave-assisted synthesis method: its application as adsorbent for removal of anionic dyes. *International Journal of Coal Preparation and Utilization*. 2022;42(7):2064-77.
67. Waseem M, Mustafa S, Naeem A, Shah K, Shah I. Mechanism of Cd (II) sorption on silica synthesized by sol-gel method. *Chemical Engineering Journal*. 2011;169:78-83.
68. Van Grieken R, Carrero A, Suarez I, Paredes B. Ethylene polymerization over supported MAO/(nBuCp)<sub>2</sub>ZrCl<sub>2</sub> catalysts: Influence of support properties. *European Polymer Journal*. 2007;43(4):1267-77.

69. Fisch A, Petry C, Pozebon D, Stedile F, Cardozo N, Secchi A, et al. Immobilization of Zirconocene into Silica Prepared by Non-Hydrolytic Sol-Gel Method. *Macromolecular Symposia*. 2006;245-246:77-86.
70. Zhou A, Zhang Y, Shi Y, Xu Q. Integrated synthesis of metallocene-supported catalysts based on glyphosate and its zirconium derivatives. *RSC Advances*. 2017;7(88):55866-73.
71. Ribeiro MR, Deffieux A, Portela MF. Supported Metallocene Complexes for Ethylene and Propylene Polymerizations: Preparation and Activity. *Industrial & Engineering Chemistry Research*. 1997;36(4):1224-37.
72. Menad K, Feddag A, Rubenis K. Synthesis and study of calcination temperature influence on the change of structural properties of the LTA zeolite. 2016;9:788-97.
73. Fan Y, Huang R, Liu Q, Cao Q, Guo R. Synthesis of zeolite A from fly ash and its application in the slow release of urea. *Waste Management*. 2023;158:47-55.
74. Robson H. Preface to the second edition. In: Robson H, Lillerud KP, editors. *Verified Syntheses of Zeolitic Materials*. Amsterdam: Elsevier Science; 2001. p. 1.
75. Prasetyo T, Soegijono B. Characterization of sonicated natural zeolite/ferric chloride hexahydrate by infrared spectroscopy. *Journal of Physics: Conference Series*. 2018;985:012022.
76. Mozgawa W, Król M, Barczyk K. FT-IR studies of zeolites from different structural groups. *Chemik*. 2011;65:667-74.
77. Guan Z, Zheng Y, Jiao S. Spherical MgCl<sub>2</sub>-supported MAO pre-catalysts: preparation, characterization and activity in ethylene polymerization. *Journal of Molecular Catalysis A: Chemical*. 2002;188(1):123-31.
78. Meshkova IN, Ushakova TM, Ladygina TA, Kovaleva NY, Novokshonova LA. Ethylene polymerization with catalysts on the base of Zr-cenes and methylaluminoxanes synthesized on zeolite support. *Polymer Bulletin*. 2000;44(5):461-8.
79. Yang H, Zhang L, Fu Z, Fan Z. Comonomer effects in copolymerization of ethylene and 1-hexene with MgCl<sub>2</sub>-supported Ziegler-Natta catalysts: New evidences from active center concentration and molecular weight distribution. *Journal of Applied*



Polymer Science. 2015;132(2).

80. Kuo S-W, Huang W-J, Huang S-B, Kao H-C, Chang F-C. Syntheses and characterizations of in situ blended metallocene polyethylene/clay nanocomposites. *Polymer*. 2003;44(25):7709-19.

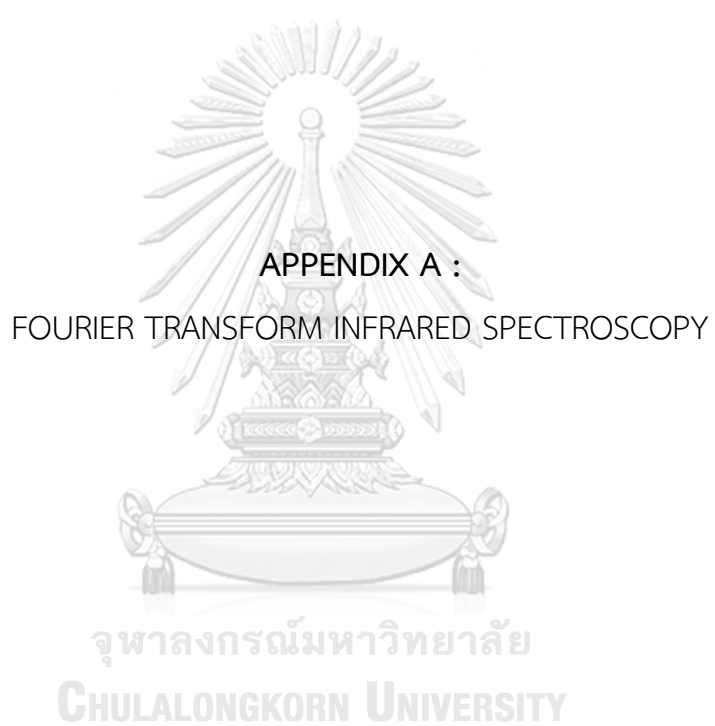
81. Kaewkrajang P. Copolymerization of ethylene/alpha-olefins on the supported zirconocene catalyst. Chulalongkorn university; 2002.

82. Chaichana E, Jongsomjit B, Praserttham P. Effect of nano-SiO<sub>2</sub> particle size on the formation of LLDPE/SiO<sub>2</sub> nanocomposite synthesized via the in situ polymerization with metallocene catalyst. *Chemical Engineering Science*. 2007;62(3):899-905.

83. Shirazi L, Jamshidi E, Ghasemi MR. The effect of Si/Al ratio of ZSM-5 zeolite on its morphology, acidity and crystal size. *Crystal Research and Technology*. 2008;43(12):1300-6.

84. Byrappa K, Kumar BVS. Characterization of zeolites by infrared spectroscopy. *Asian Journal of Chemistry*. 2007;19:4933-5.

85. Velthoen MEZ, Muñoz-Murillo A, Bouhmadi A, Cecius M, Diefenbach S, Weckhuysen BM. The Multifaceted Role of Methylaluminoxane in Metallocene-Based Olefin Polymerization Catalysis. *Macromolecules*. 2018.



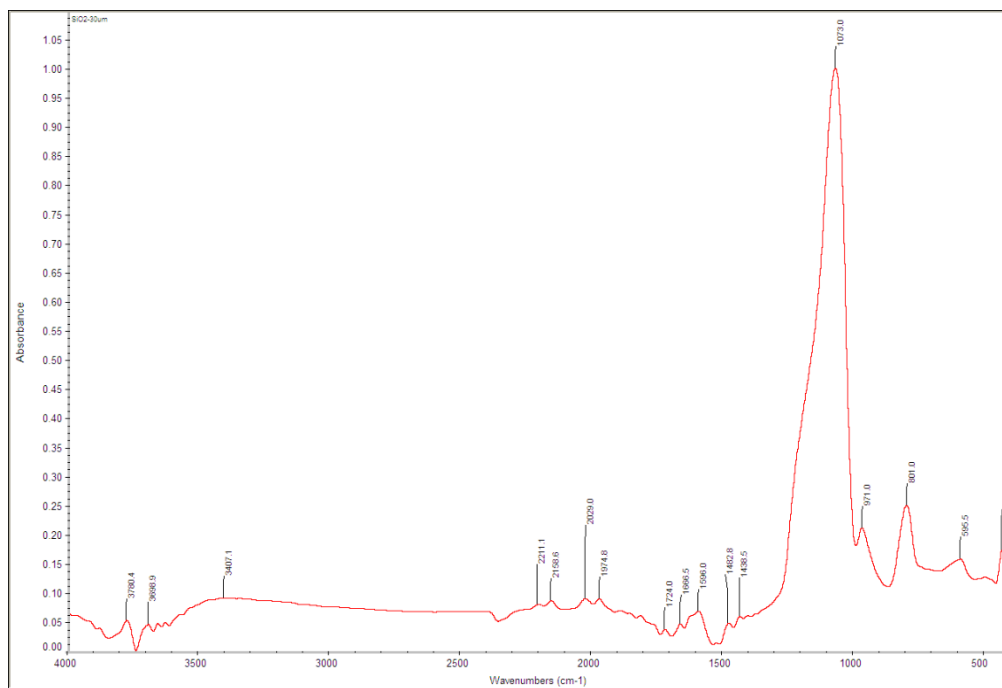


Figure A-1 FT-IR of silica support

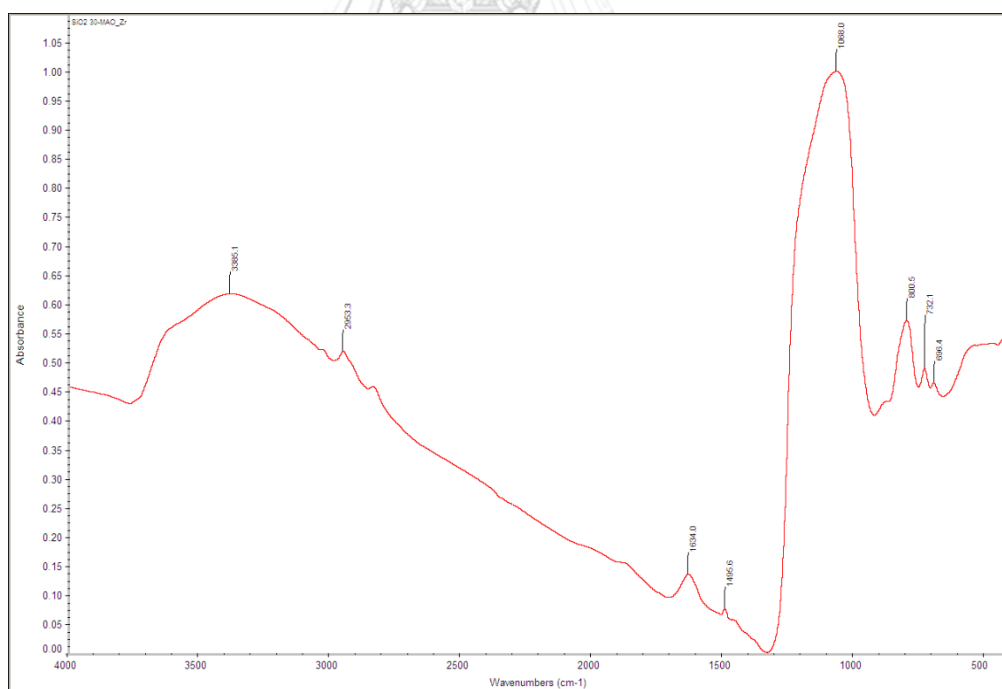


Figure A-2 FT-IR of silica support after immobilization with catalyst and MAO (SMAO/Zr)

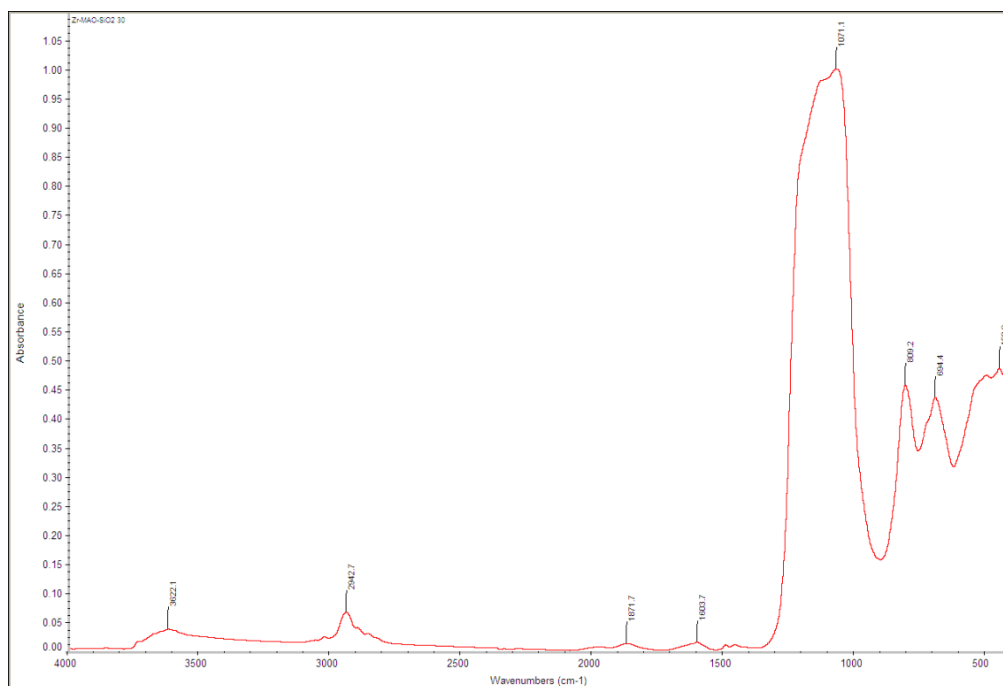


Figure A-3 FT-IR of silica support after immobilization with catalyst and MAO (SMix)

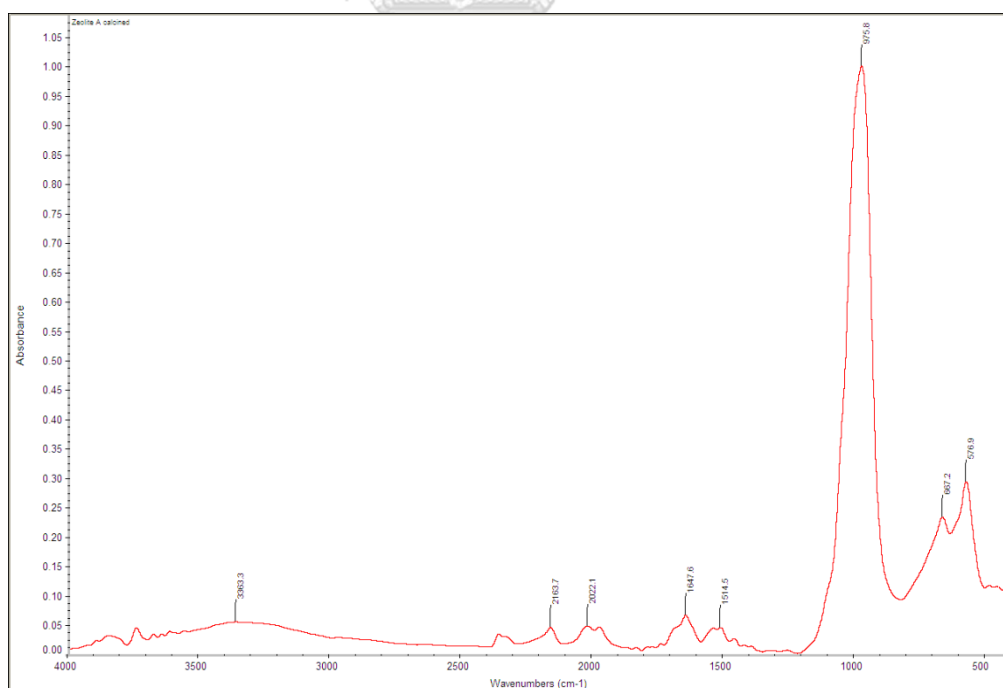


Figure A-4 FT-IR of zeolite A support (LTA)

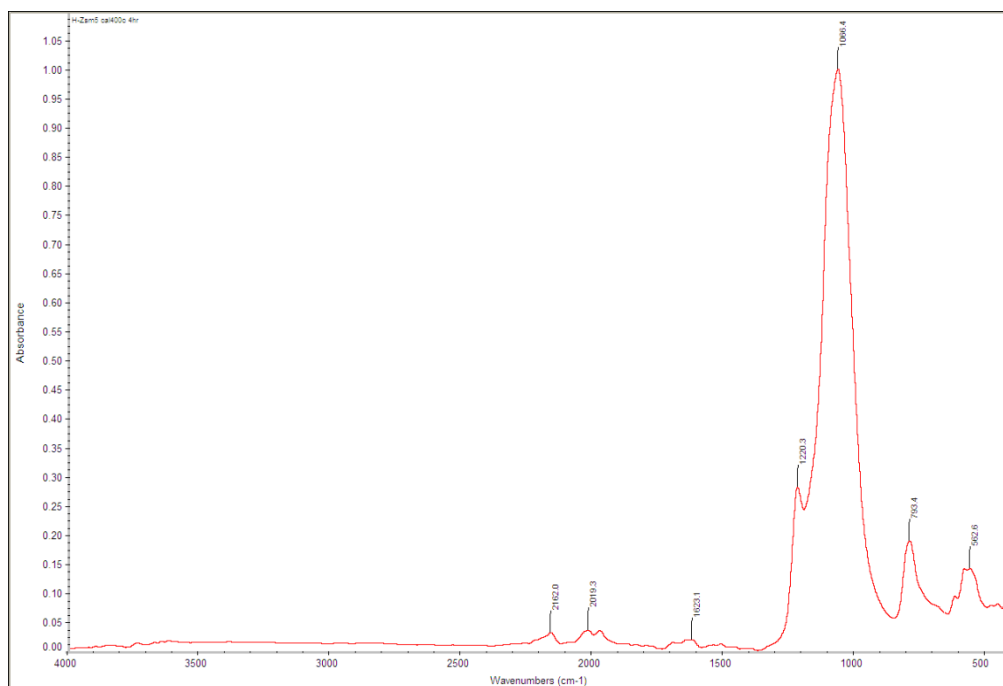


Figure A-5 FT-IR of ZSM5 support

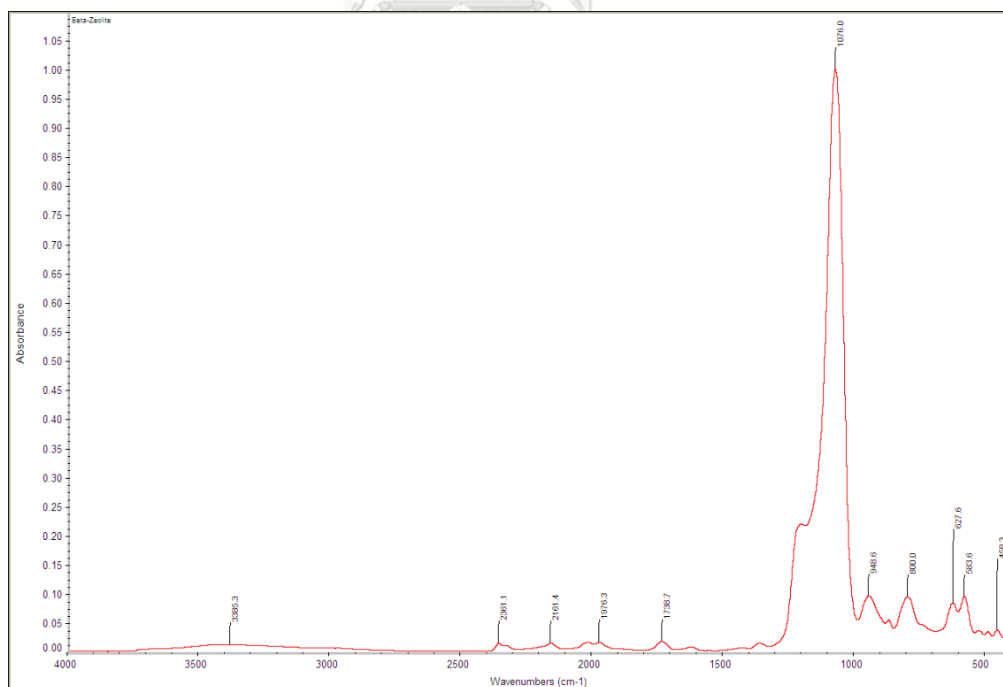


Figure A-6 FT-IR of beat zeolite support (BEA)

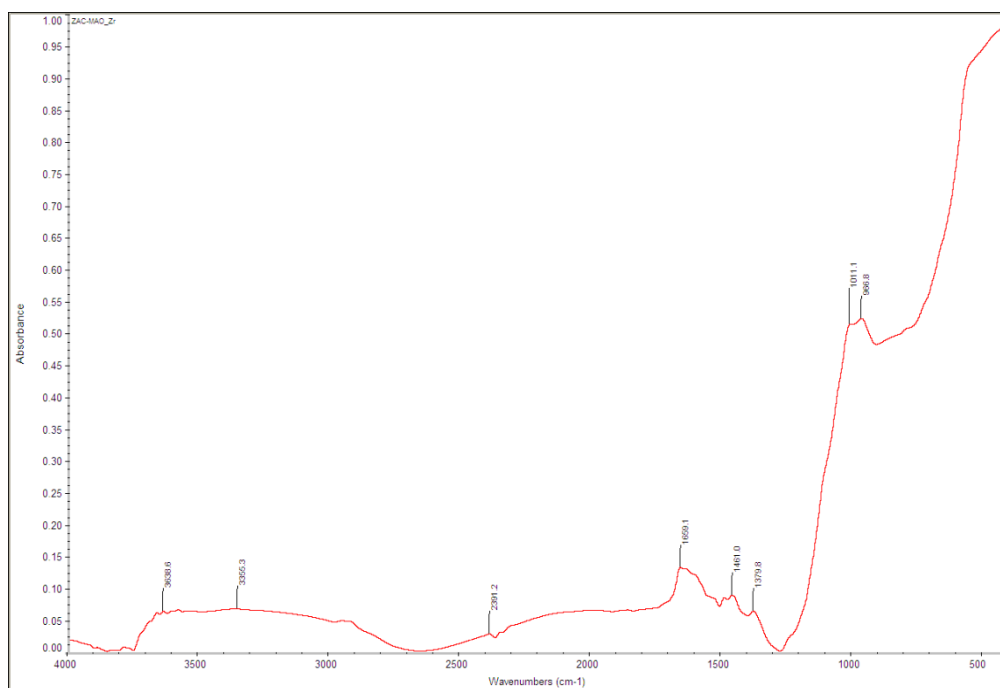


Figure A-7 FT-IR of zeolite A support after immobilization with catalyst and MAO (LTA-MAO/Zr)

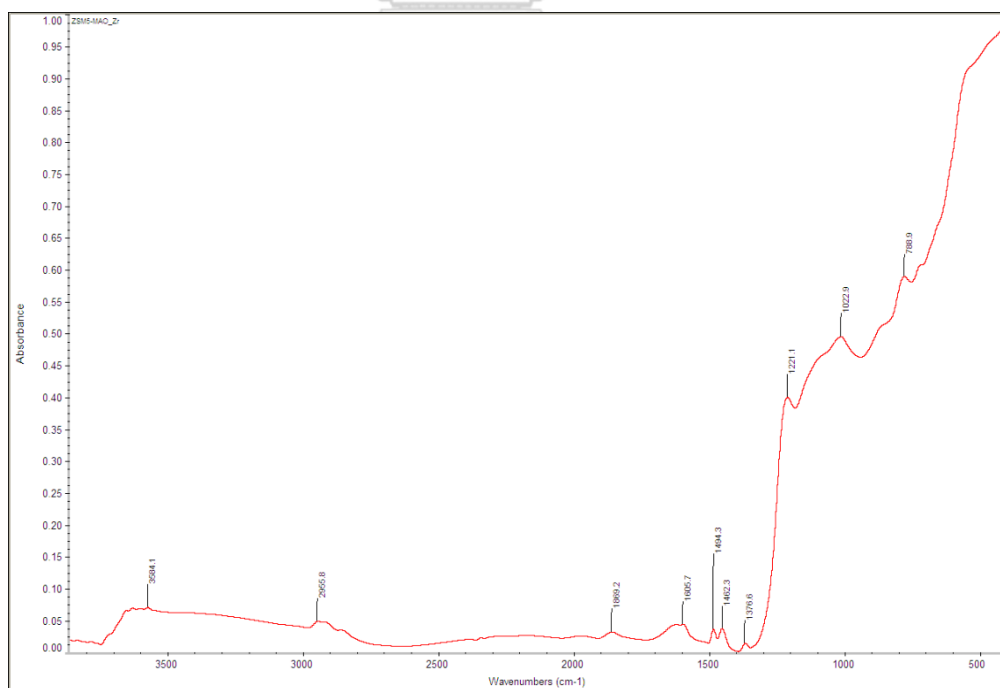


Figure A-8 FT-IR of ZSM5 support after immobilization with catalyst and MAO (ZSM5-MAO/Zr)

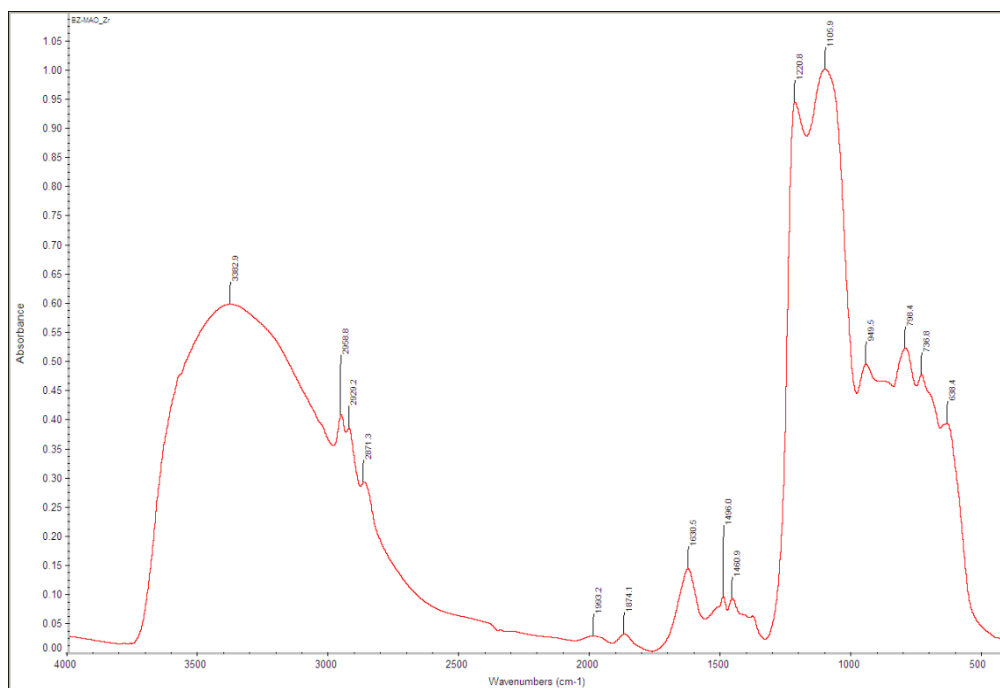


Figure A-9 FT-IR of beta zeolite support after immobilization with catalyst and MAO (BEA-MAO/Zr)

**APPENDIX B :**  
THERMAL GRAVIMETRIC ANALYSIS AND DIFFERENTIAL SCANNING  
CALORIMETRY



จุฬาลงกรณ์มหาวิทยาลัย  
**CHULALONGKORN UNIVERSITY**



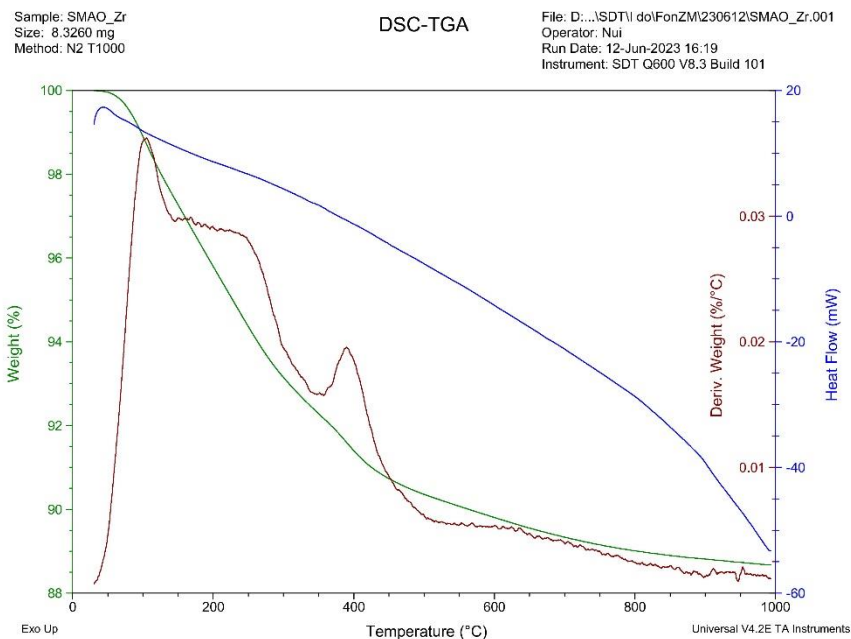


Figure B-1 TGA of silica support after immobilization with catalyst and MAO (SMAO/Zr)

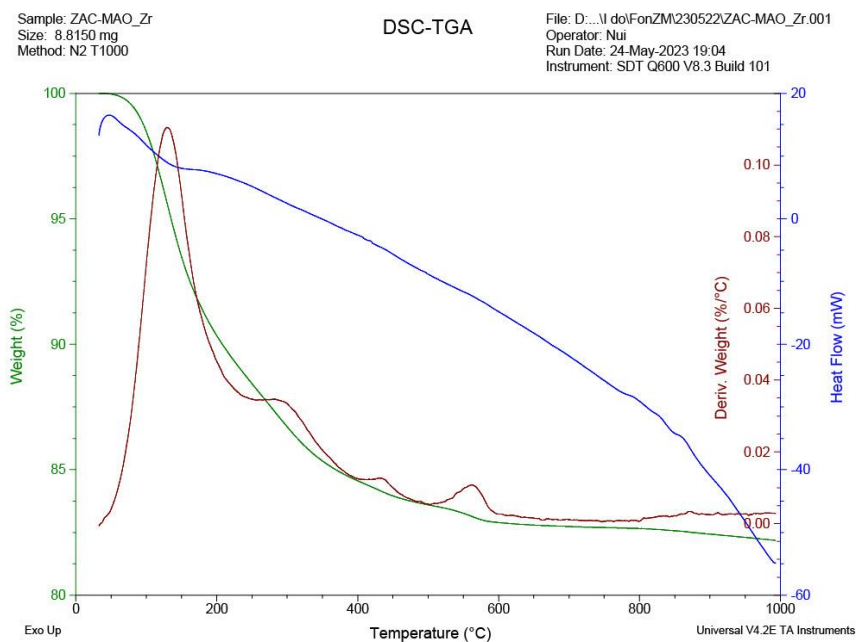


Figure B-2 TGA of zeolite A support after immobilization with catalyst and MAO (LTA-MAO/Zr)

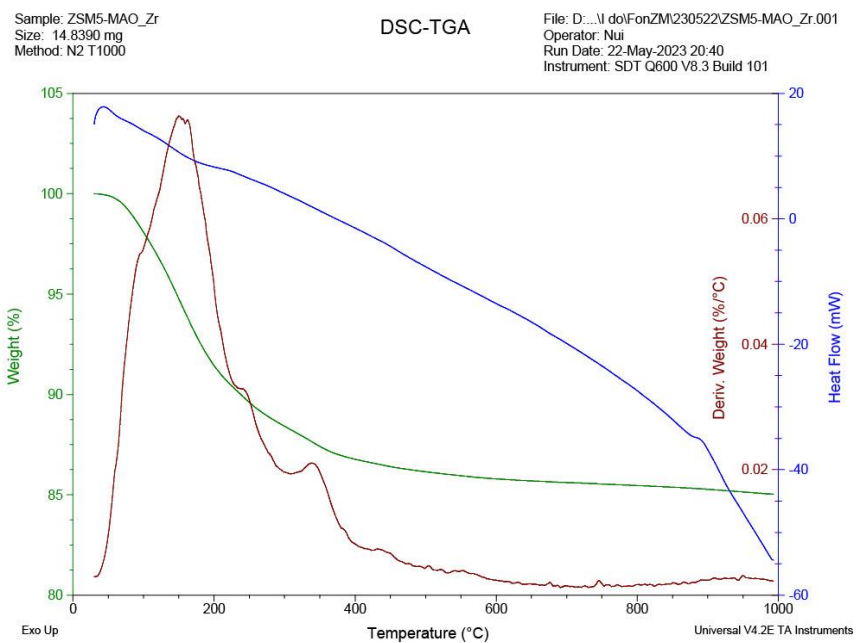


Figure B-3 TGA of ZSM5 support after immobilization with catalyst and MAO (ZSM5-MAO/Zr)

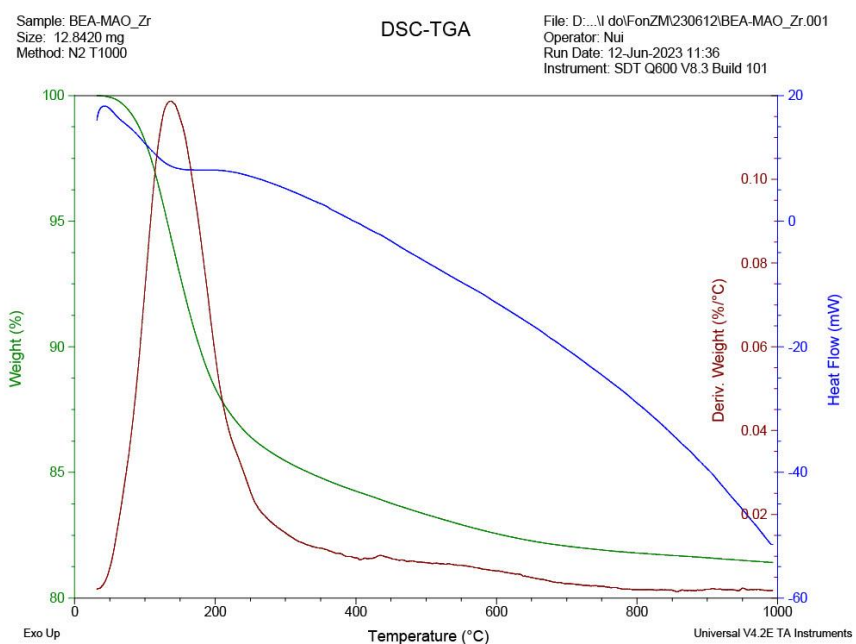


Figure B-4 TGA of beta zeolite support after immobilization with catalyst and MAO (BEA-MAO/Zr)

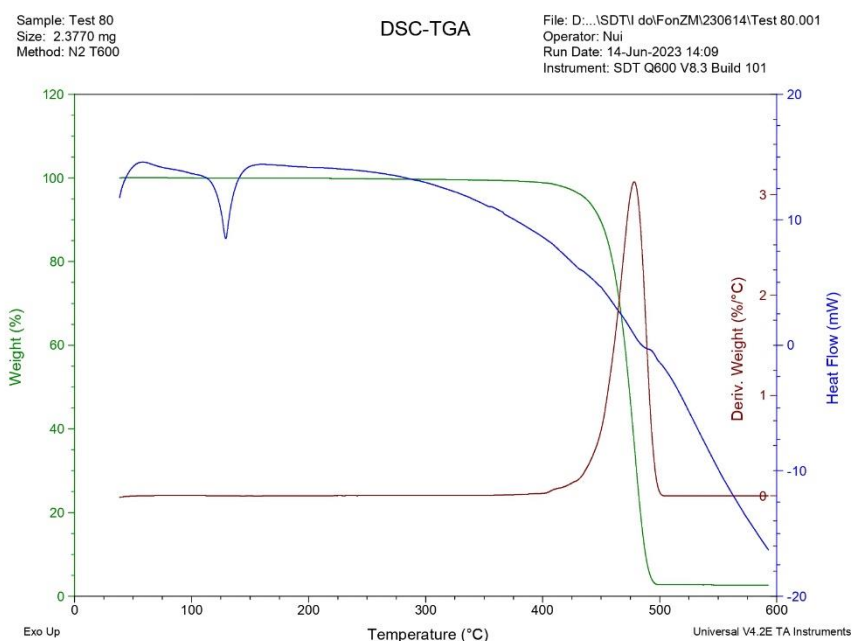


Figure B-5 TGA of polyethylene at 80°C with homogeneous system

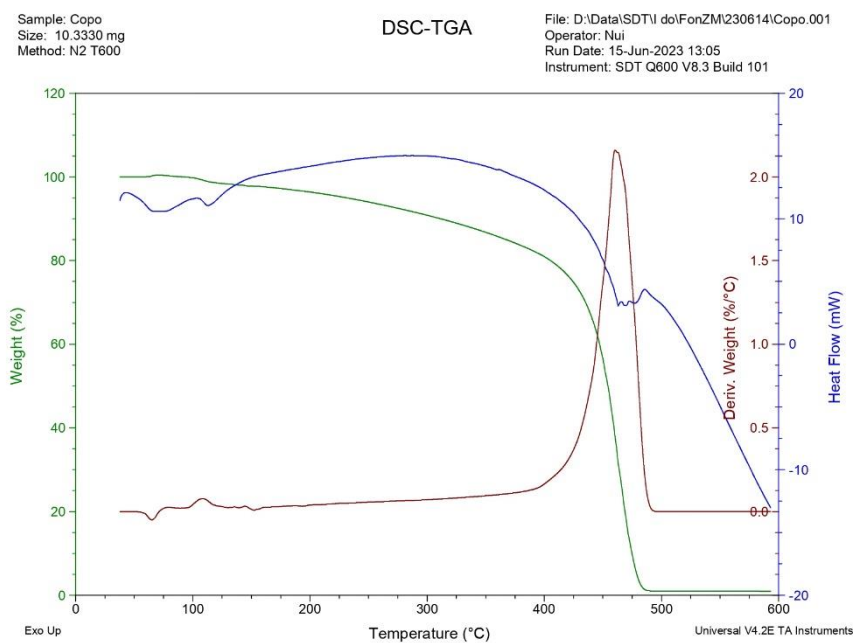


Figure B-6 TGA of ethylene/1-hexene copolymer at 80°C with homogeneous system

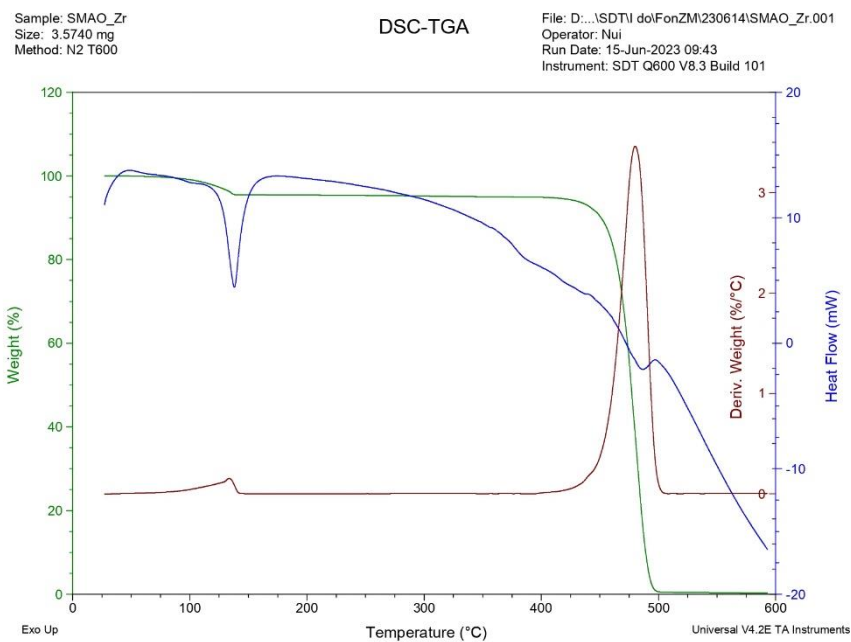


Figure B-7 TGA of PE-SMAO/Zr at 80°C

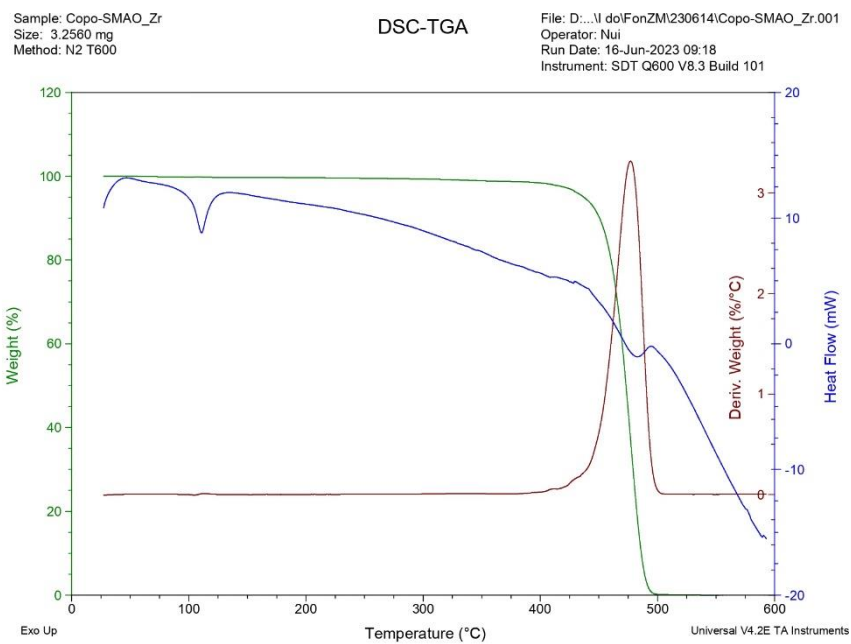


Figure B-8 TGA of CoPE-SMAO/Zr at 80°C

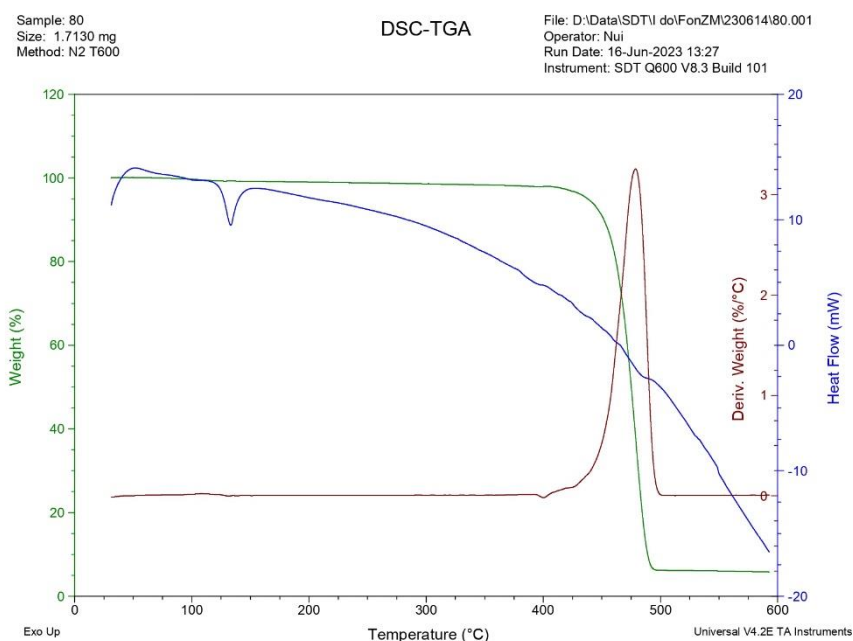


Figure B-9 TGA of PE-LTA-MAO/Zr at 80°C

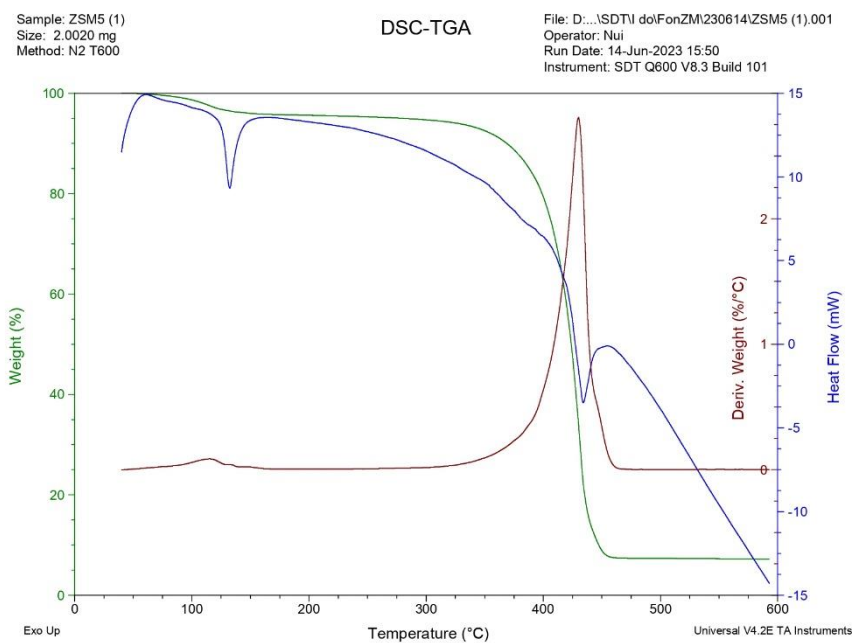


Figure B-10 TGA of PE-ZSM5-MAO/Zr at 80°C

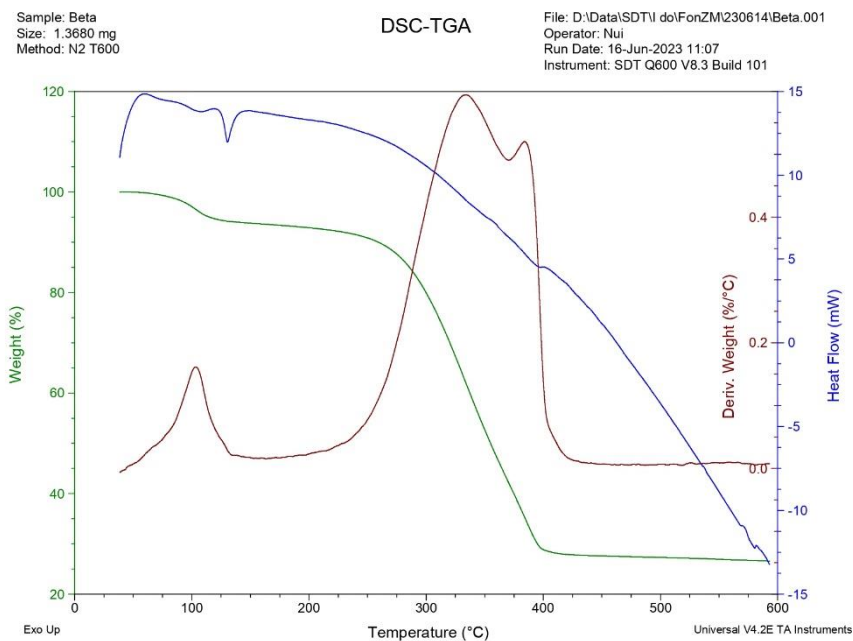


Figure B-11 TGA of PE-BEA-MAO/Zr at 80°C

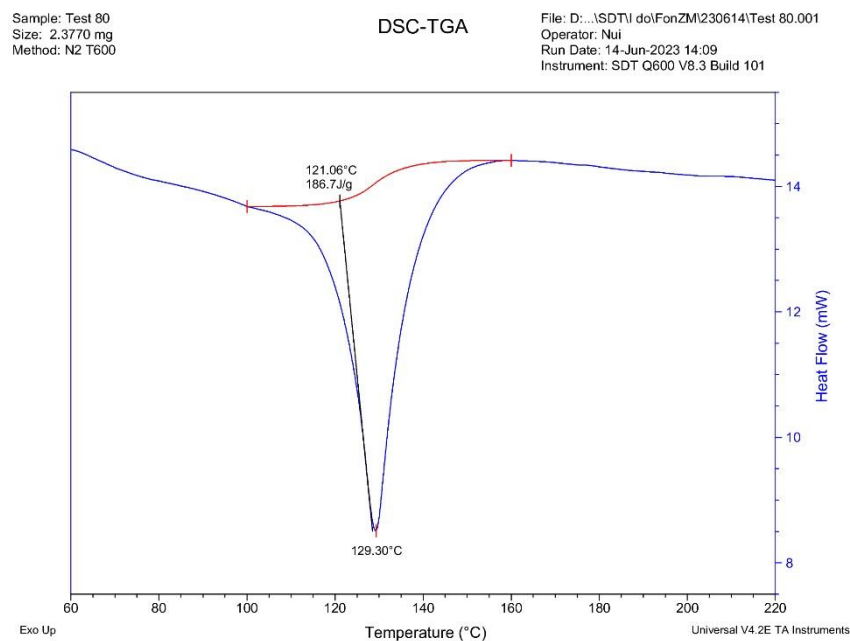


Figure B-12 DSC of polyethylene at 80°C with homogeneous system

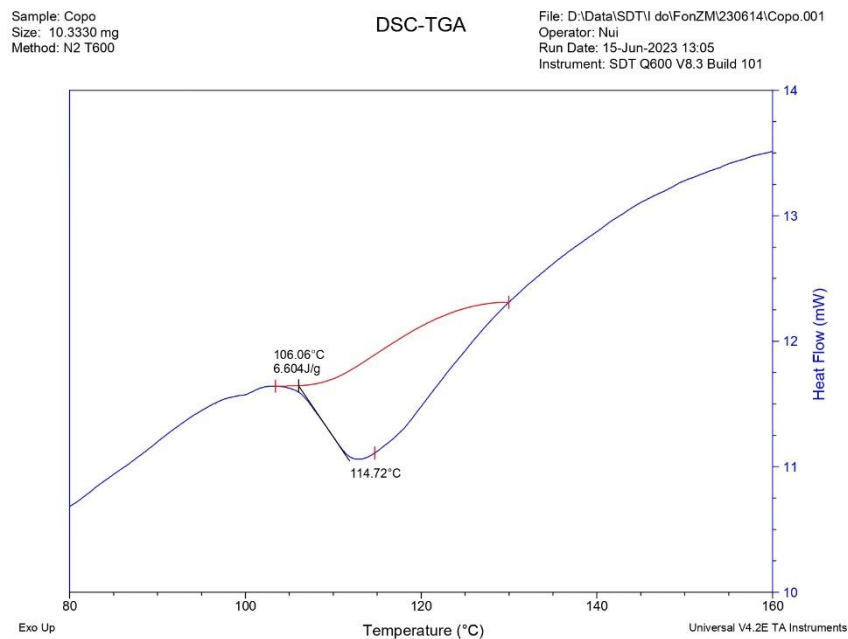


Figure B-13 DSC of ethylene/1-hexene copolymer at 80°C with homogeneous system

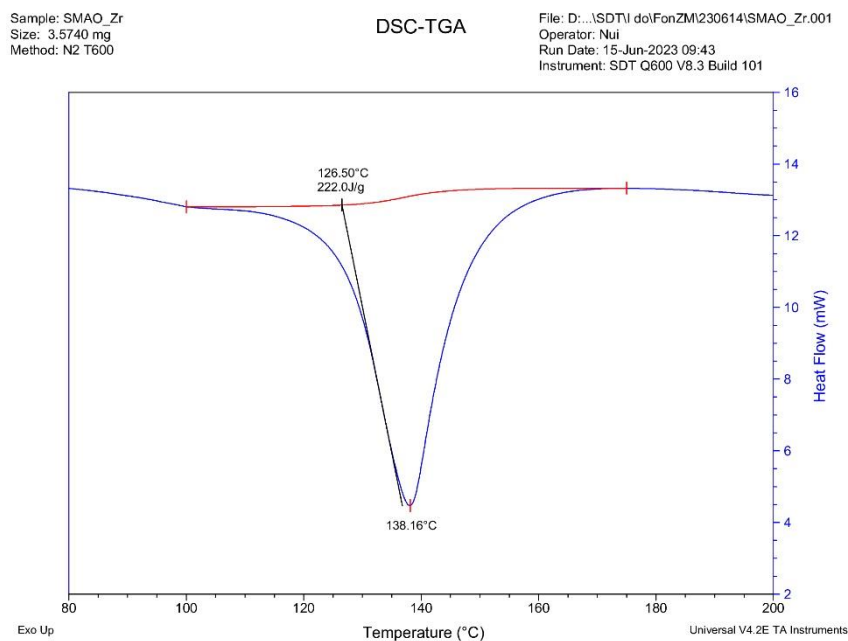


Figure B-14 DSC of PE-SMAO/Zr at 80°C

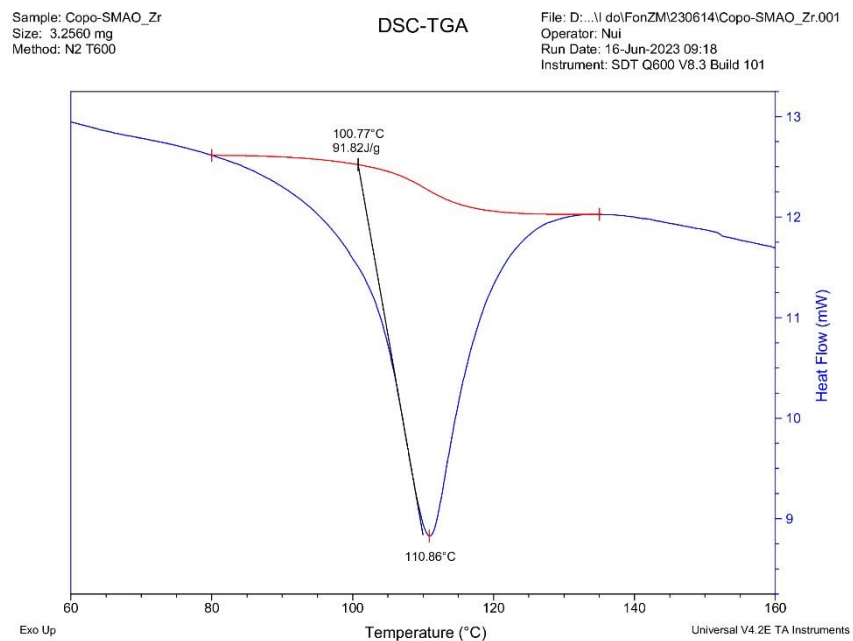


Figure B-15 DSCA of CoPE-SMAO/Zr at 80°C

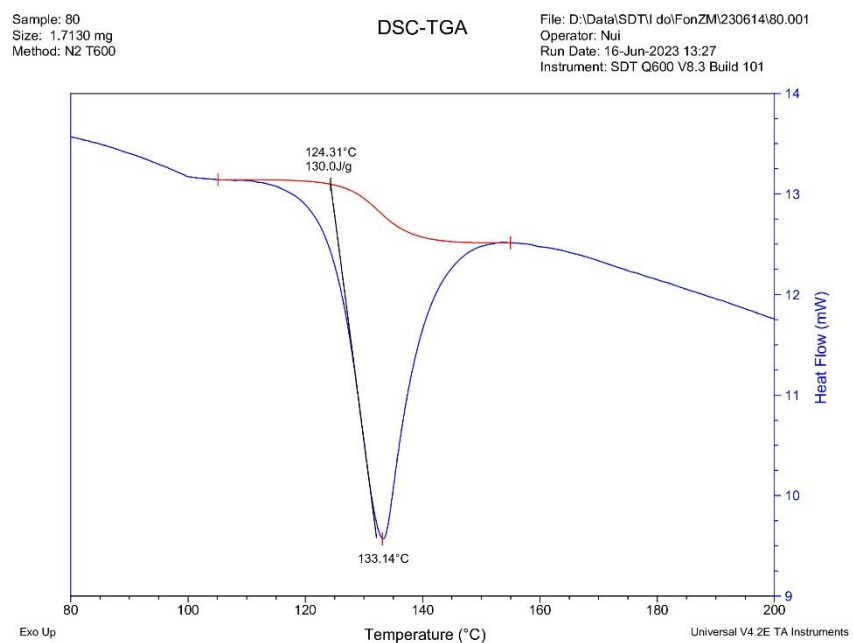


Figure B-16 DSC of PE-LTA-MAO/Zr at 80°C



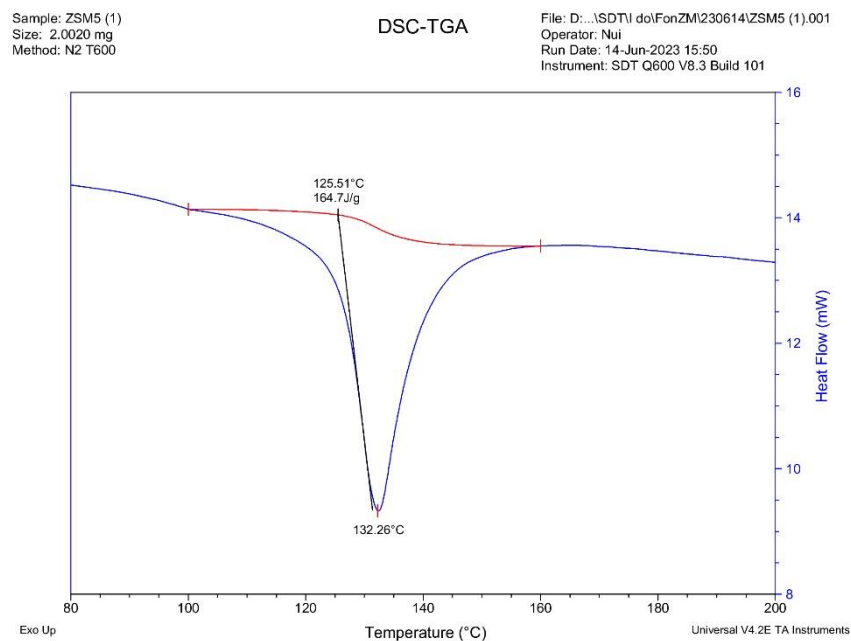


Figure B-17 DSC of PE-ZSM5-MAO/Zr at 80°C

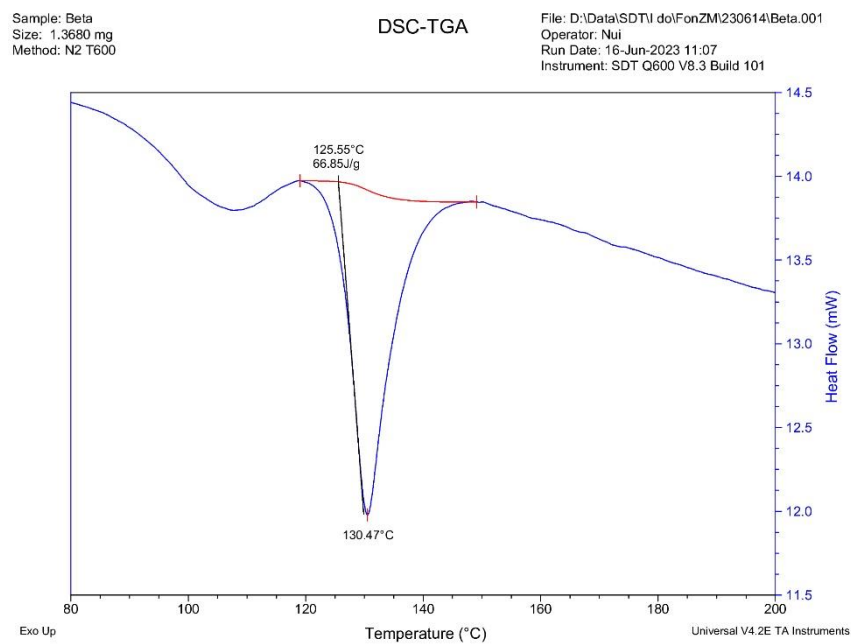
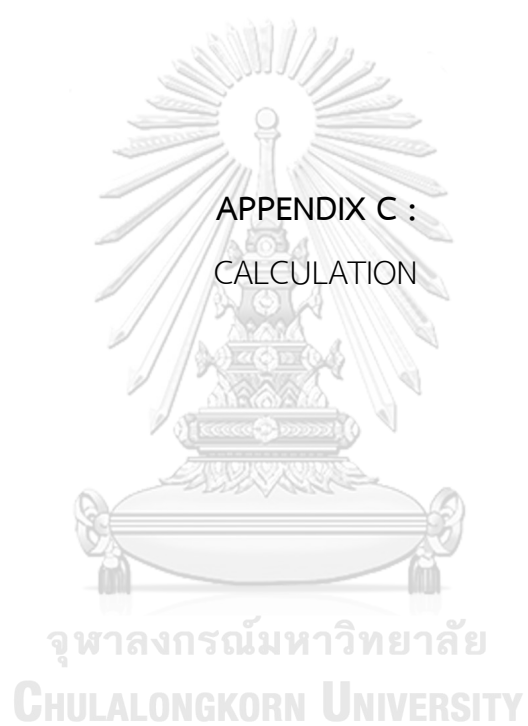


Figure B-18 DSC of PE-BEA-MAO/Zr at 80°C



## 1. Polymer yield

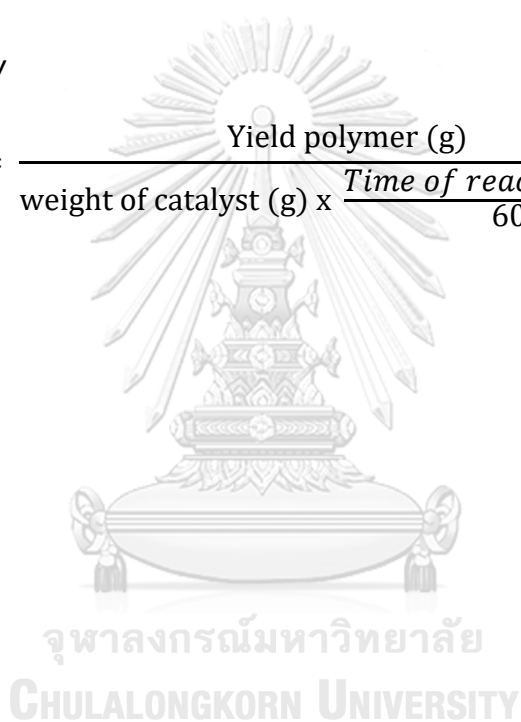
$$\text{Yield polymer (g)} = \text{obtain polymer}^1(\text{g}) - \text{support}^2(\text{g})$$

<sup>1</sup>Obtain polymer after run ethylene polymerization with filtrated and dried at room temperature.

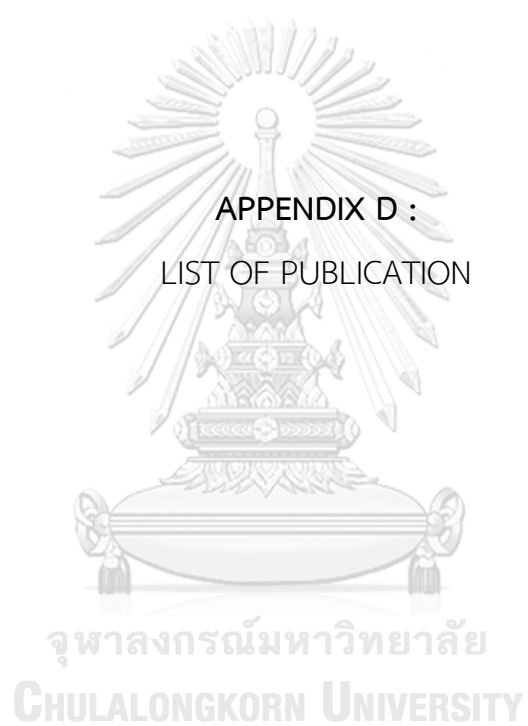
<sup>2</sup>Support for addition in ethylene polymerization

## 2. Catalyst activity

$$\text{Activity} = \frac{\text{Yield polymer (g)}}{\text{weight of catalyst (g)} \times \frac{\text{Time of reaction (min)}}{60}}$$



APPENDIX D :  
LIST OF PUBLICATION



Natthapat Warintha and Bunjerd Jongsomjit. “Effect of Silica Particle Size for Zirconocene-MAO/SiO<sub>2</sub> Catalysts on Ethylene Polymerization Behaviors” (The 32<sup>nd</sup> Thai Institute of chemical engineering and applied chemistry International conference (TICHe 2023), Nakhon Prathom, Thailand)

Natthapat Warintha and Bunjerd Jongsomjit. “Application of zeolite a derived from fly ash as a support of zirconocene/mao catalyst for ethylene and ethylene/1-hexene polymerization” (The 29<sup>th</sup> PPC Symposium on Petroleum, Petrochemicals, and Polymers and The 14<sup>th</sup> Research Symposium on Petrochemical and Materials Technology, Bangkok, Thailand)



**VITA**

<b>NAME</b>	Natthapat Warintha
<b>DATE OF BIRTH</b>	19 October 1998
<b>PLACE OF BIRTH</b>	Bangkok
<b>INSTITUTIONS ATTENDED</b>	Chemical Technology, Chulalongkorn University, Bangkok, Thailand
<b>HOME ADDRESS</b>	735 Soi 43, Rama II Road., Bangmod Sub-District, Chom Thong District, Bangkok, 10150
<b>AWARD RECEIVED</b>	1st Runner Up, TiChE National Chemical Student Design Competition 2020-2021

